THEORY AND IMPLEMENTATION OF COUPLED-CLUSTER METHODS FOR DIRECT CALCULATION OF IONIZATION ENERGIES

By

RENÉE PELOQUIN MATTIE

A DISSERTATION PRESENTED TO THE GRADUATE SCHOOL
OF THE UNIVERSITY OF FLORIDA IN PARTIAL FULFILLMENT
OF THE REQUIREMENTS FOR THE DEGREE OF
DOCTOR OF PHILOSOPHY

UNIVERSITY OF FLORIDA

1995

DEDICATION

To Robert,

You encouraged, supported, and pushed me throughout the process.

If anyone is happier than I am to see this in its final form, it must be you.

ACKNOWLEDGEMENTS

My thanks to: Professor Bartlett for sharing his knowledge and wisdom and for bringing me into his group; my entire committee for their patience; John Stanton and Jürgen Gauss for teaching me the joy of scientific collaboration; Anna Balkova and Hideo Sekino for much practical advice, abstract dialogues, tea, philosophical discussions, and late-night rides back from campus; Ajith Perera and all the students in the group for taking care of details long-distance; Karen Yanke for her help above and beyond the call of duty; Jan Musfeldt and David Bernholdt, Johna Till and Ted Johnson, for all kinds of help and encouragement, both scientific and nonscientific; and everyone else who gave me a kick when I needed it.

TABLE OF CONTENTS

LIST OF TABLES

LIST OF FIGURES

Abstract of Dissertation Presented to the Graduate School
of the University of Florida in Partial Fulfillment
of the Requirements for the Degree of
Doctor of Philosophy

THEORY AND IMPLEMENTATION OF COUPLED-CLUSTER METHODS FOR DIRECT CALCULATION OF IONIZATION ENERGIES

By

Renée Peloquin Mattie

August 1995

Chairman: Rodney J. Bartlett
Major department: Chemistry

The coupled-cluster equation-of-motion (CC-EOM) method, formally equivalent to the Fock-space coupled-cluster (FSCC) and coupled-cluster linear-response (CCLRT) methods for electron detachment energies, offers distinct advantages over the single-reference coupled cluster (SRCC) approach when several electron-detached states are to be calculated. The method is capable of providing transition energies for several states at a computational cost less than that of an SRCC calculation for one of them.

The equation-of-motion ionization potential (EOMIP) method is implemented using a Davidson-type algorithm for extracting selected roots from a large symmetric matrix, making it possible to selectively search for the difficult-to-characterize "shake-up" satellite peaks often found in inner valence structure, and several approximations to the ionization intensities are available, making it possible to simulate electron detachment spectra.

The EOMIP method is calibrated against experimental results for several small molecules, where the outer- and inner-valence regions are explored, with special attention to shake-up transitions. Results compare favorably with the coupled-cluster singles and doubles (CCSD) approach in most cases. The method is also applied to the interpretation of the electron detachment spectra of the linear carbon cluster anions, C_2^- through C_9^-.

CHAPTER 1

INTRODUCTION

1.1 Correlated Methods in Quantum Chemistry

In the early days of quantum chemistry, the only *ab initio* method available was the self-consistent field (SCF) approximation. This approximation to the electronic Hamiltonian neglects the interaction between individual electrons (electron correlation), placing each one in an average field of all the other electrons. The approach yields a simple molecular orbital picture of atoms and molecules and, in many cases, yields qualitatively good results for the energy differences between states of a molecule or reactive system. The molecular orbital (MO) picture can provide simple, useful concepts of physical processes, such as reaction, excitation, and ionization. But in many cases this simple picture is not even qualitatively correct. And there are many physical processes for which it is not capable of providing any explanatory tools.

The case in point is the photoelectron process. When electromagnetic radiation in the proper frequency range strikes an atom or molecule, an electron will be excited into the free-electron continuum. Photoelectron spectroscopists then observe the absorption spectrum or the spectrum of the free electron kinetic energies. Koopmans' theorem[1] is an SCF-based approach which states that the detached electron

is removed from a specific MO, and that the energy required is approximately the energy of that orbital. This approximation gives, in many cases, a qualitatively useful prediction of the principal peaks of the photoelectron spectrum, but it is incapable of making any prediction for the satellite peaks which are close in energy to these principal peaks. These so-called shake-up peaks are, in the MO picture, the result of a mixing of the primary hole-state process (ejection of an electron from a previously occupied orbital) with a two-hole, one-particle process (simultaneous ejection from an occupied orbital and excitation of an electron from an occupied to a virtual orbital). In order to predict these states, it is necessary to improve upon the SCF approximation -- to introduce electron correlation.

The configuration interaction (CI) method has been widely used to introduce correlation. In the single-reference formulation, it is simple in concept. Moving an electron from an "occupied" orbital (creating a "hole") to an unoccupied or "virtual" orbital (creating a "particle") defines a single excitation. Doing this twice defines a double excitation, etc. The correlated wavefunction is defined as a linear combination of the reference function and all possible single, double, etc., excitations from it. The coefficients are the eigenvectors of the matrix representation of the full electronic Hamiltonian in the basis of all these functions. The lowest-energy solution yields the correlated energy and wavefunction corresponding to the SCF reference, and the higher roots correspond to excited electronic states. The "full CI" solution, as it is called, is the best possible wavefunction for a given basis set and satisfies the variational principle. In practice, however, the full CI problem can rarely be solved. As

the number of basis functions (M) increases, the number of possible excited determinants increases as a function approaching $M!$. Standard implementations therefore truncate the expansion space, typically to only a subset of single and double excitations from the reference. But this truncation introduces a particularly troublesome error -- the energy of the system no longer scales properly with the size of the system being studied. The percentage error in the calculated correlation energy increases rapidly as the size of the system increases, more than doubling each time the size of the system doubles. The error in the energy is reflective of errors in the wavefunction, and calculations of observable properties, which depend on the wavefunction, will not scale properly with size. Typically, these truncated CI methods cannot be applied reliably to systems larger than benzene.

The many-body perturbation theory and coupled-cluster (CC)[2] methods have been developed specifically to avoid the deficiencies of the CI method. These methods are "size-extensive"; they scale properly with the size of the system. Implementations of these methods have become increasingly available in the past 10 years and have been shown to be very powerful, capable of predicting experimental results for many types of molecular systems to a high degree of accuracy. Second-order many-body perturbation theory (MBPT-2) calculations, which generally provide 80% or more of the correlation energy, require no more computational resources than do SCF calculations. Coupled-cluster singles and doubles (CCSD) calculations are routinely performed on systems up to the size of benzene. With the increasing availability of supercomputer time, it is easy to consider such calculations on molecules up to twice that large.

1.2 The Electron Detachment Problem

Since the mid-60s, "Molecular Photoelectron Spectroscopy has been recognized as an especially unambiguous method for the study of the molecular electronic structures of substances in the vapor state"[3]. In these experiments, light from an intense source is directed into a molecular gas or beam. The resulting detached electrons are collected and their kinetic energies recorded. At one time, it was common to record the absorption spectrum as well. In some cases fluorescence studies of the gas are performed as well.

From the beginning, theoretical methods have been an important tool in interpreting the photoelectron spectra. Koopmans' theorem predictions of ionization energies made it possible to identify principal peaks, and later CI singles and doubles (CISD) and electron propagator approaches were used with some success to identify the satellites. In the late seventies, several approaches were used to predict the intensities of these principal peaks and their satellites[4, 5, 6]. Nakatsuji and coworkers[7, 8, 9] introduced the symmetry-adapted-cluster (SAC) and symmetry-adapted-cluster CI (SAC-CI) approaches to calculating the ionization energies and intensities of molecules. The Fock-space coupled-cluster approach, introduced by Mukherjee and Lindgren[10, 11] and developed by others[12, 13, 14, 15] has recently provided a convenient formalism for a computationally advantageous approach to the direct calculation of energies. The CC EOM approach, closely related to CC linear-response theory (LRT)[16], is based upon a coupled-cluster reference. For the

calculation of principal ionization energies, this theory can be shown to be formally equivalent to the Fock-space coupled-cluster (FSCC) method.

In this dissertation, derivations of the CC EOM and FS EOM methods for calculation of ionization energies will be given, and the formal equivalence of these two methods will be demonstrated. The CC linear-response-theory will be derived for the ionization problem, and expressions for calculation of transition intensities will be developed as well.

Finally, the CC EOMIP method will be applied to several small molecules and to the linear carbon cluster anions, C_2^- through C_9^-.

CHAPTER 2

ELECTRON CORRELATION

2.1 The Schrödinger Equation

All electronic structure methods seek solutions or approximate solutions to the Born-Oppenheimer approximation to the Schrödinger equation,

$$\begin{aligned} H\Psi &= E\Psi \\ E &= \frac{\Psi^* H \Psi}{\Psi^* \Psi} \end{aligned} \tag{2.1}$$

where H is expressed in Hartree units as

$$H = -\frac{1}{2}\sum_i \nabla_i^2 - \sum_{i,\alpha} Z_\alpha r_{\alpha i}^{-1} + \sum_{i>j} r_{ij}^{-1}, \tag{2.2}$$

which is the sum of a one-electron and a two-electron portion,

$$\begin{aligned} h = H(\text{one}) &= -\frac{1}{2}\sum_i \nabla_i^2 - \sum_{i,\alpha} Z_\alpha r_{\alpha i}^{-1} \\ V_2 = H(\text{two}) &= \sum_{i>j} r_{ij}^{-1}, \end{aligned}$$

where i, j are indices over all electrons in the system and α over all nuclei, and Z_α is the charge of nucleus α. Unfortunately, the kinetic energy term of the Hamiltonian

$$-\frac{1}{2}\sum_i \nabla_i^2 = -\frac{1}{2}\sum_i \left(\left(\frac{\partial}{\partial x_i}\right)^2 + \left(\frac{\partial}{\partial y_i}\right)^2 + \left(\frac{\partial}{\partial z_i}\right)^2 \right), \tag{2.3}$$

taken with the two-electron term, gives a second-order differential equation in many variables, for which there is no general analytic solution. It is possible to solve certain approximations to the Schrödinger Equation.

2.1.1 The Independent Electron Approximation and Fock space

All the methods to be discussed are based on a finite set of spin orbitals, $\phi_p(\zeta)$, one-electron functions of the combined space and spin coordinate $\zeta = \{\mathbf{r}; \omega\}$. For molecular calculations, the spin orbitals are referred to as molecular orbitals and generated using an independent particle method – in which the V_2 portion of the Hamiltonian is replaced by an independent particle potential V_F. The ultimate form of the ϕ orbitals is generally arrived at by a self-consistent field method, such as the Hartree-Fock theory. In the Hartree-Fock approximation, the approximate Hamiltonian is referred to as the Fock operator.

$$\begin{aligned} F &= h + V_F \\ H &= F + (V_2 - V_F) \end{aligned} \tag{2.4}$$

The basic component of an N-electron wavefunction is a single Slater determinant Φ_ν^N,

$$\begin{aligned} \Phi_\nu^N &= \frac{1}{\sqrt{N!}} \mathcal{A} \left(\prod_{p=1,N} \phi_p(\zeta_{p\nu}) \right) \\ &= \frac{1}{\sqrt{N!}} \left| \phi_{1\nu}(\zeta_1) \phi_{2\nu}(\zeta_2) \ldots \phi_{N\nu}(\zeta_N) \right|, \end{aligned}$$

where N can be any number from 0 to the total number of molecular orbitals available, and the index ν distinguishes among the $\binom{M}{N}$ possible choices of N orbitals from a set of M. Φ^0 is the trivial case, with no electrons chosen, and is referred to as the *vacuum* state.

The Slater determinant is an antisymmetrized product of N one-electron functions, ensuring that fermion statistics are obeyed – the sign of the wavefunction will change if the ζ coordinates of any two electrons are exchanged. Any many-electron wavefunction within this truncated space can be represented as a linear combination of Slater determinants.

The finite space spanned by the Slater determinants is

$$\sum_{N\nu} \Phi_\nu^N,$$

which is generally a subset of the space spanned by the eigenfunctions of the Hamiltonian. The Slater determinants span the eigenspace of the truncated Hamiltonian – the Hamiltonian projected into the space of the Slater determinants,

$$\begin{aligned} &\sum_{N\nu}\sum_{M\mu} \Phi_\nu^N \left(\int \Phi_\nu^{N*} H \Phi_\mu^M \right) \Phi_\mu^{M*} \\ &= \sum_{N\nu}\sum_{M\mu} \left|\Phi_\nu^N\right\rangle \left\langle \Phi_\nu^N \right| H \left|\Phi_\mu^M\right\rangle \left\langle \Phi_\mu^M \right|. \end{aligned}$$

2.1.2 Second Quantization

The second quantized notation is a convenient one which will be used throughout this work. The Hamiltonian can be written in second-quantized form as

$$H = \sum_{pq} h_{pq} p^\dagger q + \frac{1}{4} \sum_{pqrs} \langle pq||rs\rangle p^\dagger r q^\dagger s \tag{2.5}$$

where

$$h_{pq} = \int \phi_p^*(1) \left(-\frac{1}{2}\nabla_1^2 - \sum_\alpha Z_\alpha r_{\alpha 1}^{-1} \right) \phi_q \, d\tau_1 d\sigma_1 \tag{2.6}$$

$$\langle pq||rs\rangle = \int\int \phi_p^*(1)\phi_q^*(2)(1 - P_{12}) r_{12}^{-1} \phi_r(1)\phi_s(2) \, d\tau_1 d\tau_2 d\sigma_1 d\sigma_2. \tag{2.7}$$

The creation ($p^\dagger$) and annihilation (p) operators represent the creation and annihilation of orbital p. The fundamental relations between these operators are

$$\left[p^\dagger, q^\dagger\right]_+ = p^\dagger q^\dagger + q^\dagger p^\dagger \equiv 0 \tag{2.8}$$

$$[p, q]_+ = pq + qp \equiv 0 \tag{2.9}$$

$$\left[p^\dagger, q\right]_+ \equiv \langle p|q\rangle. \tag{2.10}$$

When the orbitals are orthonormal, equation 2.10 becomes $\left[p^\dagger, q\right]_+ \equiv \delta_{pq}$.

Any Slater determinant can be constructed through the action of creation operators on the vacuum determinant ($\Phi^0 = |-\rangle$).

$$q^\dagger ... p^\dagger \, |-\rangle = \frac{1}{\sqrt{N!}} \left| \phi_p(\zeta_1) ... \phi_q(\zeta_N) \right|.$$

The properties of these operators ensure the Pauli principle is obeyed

$$p^\dagger p^\dagger = 0 - p^\dagger p^\dagger = 0$$

$$p^\dagger p^\dagger \, |-\rangle = 0;$$

a given spin orbital cannot be occupied more than once in the same determinant.

If one Slater determinant is chosen as a reference, the operators can be separated into occupied or hole ($i^\dagger$, i) and virtual or particle ($a^\dagger$, a) creation and annihilation operators. Any Slater determinant can created from a given reference determinant $|0\rangle$ by first annihilating zero or several occupied orbitals (creating zero or several holes), then creating 0 or several virtual orbitals (creating zero or several particles), for example $a^\dagger i\,|0\rangle$ represents the excitation of a single electron from occupied orbital ϕ_i to virtual orbital ϕ_a, while the operator string $a^\dagger ji$ operating on the same reference excites one electron while annihilating another, reducing the number of electrons in the wavefunction by one. A thorough discussion of the nature of second-quantized operators can be found in the first chapter of Jørgensen and Simons' work[17].

In order to simplify further discussions and diagrammatics, it is useful to write operators in *normal ordered* (or normal product) form[2, 18], represented by placing "{ }" around the product of operators. The normal order of a product of operators is that ordering of the operators whose expectation value with respect to the reference, $|0\rangle$, is zero. In practice, this means "moving" all particle annihilation operators (a) and hole annihilation operators ($i^\dagger$) to the right, using the fundamental anti commutation relations given in equations 2.8 through 2.10. Interchanging any two single-particle operators within a string of operators results in a change in sign of the normal-ordered product,

$$\begin{aligned} \{pqsr^\dagger\} &= -\{pqr^\dagger s\} = \{pr^\dagger qs\} = -\{r^\dagger pqs\} \\ \{j^\dagger i\} &= -\{ij^\dagger\} = -ij^\dagger \end{aligned}$$

$$\{a^\dagger i\} = a^\dagger i.$$

The last of these, $a^\dagger i$, composed only of hole- and particle-creation operators, is the only type of normal-ordered string which may act on the reference $|0\rangle$ without destroying it. With normal order defined, the *contraction* between any two operators, designated as $(pq)_C$ or $\overline{pq}$ is defined as the difference between the product and the normal order of the product

$$pq \equiv \{pq\} + \overline{pq}.$$

Using the fundamental anti commutation relations, the contractions can be evaluated as

$$\begin{aligned}
\overline{pq} &= \overline{p^\dagger q^\dagger} = 0 \\
\overline{ij^\dagger} &= \overline{a^\dagger b} = 0 \\
\overline{i^\dagger j} &= \delta_{ij} \\
\overline{ab^\dagger} &= \delta_{ab}.
\end{aligned}$$

Another common normal ordering is that with respect to the vacuum state $|-\rangle$. In this ordering, all orbitals are "virtual", and the second quantized operator in equation 2.5 is already in normal order. This is not, however, the case with the normal ordering used here. The normal-ordered Hamiltonian, H_N is that part of the Hamiltonian whose expectation with respect to the reference $|0\rangle$ is non-zero

$$H_N = H - \langle 0| H |0\rangle \tag{2.11}$$

$$= H - E_{\mathrm{SCF}}$$

$$= f_N + W_N$$

$$= H_N(\mathrm{one}) + H_N(\mathrm{two})$$

$$f_N = \sum_{pq} F_{pq} p^\dagger q \tag{2.12}$$

$$W_N = \frac{1}{4} \sum_{pqrs} \langle pq||rs\rangle p^\dagger q^\dagger sr. \tag{2.13}$$

Writing H_N in terms of normal ordered operators makes this partitioning into F and

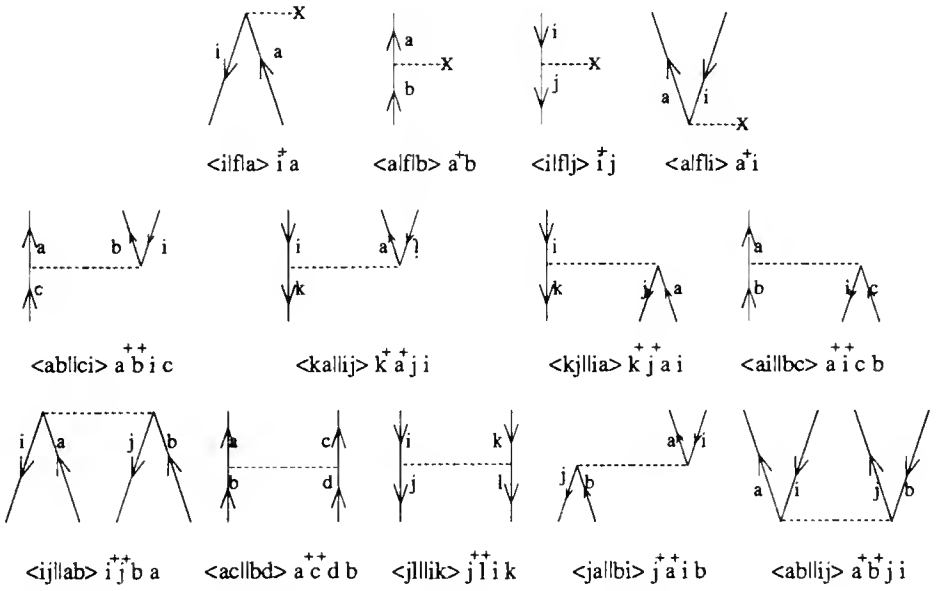

Figure 2.1: The H_N operator

non-F pieces possible, and is convenient when it comes to developing diagrammatics. A diagrammatic representation of these H_N elements is given in figure 2.1.

2.2.1 The Coupled-Cluster Operators

The coupled-cluster theory defines a wavefunction $|CC\rangle$ which is an eigenfunction of the full Hamiltonian

$$H\,|CC\rangle = E\,|CC\rangle \tag{2.14}$$

$$(H - \langle 0|\,H\,|0\rangle)\,|CC\rangle = H_N\,|CC\rangle = E_{CC}\,|CC\rangle\,, \tag{2.15}$$

where E_{CC} is the correlation energy obtained from the application of coupled-cluster theory.

The CC wavefunction is defined in terms of excitation operators T as

$$|CC\rangle = e^T\,|0\rangle \tag{2.16}$$

The operator T is defined as

$$T_1 + T_2 + T_3 + \cdots$$

$$\begin{aligned} T_1 &= \sum_{ia} t_i^a a^\dagger i \\ T_2 &= \frac{1}{4}\sum_{ijab} t_{ij}^{ab} a^\dagger b^\dagger j i, \\ T_3 &= \frac{1}{3!^2}\sum_{ijkabc} t_{ijk}^{abc} a^\dagger b^\dagger c^\dagger i j k, \end{aligned}$$

etc. The inverse of this exponential is simply $\exp(-T)$. Therefore

$$\begin{aligned} e^{-T}H\,|CC\rangle &= e^{-T}Ee^T\,|0\rangle \\ &= E\,|0\rangle \\ E &= \langle 0|\,e^{-T}He^T\,|0\rangle\,. \end{aligned}$$

The correlation energy, $E_{CC} \equiv E - E_{\mathsf{SCF}}$, is

$$\begin{aligned} E_{CC} &= \langle 0|\, e^{-T} H e^{T}\, |0\rangle - \langle 0|\, H\, |0\rangle \\ &= \langle 0|\, e^{-T} H_N e^{T}\, |0\rangle \end{aligned} \tag{2.17}$$

2.2.2 The $\bar{H}$ Operator

The quantity $\exp(-T)H\exp(T)$, referred to as $\bar{H}$, shows up again and again in coupled-cluster based methods, so it is worth looking at it in detail. $\bar{H}$, expanded in terms of T in the Baker-Campbell-Hausdorff expansion, is

$$\begin{aligned} \bar{H} &= H + HT - TH + \frac{1}{2}HT^2 - \frac{1}{2}T^2H - THT + \cdots \\ &= H + [H,T] + \frac{1}{2}[[H,T],T] + \frac{1}{3!}[[[H,T],T],T] + \frac{1}{4!}[[[[H,T],T],T],T]. \end{aligned} \tag{2.18}$$

The commutators can be written in terms of their connected and disconnected parts, and it can be shown that the disconnected parts cancel, allowing $\bar{H}$ to be expressed as a sum of only connected pieces, in which H is contracted to any T operators in the expression

$$\bar{H} = H + (HT)_C + \frac{1}{2}\left(HT^2\right)_C + \frac{1}{3!}\left(HT^3\right)_C + \frac{1}{4!}\left(HT^4\right)_C \tag{2.19}$$

$$= \left(He^{T}\right)_C. \tag{2.20}$$

The connectedness of the $\bar{H}$ elements is what establishes the size-extensivity of the coupled-cluster method.

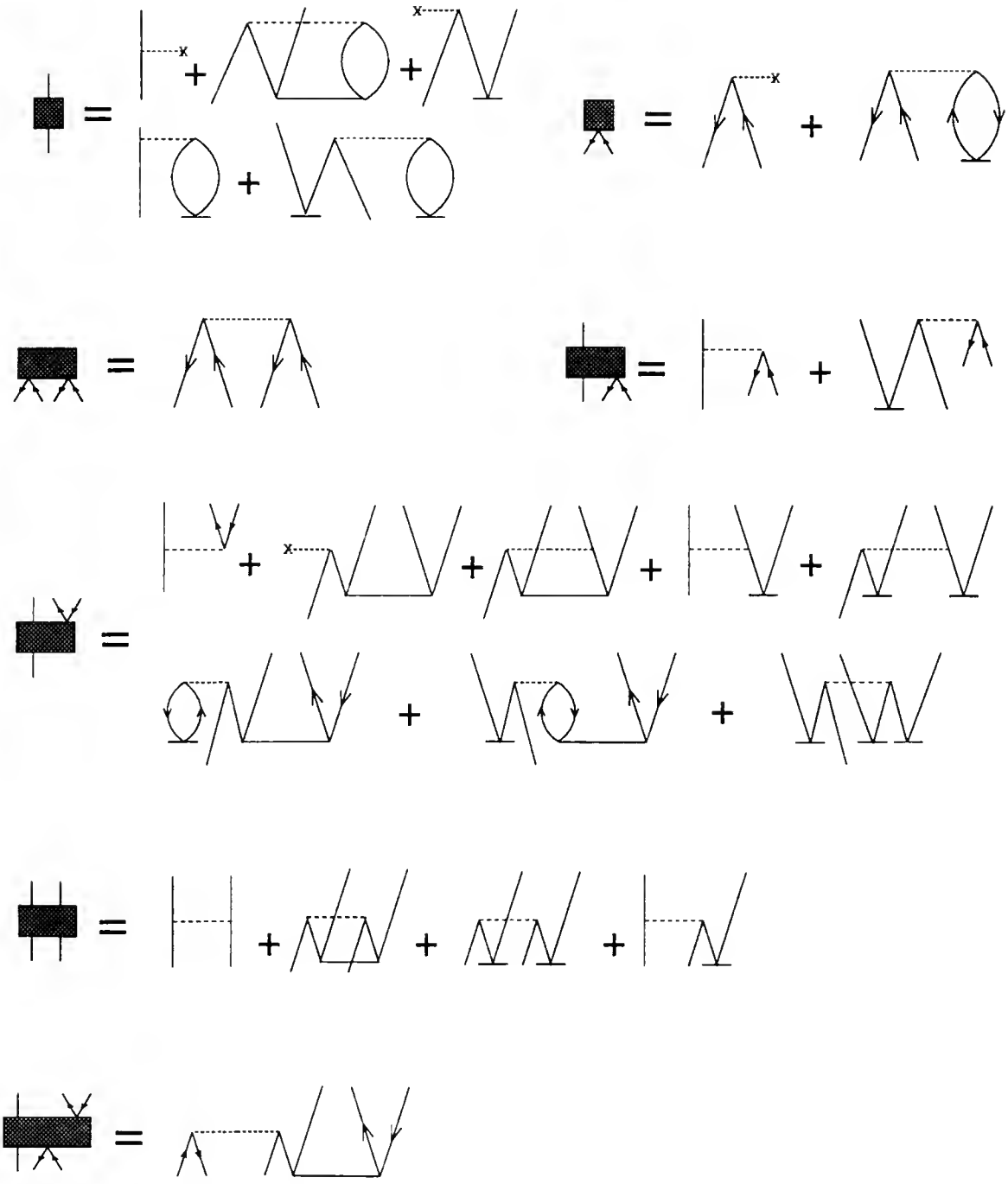

Figure 2.2: $\bar{H}_N$ elements required for CC EOMIP-SD and FSIP equations

2.2.3 The Coupled-Cluster Equations

Similar to $\bar{H}$ is $\bar{H}_N = e^{-T} H_N e^T = (H_N e^T)_C$, which appears in the coupled-cluster energy expression in equation 2.17. Using this formulation, we have

$$E_{CC} = \langle 0 | (H_N e^T)_C | 0 \rangle \tag{2.21}$$

Since $\bar{H}_N | 0 \rangle = E | 0 \rangle$, it is clear that

$$\left\langle \psi | \bar{H}_N | 0 \right\rangle = 0 \tag{2.22}$$

for any state ψ orthogonal to the $|0\rangle$ state. This fact is used to define the T amplitudes. If

$$\left| \begin{matrix} a \\ i \end{matrix} \right\rangle = a^\dagger i \, | 0 \rangle \,, \tag{2.23}$$

$$\left| \begin{matrix} ab \\ ij \end{matrix} \right\rangle = a^\dagger i b^\dagger j \, | 0 \rangle \,, \tag{2.24}$$

then the singles and doubles equations are defined by

$$\left\langle \begin{matrix} a \\ i \end{matrix} \right| \bar{H}_N | 0 \rangle = 0 \tag{2.25}$$

$$\left\langle \begin{matrix} ab \\ ij \end{matrix} \right| \bar{H}_N | 0 \rangle = 0 \tag{2.26}$$

$$\cdots \,,$$

Figure 2.2 contains the diagrammatic expressions for the $\bar{H}$ terms which are necessary for the methods to be discussed in this work. For example, the algebraic expression for the term  $(= \langle i | \bar{f} | a \rangle)$ is

$$\langle i | \bar{f} | a \rangle + \sum_{me} t_i^a \langle im | | ae \rangle \,.$$

2.3 Configuration Interaction

2.3.1 The CI Operators

In configuration interaction, electron correlation is introduced by constructing a wavefunction from all possible Slater determinants with the same number of occupied orbitals as the reference. This means each additional determinant is related to the reference by an excitation operation – $a^\dagger i$ represents a single excitation, while $a^\dagger b^\dagger ji$ represents a double excitation. The CI wavefunction is represented as

$$|CI\rangle = (1 + C)\,|0\rangle\,, \tag{2.27}$$

where C is defined as

$$C_1 + C_2 + C_3 + \cdots$$

$$\begin{aligned} C_1 &= \sum_{ia} c_i^a a^\dagger i \\ C_2 &= \frac{1}{4}\sum_{ijab} c_{ij}^{ab} a^\dagger i b^\dagger j, \\ C_3 &= \frac{1}{3!^2}\sum_{ijkabc} c_{ijk}^{abc} a^\dagger i b^\dagger j c^\dagger k \end{aligned}$$

etc.

2.3.2 The CI Equations

The CI energy is calculated from

$$\begin{aligned} H\,|CI\rangle &= E\,|CI\rangle \\ E &= \langle 0|\,H\,|CI\rangle = E(\langle 0|\,|0\rangle + \langle 0|\,C\,|0\rangle) \\ E_{CI} + E_{\mathsf{SCF}} &= \langle 0|\,(H_N + \langle 0|\,H\,|0\rangle)(1+C)\,|0\rangle \\ E_{CI} &= \langle 0|\,H_N(1+C)\,|0\rangle \end{aligned}$$

and the C operator satisfies

$$\left\langle \begin{matrix} a \\ i \end{matrix} \right| H_N(1+C)\,|0\rangle = E_{CI}C_i^a \tag{2.28}$$

$$\left\langle \begin{matrix} ab \\ ij \end{matrix} \right| H_N(1+C)\,|0\rangle = E_{CI}C_{ij}^{ab} \tag{2.29}$$

etc., (2.30)

which can be solved via a matrix eigenvalue approach.

In the CI approach, there is no Baker-Campbell-Hausdorff expansion to force the connectedness of H to the wavefunction operator C.

CHAPTER 3

THE COUPLED-CLUSTER EQUATION-OF-MOTION METHOD

3.1 The EOM Equations

Beginning with the exact coupled-cluster ground state $|CC\rangle$, an EOM wavefunction is created using a linear operator Ω, the full set of which spans the space of excitations from the SCF reference, and therefore the space of eigenfunctions of the second-quantized H_N of the appropriate number of electrons. A particular EOM state will be referred to by the index $\mathcal{K}$.

$$H_N |CC\rangle = E_{CC} |CC\rangle = E_{CC} e^T |0\rangle \tag{3.1}$$

$$\begin{aligned} H_N |\mathcal{K}_{CC}\rangle &= (E^{\mathcal{K}} - E_{\mathsf{SCF}}) |\mathcal{K}_{CC}\rangle \\ &= (E^{\mathcal{K}} - E_{\mathsf{SCF}}) \Omega^{\mathcal{K}} |CC\rangle = (E^{\mathcal{K}} - E_{\mathsf{SCF}}) \Omega^{\mathcal{K}} e^T |0\rangle . \end{aligned} \tag{3.2}$$

When $\Omega^{\mathcal{K}}$ is limited to contain excitation-type operators only, it commutes with T, and we derive the expression

$$\begin{aligned} H_N |\mathcal{K}_{CC}\rangle - \Omega^{\mathcal{K}} H_N |CC\rangle &= (E^{\mathcal{K}} - E) |\mathcal{K}_{CC}\rangle = \left[H_N, \Omega^{\mathcal{K}}\right] |CC\rangle \\ \omega^{\mathcal{K}} e^T \Omega^{\mathcal{K}} |0\rangle &= \left[H_N, \Omega^{\mathcal{K}}\right] e^T |0\rangle = \left[H_N e^T, \Omega^{\mathcal{K}}\right] |0\rangle \\ e^{-T} \omega^{\mathcal{K}} e^T \Omega^{\mathcal{K}} |0\rangle &= \left[e^{-T} H_N e^T, \Omega^{\mathcal{K}}\right] |0\rangle \end{aligned}$$

$$\omega^{\mathcal{K}}\Omega^{\mathcal{K}}\left|0\right\rangle \;=\; \left[\bar{H}_N,\Omega^{\mathcal{K}}\right]\left|0\right\rangle \tag{3.3}$$

where $\omega^{\mathcal{K}} \equiv E^{\mathcal{K}} - E$ and $\bar{H}_N \equiv e^{-T}H_N e^{T} = (H_N e^{T})_C$.

Projection of equation 3.3 on the left by $|\mathbf{h}\rangle$, the orthogonal complement to the reference function $|0\rangle$, and by $|0\rangle$ itself yield

$$\omega^{\mathcal{K}}\left\langle\mathbf{h}\right|\Omega^{\mathcal{K}}\left|0\right\rangle \;=\; \left\langle\mathbf{h}\right|\left[\bar{H}_N,\Omega^{\mathcal{K}}\right]\left|0\right\rangle \tag{3.4}$$

This equation defines an eigenvalue problem which is solved to yield the energies (eigenvectors) ω (Ω).

The second term of the commutator, $\Omega^{\mathcal{K}}\bar{H}_N$, contains only uncontracted terms. Dividing the commutator into contracted and uncontracted terms gives

$$\begin{aligned}
\left[\bar{H}_N,\Omega^{\mathcal{K}}\right] &= \left(\bar{H}_N\Omega^{\mathcal{K}}\right)_C + \left(\bar{H}_N\Omega^{\mathcal{K}}\right)_U - \left(\bar{H}_N\Omega^{\mathcal{K}}\right)_C \\
&= \left(\bar{H}_N\Omega^{\mathcal{K}}\right)_C + \left(\bar{H}_N\Omega^{\mathcal{K}}\right)_U - \left(\Omega^{\mathcal{K}}\bar{H}_N\right)_U \\
&= \left(\bar{H}_N\Omega^{\mathcal{K}}\right)_C \\
\omega^{\mathcal{K}}\Omega^{\mathcal{K}}\left|0\right\rangle &= \left(\bar{H}_N\Omega^{\mathcal{K}}\right)_C\left|0\right\rangle .
\end{aligned} \tag{3.5}$$

The commutator in the EOM equations has the effect of removing all the uncontracted terms from the equations. The EOMIP equations become

$$\omega^{\mathcal{K}}\left\langle\mathbf{h}\right|\Omega^{\mathcal{K}}\left|0\right\rangle = \left\langle\mathbf{h}\right|\left(\bar{H}_N\Omega^{\mathcal{K}}\right)_C\left|0\right\rangle , \tag{3.6}$$

an eigenvalue problem in terms of the transformed Hamiltonian $\bar{H}_N$.

The expansion of the $\bar{H}_N$ terms is limited to a maximum $\bar{H}_N$ excitation level of $(L_\Omega - 1)$, where L_Ω is the highest level of excitation included in $\Omega^{\mathcal{K}}$, and again by the maximum number of up-going lines in $\Omega^{\mathcal{K}}$ available for contraction. This will be $2L_\Omega - 1$ for the IP problem and $2L_\Omega$ for excitation energies.

3.2 Size-Extensivity and the EOM problem

The EOM problem is similar, from a computational standpoint, to an ordinary CI problem except that $\bar{H}_N$ is not symmetric and is not limited to one- and two-body terms. From a theoretical standpoint however, it differs considerably from the CI problem, in that all the terms of the $\bar{H}_N \Omega^K$ product are contracted.

Within this framework, a perturbation theory which is connected to every order, and at any level of truncation of the theory, can be constructed[10] for the principal ionization energy and electron affinity cases (see appendix B). Since the $\bar{H}_N$ operator, being based on the CC solution, is also connected, the EOMIP and EOMEA principal energies are connected, and the solutions are therefore size-extensive. CI-based methods, being unconnected, do not offer this advantage.

3.3 The EOM Wavefunction

For the EOM problem, Ω^K is a linear operator,

$$\Omega^K = \sum_\mu C_\mu^K \tau_\mu \tag{3.7}$$

where

$$\tau_\mu |0\rangle = |\mu\rangle . \tag{3.8}$$

The operator τ_μ consists of a normal-ordered product of creation and annihilation operators which, acting on the Hartree-Fock reference $|0\rangle$, create new determinants. For excited wavefunctions, the set $\{\tau_\mu\}$ contains the identity operator, as well as

excitation operators $a^\dagger i$, $a^\dagger i b^\dagger j$, $\cdots$. For the electron-detached case, $\{\tau_\mu\}$ contains i, $a^\dagger ij \cdots$, operator products which will create N$-$1 electron determinants.

Because the equation-of-motion problem is treated as an eigen problem of the $\bar{H}_N$ operator, the solution wavefunctions,

$$|\mathcal{K}\rangle \;=\; \Omega^{\mathcal{K}}\,|0\rangle$$

are eigenfunctions of $\bar{H}_N$ within the truncated space defined by the highest level of excitation in $\{\tau_\mu\}$. But in general, we are interested in wavefunctions of the Hamiltonian H, and so must go back to the expression

$$|\mathcal{K}_{CC}\rangle \;=\; e^T\Omega^{\mathcal{K}}\,|0\rangle\,, \tag{3.9}$$

an approximation to an eigenfunction of H.

If we define a matrix C with vectors $\mathsf{C}^{\mathcal{K}}$ corresponding to the $C_\mu^{\mathcal{K}}$ which appear in the definition of $\Omega^{\mathcal{K}}$, then Ω (the entire set of $\Omega^{\mathcal{K}}$ solution operators) can be written as

$$\begin{aligned}\Omega \;&=\; \tau\mathsf{C}\\ &=\; \begin{pmatrix}\tau_1 & \tau_2 & \cdots & \tau_\mu\end{pmatrix}\begin{pmatrix} C_1^1 & C_1^2 & \cdots & C_1^{\mathcal{K}} \\ C_2^1 & C_2^2 & \cdots & C_2^{\mathcal{K}} \\ \vdots & \vdots & \ddots & \vdots \\ C_\mu^1 & C_\mu^2 & \cdots & C_\mu^{\mathcal{K}}\end{pmatrix},\end{aligned} \tag{3.10}$$

the solution space for a given EOM problem can be represented as

$$\begin{aligned}\langle 0|\,\tau\bar{H}_N\tau\mathsf{C}\,|0\rangle \;&=\; \omega\mathsf{C}\\ \langle\mu|\,\bar{H}_N\,|\mu\rangle\,\mathsf{C} \;&=\; \omega\mathsf{C}\\ \mathsf{C}^{-1}\,\langle\mu|\,\bar{H}_N\,|\mu\rangle\,\mathsf{C} \;&=\; \omega\\ \mathsf{D}^\dagger\,\langle\mu|\,\bar{H}_N\,|\mu\rangle\,\mathsf{C} \;&=\; \omega.\end{aligned} \tag{3.11}$$

The matrix $\mathsf{D}^\dagger \equiv \mathsf{C}^{-1}$, defines a new operator $Y = \tau\mathsf{D}$. D and Y can also be used to represent the solution space of the EOM equations:

$$\mathsf{D}^\dagger \langle\mu| \bar{H}_N |\mu\rangle = \mathsf{D}\omega. \tag{3.12}$$

It is clear that these D vectors, the left-hand eigenvectors of the non Hermitian $\bar{H}_N$, yield left-hand eigenfunctions of $\bar{H}_N$,

$$\mathsf{D}^\dagger \langle 0| \tau\bar{H}_N\tau |0\rangle = \mathsf{D}^\dagger\omega \tag{3.13}$$

$$\langle 0| Y^{\mathcal{K}\dagger}\bar{H}_N = \langle 0| Y^{\mathcal{K}\dagger}\omega^{\mathcal{K}}, \tag{3.14}$$

and therefore the projection of the full-space left-hand eigenfunction into the reduced space,

$$\langle 0| Y^{\mathcal{K}\dagger}e^{-T}H_N \approx \langle 0| Y^{\mathcal{K}\dagger}e^{-T}E^{\mathcal{K}}, \tag{3.15}$$

just as the right-hand eigenvectors, C, yield the projection of the full-space right-hand eigenfunction into the reduced space,

$$H_N\Omega^{\mathcal{K}}e^T |0\rangle \approx E^{\mathcal{K}}\Omega^{\mathcal{K}}e^T |0\rangle . \tag{3.16}$$

It should be noted that, since the untransformed H is a Hermitian operator, its right- and left- hand eigenfunctions are of course merely the transpose of one other:

$$\begin{aligned} H |R_i\rangle &= E_i |R_i\rangle \\ \langle L_i| H &= \langle L_i| E_i \\ \langle L_i| &= \{|R_i\rangle\}^\dagger. \end{aligned}$$

Up to this point, there has not been much attention paid to the T and $\Omega^{\mathcal{K}}/Y^{\mathcal{K}}$ operators actually used in practical calculations. Although it is easy to show that,

in the full expansion of the operators, the left-hand side ground state coupled cluster wavefunction and the transpose of the right-hand side wavefunction are identical up to a normalization constant,

$$\langle 0|\,(1+\Lambda)e^{-T} \;=\; \langle 0|\,e^{T^\dagger}e^{T}\,|0\rangle^{-1}\,\langle 0|\,e^{T^\dagger},$$

qualitative differences between the two wavefunctions are apparent in the usual CCSD approximation (John Stanton, private communication), because of the truncation in the operator space.

3.4 The Ionization Energy Equations

In an ionization potential problem, the reference state $|0\rangle$ is an N-particle function, whereas the solution $\Omega^{\mathcal{K}}|0\rangle$ is an $(N-1)$ particle function. The operator $\Omega^{\mathcal{K}}$ must therefore contain terms which annihilate on electron in addition to any excitation they might also perform:

$$\Omega^{\mathcal{K}} \;=\; C_1^{\mathcal{K}} + C_2^{\mathcal{K}} + \cdots \tag{3.17}$$

$$\;=\; \sum_i c_i^{\mathcal{K}} i + \frac{1}{2}\sum_{ija} c_{i\;j}^{\mathcal{K}a}\, i a^\dagger j + \cdots \tag{3.18}$$

$$|\mathcal{K}\rangle = \Omega^{\mathcal{K}}|0\rangle \;=\; \sum_i c_i^{\mathcal{K}} \left|\, {}_i \right\rangle + \frac{1}{2}\sum_{ija} c_{i\;j}^{\mathcal{K}a} \left|\, {}^{a}_{i\;j} \right\rangle . \tag{3.19}$$

The IP coefficients $c_i^{\mathcal{K}}$, $c_{i\;j}^{\mathcal{K}a}$ are indexed by $\mathcal{K}$ for convenience. The similarity of this notation to that for the coupled-cluster amplitudes t_i^a and t_{ij}^{ab} implies that an electron is being excited out of orbital i and into $\mathcal{K}$, but this $\mathcal{K}$ does not represent one of the reference orbitals. It may be taken to indicate that the electron has been excited into an "unbound orbital," but this interpretation is not important to the solution of

the EOMIP equations. It is important to remember that, when constructing EOMIP equation terms, no contractions may be made to the "free-electron" index.

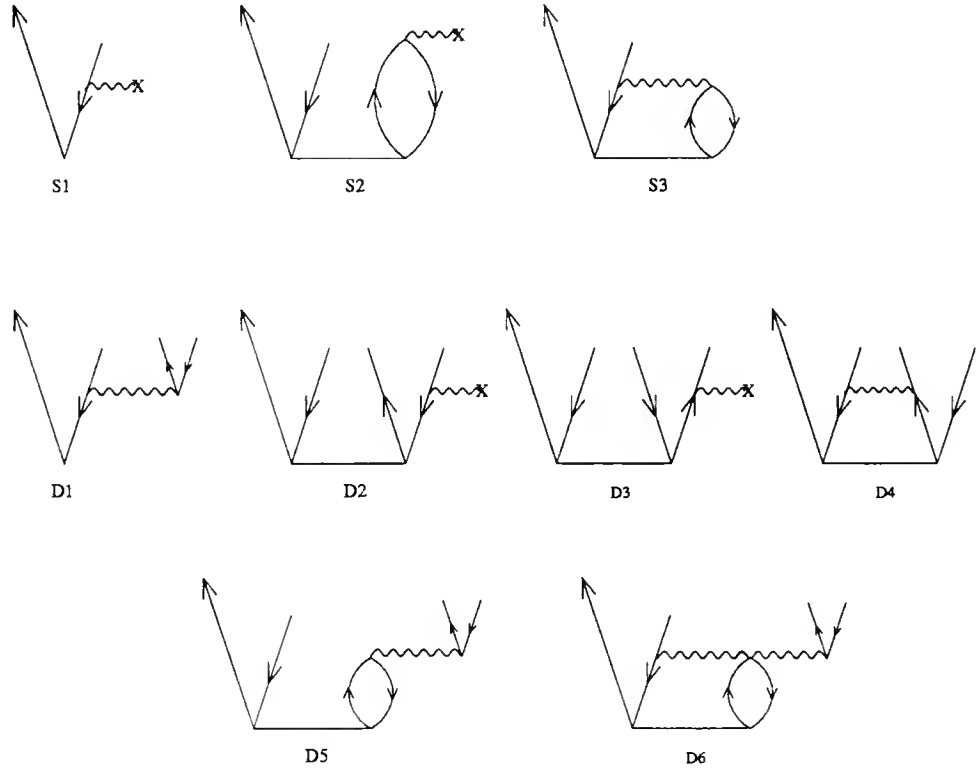

Figure 3.1: The EOMIP equation diagrams.

The EOMIP singles and doubles (EOMIP-SD) equations, for which the terms are shown diagrammatically in figure 3.1, can be written as

$$\begin{aligned}(\text{SINGLES})\omega^{\mathcal{K}} c_i^{\mathcal{K}} &= -\sum_n \langle n|\,\bar{f}\,|i\rangle\, c_n^{\mathcal{K}} + \sum_{na} \langle n|\,\bar{f}\,|a\rangle\, c_{i\,n}^{\mathcal{K}a} \\ &\quad -\frac{1}{2}\sum_{nma} c_{n\,m}^{\mathcal{K}a} \left\langle nm\bar{||}ia\right\rangle \end{aligned} \tag{3.20}$$

$$\begin{aligned}(\text{DOUBLES})\omega^{\mathcal{K}} c_{i\,j}^{\mathcal{K}a} &= -\sum_n \left\langle na\bar{||}ij\right\rangle c_n^{\mathcal{K}} - \sum_n \left(\langle n|\,\bar{f}\,|i\rangle\, c_{n\,j}^{\mathcal{K}a} - \langle n|\,\bar{f}\,|j\rangle\, c_{n\,i}^{\mathcal{K}a}\right) \\ &\quad + \sum_b \langle a|\,\bar{f}\,|B\rangle\, c_{i\,j}^{\mathcal{K}b} + \frac{1}{2}\sum_{nm} \left\langle nm\bar{||}ij\right\rangle c_{n\,m}^{\mathcal{K}a} \\ &\quad + \sum_{nb} \left(\left\langle na\bar{||}bj\right\rangle c_{i\,n}^{\mathcal{K}b} - \left\langle na\bar{||}bi\right\rangle c_{j\,n}^{\mathcal{K}b}\right) \end{aligned}$$

$$-\frac{1}{2}\sum_{nmb}\left(\sum_{e}\langle nm||be\rangle\, t_{ij}^{ea}\right)c_{n\,m}^{\mathcal{K}b}, \tag{3.21}$$

Where the notations $\bar{f}$ and $\left\langle\cdots\bar{||}\cdots\right\rangle$ indicated, respectively, one- and two-body $\bar{H}$ elements. The final term of the doubles equation involves the 3-electron $\bar{H}_N$ term $\left\langle nma|\bar{H}|ijb\right\rangle$ (figure 2.2). These equations form an eigenvalue problem which may be solved by any number of diagonalization procedures.

3.5 The EOMIP Wavefunction

The EOMIP-SD wavefunction expressed in equation 3.19 is an eigenfunction of the $\bar{H}_N$ operator projected into the reduced EOMIP-SD space. The full wavefunction, $e^T\Omega^{\mathcal{K}}\,|0\rangle$, is an approximation to an eigenfunction of H, and can be written

$$\begin{aligned}
|\mathcal{K}_{CC}\rangle \;=\; & \sum_i c_i^{\mathcal{K}}\left|{}_i\right\rangle + \left(\frac{1}{2}\sum_{ija} c_{i\;j}^{\mathcal{K}a} + P(ij)\sum_{ija} c_i^{\mathcal{K}}t_j^a\right)\left|{}^{a}_{i\,j}\right\rangle \\
& + \frac{1}{2}\left(P(i/jk)\sum_{ijkab} c_i^{\mathcal{K}}\left(t_{jk}^{ab} + (t_j^a t_k^b - t_k^a t_j^b)\right) + P(ij/k)P(ab)\sum_{ijkab} c_{i\;j}^{\mathcal{K}a}t_k^b\right)\left|{}^{ab}_{i\,jk}\right\rangle \\
& + \frac{1}{2}\left(P(i/j/kl)P(a/bc)\sum_{ijklabc} c_i^{\mathcal{K}}t_j^a t_{kl}^{bc} + \frac{1}{3}P(ijkl)P(abc)\sum_{ijklabc} c_i^{\mathcal{K}}t_j^a t_k^b t_l^c\right. \\
& \left. + P(ij/kl)P(a/bc)\sum_{ijklabc} c_{i\;j}^{\mathcal{K}a}\left(t_{kl}^{bc} + (t_j^a t_k^b - t_k^a t_j^b)\right)\right)\left|{}^{abc}_{i\,jkl}\right\rangle \;+\; \cdots
\end{aligned} \tag{3.22}$$

CHAPTER 4

THE FOCK-SPACE COUPLED-CLUSTER METHOD

4.1 Fock-Space Theory

The Fock-space coupled-cluster method (FSCC) uses an exponential operator to describe electron attached, electron-detached, and excited states relative to one single-determinant reference. Like EOMIP, it gives direct differences between the correlated reference energy and the energy of the calculated state. The FSCC approaches to the calculation of single electron ionizations and attachments are formally equivalent to the EOMIP approaches to the same, as will be demonstrated for the IP case in section 4.2. The Fock space coupled-cluster method is based upon a valence universal operator Ω that, when acting upon the appropriate model space, yields the desired wavefunction(s). If we begin with a single determinant function, such as a Hartree-Fock wavefunction, a *model space* can be defined by annihilating n electrons from occupied orbitals (also referred to as creating holes) and creating m electrons in virtual (unoccupied) orbitals (also referred to as creating particles). This is called a rank (m, n) model space, one with *particle-hole rank* (m, n). The rank (m, n) part of the problem is also referred to as the (m, n) *sector*. For example, the usual coupled-cluster problem has particle-hole rank $(0, 0)$, while the single electron detachment

problem is of rank $(0,1)$. An *active space* of occupied and virtual orbitals is chosen in which electrons can be created and annihilated to produce model space determinants.

The operator Ω is defined by $\left\{e^S\right\}$, where the braces, $\{\}$, denote *normal ordering.* Normal ordering of a product of operators prevents the operators from contracting with, or operating on, each other. For this reason, model spaces of different hole-particle ranks are decoupled, and the solution of the equations is hierarchical, starting with the usual coupled-cluster equations, and building solutions to sectors with successively higher rank (the sum of m and n) upon the solutions of lower sectors.

The valence universal operator Ω can be written

$$\Omega_{tot} = \left\{e^X\right\} \tag{4.1}$$

where $X = S^{(0,0)} + S^{(0,1)} + S^{(1,0)} + \cdots$. Because of the properties of normal ordered products, Ω_{tot} can be written as a product of terms

$$\begin{aligned} \Omega_{tot} &= \left\{\Omega^{(0,0)} * \Omega^{(0,1)} * \cdots\right\} \\ \text{where } \Omega^{(m,n)} &= \left\{\exp(S^{(m,n)})\right\} = 1 + S^{(m,n)} + \frac{1}{2}\left\{(S^{(m,n)})^2\right\} + \cdots. \end{aligned} \tag{4.2}$$

$S^{(m,n)}$ is always chosen so that, when acting on the (m,n) model space $P^{(m,n)}$, it does not cause scattering between model determinants. That is, $P^{(m,n)}S^{(m,n)}P^{(m,n)} = 0$, or $S^{(m,n)}P^{(m,n)} = Q^{(m,n)}S^{(m,n)}P^{(m,n)}$, where $Q^{(m,n)}$ is the complement to $P^{(m,n)}$. The $(0,0)$ sector, as was noted above, corresponds to the usual single-reference coupled-cluster problem. The operator $\exp(S^{(0,0)})$ is identical to the usual e^T operator encountered in the coupled-cluster equations. Because T-to-T contractions are impossible, imposing normal order does not change the operator.

The operator Ω_{tot} has an inverse,

$$\Omega_{tot}{}^{-1} = \left\{ \Omega^{(0,0)^{-1}} * \Omega^{(0,1)^{-1}} * \cdots \right\}. \tag{4.3}$$

In the $(0,0)$ case this is $\Omega^{(0,0)} = e^{-T}$ but in the higher sectors, the form becomes more complicated because of the normal-ordering constraint. These terms can easily be derived using a Taylor series expansion of the inverse of $\Omega^{(m,n)}$, or by other approaches, but are not important to the following discussion.

To begin, an N–electron single determinant reference $|0\rangle$ is chosen, which may be an SCF wavefunction. The reference wavefunction defines a complement, Q, which contains all N–electron functions orthogonal to the reference. The single-reference coupled-cluster problem is solved, yielding $\bar{H}_N$, which is an *effective Hamiltonian* for the $(0,0)$ sector. This is a canonical (eigenvalue-preserving) transformation of the Hamiltonian, chosen so that it is the eigen-operator of the reference function, yielding the desired coupled-cluster energy (E_{CC}) as its eigenvalue.

The coupled-cluster equations can now be expressed in a compact form.

$$\langle Q | \bar{H}_N | 0 \rangle = 0, \tag{4.4}$$

and the equations are solved for the T amplitudes.

In further discussions, the following quantity will be useful:

$$\Omega_{old}^{(m,n)} = \left\{ \prod_{0<l+k} \Omega^{(l,k)} \Omega^{(m,n)^{-1}} \right\} \tag{4.5}$$

While $\Omega_{old}^{(m,n)}$ contains all the contributions from all the Ω's of different sectors, the projection of equations by $P^{(m,n)}$ and $Q^{(m,n)}$ limits the contributions to the energy and wavefunction expressions to only certain lower-ranked sectors. The $(0,0)$ sector

contributes to all higher-ranked sectors, and is the only one contributing to the $(0,1)$ and $(1,0)$ sectors. The $(1,1)$ sector has contributions from all lower-ranked sectors, while the $(0,2)$ has contributions only from $(0,1)$ and $(0,0)$.

For a given sector, an effective Hamiltonian is also defined, $H_{eff}^{(m,n)}$, defined

$$H_{eff}^{(m,n)} = \Omega^{(m,n)^{-1}} \bar{H}_N \Omega_{old} \Omega^{(m,n)}, \tag{4.6}$$

which will prove useful in the following discussion. Now, with the model space and the Ω operator defined, we can begin to define the (m,n) problem.

While $H_{eff}^{(0,0)} P^{0,0} = E_{CC} P^{(0,0)}$ works fine for the one-dimensional problem, it is clear that something more is needed to deal with the multi-determinant model space. It is necessary to introduce $C^{(m,n)}$, or C for short. The matrix C causes a linear transformation of the model-space functions. If $P^{(m,n)}$ includes a set of functions $|p_i\rangle$, then a linear transformation of these functions results in another set

$$\mathcal{K}^{(m,n)} = P^{(m,n)} C_{\mathcal{K}}^{(m,n)}$$

or

$$|p_{\mathcal{K}}\rangle^{(m,n)} = \sum_i |p_i\rangle^{(m,n)} C_{\mathcal{K}i}^{(m,n)}. \tag{4.7}$$

The $\mathcal{K}^{\text{th}}$ wavefunction of the sector then is defined to be $\Omega_{tot} C_{\mathcal{K}}^{(m,n)} P^{(m,n)}$ and should satisfy

$$H \Omega_{tot} P^{(m,n)} C_{\mathcal{K}}^{(m,n)} = \Omega_{tot} P^{(m,n)} C_{\mathcal{K}}^{(m,n)} \omega_{\mathcal{K}}^{(m,n)}.$$

If the full C matrix is used, the result is

$$H \Omega_{tot} P^{(m,n)} C^{(m,n)} = \Omega_{tot} P^{(m,n)} C^{(m,n)} \mathcal{W}^{(m,n)}, \tag{4.8}$$

where $\mathcal{W}^{(m,n)}$ is a diagonal matrix containing the eigenvalues.

This equation, like the analogous $(0,0)$ equation, can be put into an "H_{eff}" form,

$$H_{eff}^{(m,n)} P^{(m,n)} = \Omega_{tot}{}^{-1} \bar{H}_N \Omega_{tot} P^{(m,n)}, \tag{4.9}$$

where

$$H_{eff}^{(m,n)} P^{(m,n)} C^{(m,n)} = \Omega_{tot}{}^{-1} \Omega_{tot} P^{(m,n)} C^{(m,n)} \mathcal{W}^{(m,n)}.$$

H_{eff} has the property

$$\begin{aligned} Q^{(m,n)} H_{eff}^{(m,n)} P^{(m,n)} C^{(m,n)} &= Q^{(m,n)} P^{(m,n)} C^{(m,n)} \mathcal{W}^{(m,n)} \\ &= 0 \end{aligned} \tag{4.10}$$

This fundamental result, unfortunately, is not nearly as useful as the similar equation from the $(0,0)$ sector is in computing the solution to the coupled-cluster equations. The complicated form of Ω^{-1} makes for a large number of algebraically messy and computationally difficult terms in the expression $Q^{(m,n)} H_{eff} C P^{(m,n)}$. Upon convergence of Ω,

$$H_{eff}^{(m,n)} P^{(m,n)} C^{(m,n)} = (P^{(m,n)} + Q^{(m,n)}) H_{eff}^{(m,n)} P^{(m,n)} C^{(m,n)} = P^{(m,n)} H_{eff} P^{(m,n)} C^{(m,n)}. \tag{4.11}$$

Since the matrix C only mixes the $P^{(m,n)}$ functions among themselves, and cannot promote $P^{(m,n)}$ functions to the $Q^{(m,n)}$ space, it is equally valid to say

$$H_{eff}^{(m,n)} P^{(m,n)} = P^{(m,n)} H_{eff}^{(m,n)} P^{(m,n)}. \tag{4.12}$$

Combining this with the identity $\bar{H}_N \Omega = \Omega H_{eff}$, we arrive at an algebraically and computationally more tractable form, $Q^{(m,n)} \left(\bar{H}_N \Omega - \Omega P^{(m,n)} H_{eff} \right) P^{(m,n)}$. Once Ω has been determined from the solution of this equation, $P^{(m,n)} H_{eff}^{(m,n)} P^{(m,n)}$ can be diagonalized to yield the $C_i^{\mathcal{K}}$ and the energies $\omega_{\mathcal{K}}^{(m,n)}$.

$$H_{ij}^{eff} = -\langle i|\,\bar{f}\,|j\rangle + \sum_{m} S_{m}^{i}\,\langle m|\,\bar{f}\,|j\rangle - \sum_{me} S_{jm}^{ie}\,\langle m|\,\bar{f}\,|e\rangle + \sum_{mne} S_{mn}^{ie}\left\langle mn\bar{||}je\right\rangle. \tag{4.13}$$

$$0 = \langle i|\,\bar{f}\,|j\rangle - \sum_{m} S_{m}^{i}\,\langle m|\,\bar{f}\,|j\rangle + \sum_{me} S_{jm}^{ie}\,\langle m|\,\bar{f}\,|e\rangle - \frac{1}{2}\sum_{mne} S_{mn}^{ie}\left\langle mn\bar{||}je\right\rangle + \sum_{m} S_{j}^{m} H_{im}^{eff} \tag{4.14}$$

$$0 = \left\langle ia\bar{||}jk\right\rangle - \sum_{m} S_{m}^{i}\left\langle ma\bar{||}jk\right\rangle - P_{(jk)}\sum_{m} S_{jm}^{ia}\,\langle m|\,\bar{f}\,|k\rangle + \sum_{e} S_{jk}^{ie}\,\langle a|\,\bar{f}\,|e\rangle - P_{(jk)}\sum_{me} S_{jk}^{ie}\left\langle ma\bar{||}ej\right\rangle + \frac{1}{2}\sum_{mn} S_{mn}^{ia}\left\langle mn\bar{||}jk\right\rangle - \frac{1}{2}\sum_{mnbc} S_{mn}^{ib}\,t_{ij}^{ca}\langle mn||bc\rangle - \sum_{m} S_{jk}^{ma} H_{im}^{eff} \tag{4.15}$$

An important feature of these equations is that the ionization energies are invariant to the choice of active space. This is because the S_1 amplitudes and the C coefficients are serving essentially the same purpose; they mix the model space functions. If all occupied orbitals are made active, there will not be any S_1 amplitudes, and an $n \times n$ matrix of C coefficients. If the number of active orbitals is decreased, there will be a decrease in the number of C coefficients and a corresponding increase in the number of S_1 amplitudes. In fact, it is easy to show that there is a simple relationship between C and S for the two cases. The proof of the invariance of the energy to the choice of active space can be found in appendix A

4.2 Comparison of EOM to FSCC

When FSCC-IP and EOMIP calculations are performed using the same active space—the complete active space, consisting of ionizations from all occupied orbitals—certain correspondences can be shown.

4.2.1 Definitions

- $\Omega^{(0,0)}$ is the usual CC wave reaction operator e^T.
- $P^{(0,1)}$, written P for convenience, is a projector over the model space, which contains all $(N-1)$ - electron determinants obtained by annihilating a single occupied electron.
- $Q^{(0,1)}$, or Q, is the complement to P $(\mathbf{1}-P)$ in the $(N-1)$ - electron space.
- $\Omega^{(0,1)} = \{\exp(S)\} = 1 + S + \frac{1}{2}\{S^2\} + \cdots$ is the solution to the FSCC equation for the (0,1) (IP) sector.
- ${\Omega^{(0,1)}}^{-1}$ satisfies ${\Omega^{(0,1)}}^{-1}\Omega^{(0,1)}P = \Omega^{(0,1)}{\Omega^{(0,1)}}^{-1}P = P$.
- $\bar{\bar{H}} = {\Omega^{(0,1)}}^{-1}{\Omega^{(0,0)}}^{-1}H\Omega^{(0,0)}\Omega^{(0,1)} = {\Omega^{(0,1)}}^{-1}\bar{H}\Omega^{(0,1)}$

4.2.2 FSCC Method

The Fock-space method defines a model space consisting of several $(N-1)$ electron determinants and a projector $P \equiv P^{(0,1)}$ over this space. An electron-detached wavefunction is defined as

$$\Omega^{(0,1)} |\mathcal{K}\rangle \equiv \Omega^{(0,1)} \mathcal{C}^{\mathcal{K}} |0\rangle = \Omega^{(0,1)} \sum_i C_i^{\mathcal{K}} i |0\rangle .$$

P can be represented as a sum over these $|\mathcal{K}\rangle$ states

$$P = \sum_{\mathcal{K}} |\mathcal{K}\rangle \langle \mathcal{K}|\mathcal{K}\rangle^{-\frac{1}{2}} \langle \mathcal{K}| .$$

The $\Omega^{(0,1)}$ and $\mathcal{C}^{\mathcal{K}}$ operators are defined so that

$$\bar{H}\Omega^{(0,1)} |\mathcal{K}\rangle = E^{\mathcal{K}} \Omega^{(0,1)} |\mathcal{K}\rangle , \tag{4.16}$$

which leads to a useful definition for H_{eff},

$$H_{eff} P = \Omega^{(0,1)^{-1}} \bar{H} \Omega^{(0,1)} P; \tag{4.17}$$

$$\begin{aligned} H_{eff} |\mathcal{K}\rangle &= \Omega^{(0,1)^{-1}} \left(\bar{H} - E_{CC}\right) \Omega^{(0,1)} |\mathcal{K}\rangle = \left(E^{\mathcal{K}} - E_{CC}\right) |\mathcal{K}\rangle \\ &= \omega^{\mathcal{K}} |\mathcal{K}\rangle , \end{aligned} \tag{4.18}$$

which has the property

$$Q H_{eff} |\mathcal{K}\rangle = Q E^{\mathcal{K}} |\mathcal{K}\rangle = 0 \tag{4.19}$$

$$H_{eff} = \Omega^{(0,1)^{-1}} \bar{H} \Omega^{(0,1)} P = P \Omega^{(0,1)^{-1}} \bar{H} \Omega^{(0,1)} P. \tag{4.20}$$

H_{eff} acting on any representation of the model space can be diagonalized to yield the entire spectrum of ionization energies $\omega^{\mathcal{K}}$

$$C^{-1} H_{eff} C |0\rangle = \omega |0\rangle \tag{4.21}$$

This operator eigenvalue equation is easily replaced by the matrix eigenvalue equation,

$$\mathrm{C}^{-1}\mathrm{H}_{\mathit{eff}}\mathrm{C} = \boldsymbol{\omega}$$

4.2.3 EOM Method

The diagonalization of $\bar{H}$ yields coefficients C and eigenvalues ω. The space of eigenvalues and eigenvectors, and hence the $\bar{H}$ matrix itself, can be partitioned into principal and shake-up portions. The principal IPs correspond to the solutions of the Fock Space method and can be labeled as the P portion of the solution space.

$$\begin{pmatrix} \bar{H}_{PP} & \bar{H}_{PQ} \\ \bar{H}_{QP} & \bar{H}_{QQ} \end{pmatrix} \begin{pmatrix} C_{PP} & C_{PQ} \\ C_{QP} & C_{QQ} \end{pmatrix} = \begin{pmatrix} C_{PP} & C_{PQ} \\ C_{QP} & C_{QQ} \end{pmatrix} \begin{pmatrix} \omega_P & 0 \\ 0 & \omega_Q \end{pmatrix}$$

or

$$\begin{pmatrix} \bar{H}_{PP}C_{PP} + \bar{H}_{PQ}C_{QP} & \bar{H}_{PP}C_{PQ} + \bar{H}_{PQ}C_{QQ} \\ \bar{H}_{QP}C_{PP} + \bar{H}_{QQ}C_{QP} & \bar{H}_{QP}C_{PQ} + \bar{H}_{QQ}C_{QQ} \end{pmatrix} = \begin{pmatrix} C_{PP}\omega_P & C_{PQ}\omega_Q \\ C_{QP}\omega_P & C_{QQ}\omega_Q \end{pmatrix}.$$

The P–P portion of this equation can be rewritten as

$$C_{PP}^{-1}\left(\bar{H}_{PP} + \bar{H}_{PQ}C_{QP}C_{PP}^{-1}\right)C_{PP} = \omega_P.$$

Since ω_P has been chosen to match the solutions to the FS equations, there is quite naturally an identification:

$$\mathrm{C}^{-1}\mathrm{H}_{\mathit{eff}}\mathrm{C} = \omega_P = \mathrm{C}_{\mathrm{PP}}^{-1}\left(\bar{\mathrm{H}}_{\mathrm{PP}} + \bar{\mathrm{H}}_{\mathrm{PQ}}\mathrm{C}_{\mathrm{QP}}\mathrm{C}_{\mathrm{PP}}^{-1}\right)\mathrm{C}_{\mathrm{PP}},$$

which will lead to

$$\mathrm{H}_{\mathit{eff}} = \left(\bar{\mathrm{H}}_{\mathrm{PP}} + \bar{\mathrm{H}}_{\mathrm{PQ}}\mathrm{C}_{\mathrm{QP}}\mathrm{C}_{\mathrm{PP}}^{-1}\right)$$

as long as the model functions chosen for both methods are identical.

4.2.4 Comparison

The eigenvalues and eigenvectors obtained from the diagonalization of the effective Hamiltonian H_{eff} are the (PP) blocks of the respective matrices obtained from the diagonalization of the full matrix $\bar{H}$

$$H_{eff} = \bar{H}_{PP} + \left(\bar{H}S\right)_{PP,c} \tag{4.22}$$

$$= \bar{H}_{PP} + (\bar{H}_{PQ}S)_c \tag{4.23}$$

$$= \bar{H}_{PP} + \bar{H}_{PQ}C_{QP}C_{PP}^{-1} \tag{4.24}$$

$$S_{QP} = C_{QP}C_{PP}^{-1} \tag{4.25}$$

$$C_{QP} = S_{QP}C_{PP} \tag{4.26}$$

This means that the eigenvectors of principal IP states obtained from an EOM calculation can be directly compared to those from the FSCC calculation of the same states. The C_{PP} vectors obtained in both examples are identical.

CHAPTER 5

THE ELECTRON PROPAGATOR

The electron propagator[19], also called the one electron Green's function, was one of the first improvements made on Koopmans' theorem for the calculation of IPs and EAs [20], and is still in use. Propagator methods are direct methods, yielding energy differences rather than state energies. Unlike the methods described so far, which are based upon correlated wavefunctions for the reference and final states, most Green's function methods provide transition properties rather than wavefunctions for the final states. And it is feasible to begin a correlated calculation of ionization energies with an uncorrelated, single determinant reference, if a suitably large manifold of annihilation/excitation operators, such as those used in the the construction of the EOMIP wavefunction, is chosen. However, the symmetric form of the electron propagator requires that the manifold include, in addition to IP-type operators, i and $a^\dagger ij$, the EA-type operators $a^\dagger$ and $a^\dagger b^\dagger i$ be included as well. Energy differences will correspond to the difference between a correlated reference and a correlated final state, neither of which wavefunction is, in general, directly constructed.

Despite these apparent differences, there are similarities between the results of electron propagator and CI calculations. More recent formal developments have bridged the theoretical gap between Green's function and coupled-cluster methods,

and propagator researchers have independently arrived at equations which are identical to those derived from coupled-cluster EOM theory.

The general form of Green's function in the energy representation is

$$\langle\langle A;B\rangle\rangle_E = \lim_{\eta\to 0_+}\left\{\sum_k \frac{\pm\langle 0|\,A\,|k\rangle\langle k|\,B\,|0\rangle}{E_0 - E_k + E + i\eta} + \sum_k \frac{\langle 0|\,B\,|k\rangle\langle k|\,A\,|0\rangle}{E_k - E_0 + E - i\eta}\right\}, \tag{5.1}$$

where the states $|k\rangle$ are eigenfunctions of the full Hamiltonian, H. The electron propagator is a matrix G of elements

$$G_{pq} = \lim_{\eta\to 0_+}\left\{\sum_{k_{N-1}} \frac{\langle 0_N|\,p^\dagger\,|k_{N-1}\rangle\langle k_{N-1}|\,q\,|0\rangle}{E_0 - E_{k_{N-1}} + E + i\eta} + \sum_{k_{N+1}} \frac{\langle 0|\,q\,|k_{N+1}\rangle\langle k_{N+1}|\,p^\dagger\,|0\rangle}{E_{k_{N+1}} - E_0 + E - i\eta}\right\}, \tag{5.2}$$

where the $|k_{N-1}\rangle$ and $|k_{N+1}\rangle$ functions are, respectively, electron-detached and electron-attached functions. The poles of this expression occur at $E_0 - E_{k_{N-1}} + E = 0$ and $E_{k_{N+1}} - E_0 + E = 0$; the residue at a particular pole yields the transition moment $\langle 0_N|\,p^\dagger\,|k_{N-1}\rangle\langle k_{N-1}|\,q\,|0\rangle$ or $\langle 0|\,q\,|k_{N+1}\rangle\langle k_{N+1}|\,p^\dagger\,|0\rangle$. This form of the Green's function is not directly useful for obtaining energies or wavefunctions, so another approach is used which calculates the energy differences and transition moments directly, without first determining $|0\rangle$, $|k\rangle$, or any of the state energies.

5.1 Superoperator Expression of the Electron Propagator

Propagator equations are most compactly written in terms of superoperator notation. For any operator C, the superoperator $\hat{C}$ acts on other operators, and a new "binary superoperator product" is defined between any two operators:

$$\hat{C}D \;=\; [C,D]_- = CD - DC \tag{5.3}$$

$$\hat{1}D \equiv D \tag{5.4}$$

$$(C|D) \equiv \langle 0|\, C^\dagger D\, |0\rangle \mp \langle 0|\, DC^\dagger\, |0\rangle\,, \tag{5.5}$$

where the sign in equation 5.5 depends on the number of creation and annihilation operators in C and D. In this notation, the Green's function can be written as

$$\langle\langle A;B\rangle\rangle_E = \left(B^\dagger|(E\hat{1}+\hat{H})^{-1}A\right). \tag{5.6}$$

Inserting the spectral resolution of the identity,

$$\hat{1} = \left|\mathbf{F}^\dagger\right)\left(\mathbf{F}^\dagger|\mathbf{F}^\dagger\right)^{-1}\left(\mathbf{F}^\dagger\right| \tag{5.7}$$

$$= \sum_{kl}\left|F^\dagger\right)\left(\mathbf{F}^\dagger|\mathbf{F}^\dagger\right)^{-1}_{kl}\left(F_l^\dagger\right|, \tag{5.8}$$

into the expression for the propagator gives

$$\begin{aligned}\langle\langle A;B\rangle\rangle_E &= \left(B^\dagger\right|\left(E\hat{1}+\hat{H}\right)^{-1}|A) \\ &= \left(B^\dagger|\mathbf{F}^\dagger\right)\left(\mathbf{F}^\dagger|\mathbf{F}^\dagger\right)^{-1}\left(\mathbf{F}^\dagger\right|\left(E\hat{1}+\hat{H}\right)^{-1}\left|\mathbf{F}^\dagger\right)\left(\mathbf{F}^\dagger|\mathbf{F}^\dagger\right)^{-1}\left(\mathbf{F}^\dagger|A\right) \\ &= \left(B^\dagger|\mathbf{F}^\dagger\right)\left(\mathbf{F}^\dagger\right|\left(E\hat{1}+\hat{H}\right)\left|\mathbf{F}^\dagger\right)^{-1}\left(\mathbf{F}^\dagger|A\right),\end{aligned} \tag{5.9}$$

which are the working equations from which propagator approximations are derived. The expression

$$\left(E\hat{1}+\hat{H}\right)^{-1}$$

is called the superoperator resolvent. The poles and residues of the resolvent give the energies and transition moments.

For the one-electron propagator, propagator matrix elements become

$$\begin{aligned}G_{pq}(E) &= \left\langle\left\langle p^\dagger;q\right\rangle\right\rangle_E = (p|\left(E\hat{1}+\hat{H}\right)^{-1}\left|q^\dagger\right) \\ &= (p|\mathbf{F})\left(\mathbf{F}|\left(E\hat{1}+\hat{H}\right)\mathbf{F}\right)^{-1}(\mathbf{F}|q).\end{aligned} \tag{5.10}$$

The manifold **F** can be separated into **a**, which contains all the one-electron operators, p and q, and its orthogonal complement **f**, which contains all higher odd-electron operators. Because the **f** portion of the manifold is orthogonal to the p and q operators, only the **a** - **a** projected portion of $\left(\mathbf{F}\right|\left(E\hat{1}+\hat{H}\right)\left|\mathbf{F}\right)^{-1}$ contributes. This portion can be written as

$$\begin{aligned} G^{-1}(E) &= \left(\mathbf{a}\right|\left(E\hat{1}+\hat{H}\right)\left|\mathbf{a}\right) - \left(\mathbf{a}\right|\left(E\hat{1}+\hat{H}\right)\left|\mathbf{f}\right)\left(\mathbf{f}\right|\left(E\hat{1}+\hat{H}\right)\left|\mathbf{f}\right)^{-1}\left(\mathbf{f}\right|\left(E\hat{1}+\hat{H}\right)\left|\mathbf{a}\right) \\ &= E\mathbf{1} - \left(\mathbf{a}|\hat{H}|\mathbf{a}\right) - \left(\mathbf{a}|\hat{H}|\mathbf{f}\right)\left(\mathbf{f}\right|\left(E\hat{1}+\hat{H}\right)\left|\mathbf{f}\right)^{-1}\left(\mathbf{f}|\hat{H}|\mathbf{a}\right) \end{aligned} \tag{5.11}$$

5.2 The Dyson Equation

The Dyson equation is an expression of the difference between the inverses of the propagator $G^{-1}(E)$ and the zeroth order propagator $G_0^{-1}(E)$, the Green's function in terms of the zeroth order Hamiltonian, H_0.

$$G^{-1}(E) = G_0^{-1}(E) - \Sigma(E) \tag{5.12}$$

where

$$G_0^{-1}(E)_{pq} = (E-\epsilon_p)\delta_{pq} \tag{5.13}$$

$$\Sigma(E) = \left(\mathbf{a}|\hat{\mathbf{H}}\mathbf{a}\right)_{\text{corr}} + \left(\mathbf{a}|\hat{H}\mathbf{f}\right)\left(\mathbf{f}\right|\left(E\hat{1}+\hat{H}\right)\mathbf{f}\Big)^{-1}\left(\mathbf{f}|\hat{H}\mathbf{a}\right) \tag{5.14}$$

$$\left(p|\hat{H}|q\right)_{\text{corr}} = \left(p|\hat{H}|q\right) - \epsilon_p\delta_{pq}.$$

In this formulation, $\Sigma(E)$, the self-energy, is the correction to the Koopmans' theorem approximation to the propagator given by $G_0(E)$. The self energy is itself divided into two parts, the energy dependent part $\Sigma'(E)$ and the constant part $\Sigma(\infty)$

$$\Sigma(E) = \Sigma(\infty) + \Sigma'(E) \tag{5.15}$$

$$\begin{aligned}\Sigma(\infty) &= \left(\mathbf{a}|\hat{H}\mathbf{a}\right)_{\text{corr}} \\ \Sigma'(E) &= \left(\mathbf{a}|\hat{H}\mathbf{f}\right)\left(\mathbf{f}|\left(E\hat{1}+\hat{H}\right)\mathbf{f}\right)^{-1}\left(\mathbf{f}|\hat{H}\mathbf{a}\right).\end{aligned} \tag{5.16}$$

A great many approaches to the electron propagator are concerned with successive orders of approximation to the energy-dependent part of the self energy[21],[22], in combination with appropriate choices for the reference state $|0\rangle$[23], and the most important portions of the manifold $\mathbf{F}$.

5.3 Non-Dyson Equation Approaches

The development, in the world of CI theory, of the Davidson procedure for convergence of selected roots of a large matrix[24] spurred Baker and Pickup to develop a method for extracting the roots of the one electron propagator matrix rather than using self-energy expressions[25]. More recently, Ortiz has experimented with the use of a highly-correlated reference based on the coupled cluster wavefunction [26], a process referred to as renormalization of the ground state, in a procedure which maintains the symmetry of the electron propagator matrix. Snijders and Nooijen [27], using an RSPT analysis of the diagrams contained in the one electron propagator, showed that they can be represented using the coupled-cluster wavefunction as the reference, with two major consequences. The symmetry of the resulting matrices is broken, and the IP-type manifold is decoupled from the EA-type manifold, decreasing the dimension

of the manifold space to less than half for the IP case when typical modern basis sets are used. The resulting equations are identical to the CCEOM equations.

One other Green's function-based approach which gives results identical to the EOM approach is the coupled-cluster response function approach developed by Koch and Jørgensen[16]. In this approach, a time dependent formulation is used to derive expressions for the linear and quadratic response functions of the coupled-cluster equations. The coupled-cluster Jacobian (the first derivative of the coupled-cluster equations with respect to the cluster amplitudes) used in their work is identical to the coupled-cluster EOM matrix. Transition matrix elements between the ground and excited states and between two excited states are derived from residuals of the quadratic response function.

CHAPTER 6

OTHER METHODS FOR IONIZATION CALCULATIONS

The many approaches to calculating ionization energies can be broken down into two main categories – *state-by-state* approaches which involve a separate SCF reference and correlated calculation for each state of interest, and *direct* methods which use a single reference (SCF or correlated) as the starting point for calculation of the energy difference between the reference state and several states of interest. State-by-state approaches can use any SCF or correlated (CI, perturbation, or coupled-cluster theory) method in the calculation of differences. Among the direct approaches include two hole–one particle CI[28, 6], the symmetry adapted cluster-CI approach of Nakatsuji[29], the Fock-Space Coupled Cluster approach[10, 13, 30, 14], and one electron propagator approaches[31, 32, 23, 33], as well as the coupled-cluster equation-of-motion approach, which has been derived independently several times, and is known variously as the coupled cluster linear response function[16] and the coupled-cluster Green's function[27] methods.

6.1 State Methods

The conceptually simplest way to consider calculating energy differences is to calculate the individual energies of the states of interest and take the differences. The problems inherent in comparing SCF energies of systems with different spins (as in the common case of the closed-shell singlet neutral reference and the doublet ionized state) are well known and tend to make the SCF energy differences not even qualitatively useful. Configuration interaction, perturbation theory, and coupled-cluster methods may all be applied, and for small molecules which are well-described by a single SCF determinant, any of these methods might give a good result for valence ionizations. There are a few difficulties which can make the problem less straightforward, however. Modern SCF programs usually can be induced to converge on valence ionized states, and the fact that core molecular orbitals are generally well described as a linear combination of core atomic orbitals and do not change much when the occupation changes means that core ionized states can be converged as well. But when an inner-shell ionization is desired, there is no good way to characterize the excited SCF state. SCF programs will quickly collapse back to the valence-ionized state. One remedy for this problem is to use a quasi-restricted Hartree-Fock (QRHF) reference, in which an SCF calculation is performed on suitable reference such as the closed-shell neutral, following which the orbitals are re-occupied and the Fock matrix recalculated. This non-Hartree-Fock reference is then used as the basis for the correlated (typically coupled-cluster) calculation[34].

Because each state is handled as a separate case, there is considerable freedom in the choice of the reference. For approximate correlation methods, poorly chosen orbitals result in a substantial shift in the energy of the state considered. And if the orbitals are chosen well for one state but poorly for another, the lack of balance means the accuracy of the difference will suffer. UHF references lack spin symmetry. ROHF and QRHF references for high-spin states will always be pure spin states, but the orbitals themselves may be unphysical. In some difficult cases, it is a matter of trial and error to determine which set of reference orbitals is best suited to the problem – the size of the correlation corrections for each reference is often the best guide.

One more factor to consider is molecular geometry. Experimentalists may report vertical or adiabatic ionizations, or may be unsure. Proper vertical ionizations can only be approximated from the optimized geometry of the N-electron species, while adiabatic ionizations involve finding the potential energy minimum for each of the $N-1$-electron states.

In most cases, a single-reference approach like CCSD(T), an approximation to the full CCSDT method, is significantly flexible to provide adequate correlation to all of the states in question. For calculations on certain open-shell systems, however, it becomes necessary to consider a multi-determinant reference. For example, the excited states of C_2 accessible from ionization of the C_2^- ion[35, 36] include open-shell singlet states. Attempting single-reference calculations on these states results in significant spin contamination, and the splittings between these and the related triplets (which can be calculated from a single high-spin determinant calculation) are too large to ignore. For such states, the multireference coupled-cluster (MRCC)

method[37, 38] can be used. In this approach, two (or more) determinants serve as the reference function, and an exponential operator (analogous to the single-reference coupled-cluster theory described in chapter 2) is applied to each reference in turn to create the correlated wavefunction. The number of amplitudes required grows as the number of unique determinants used in the reference; a typical application of the theory might require two or four reference determinants. Since higher and higher levels of SRCC theory are required to obtain better spin-projection, approaching a pure-spin result, the MRCC method gives substantial savings in cases where a full triples or even CCSDTQ approach might be required to gain the desired degree of projection.

6.2 Direct Approaches

6.2.1 Two-Hole One-Particle Configuration Interaction

Configuration interaction approaches can also be applied to the direct calculation of a spectrum of ionized states based on a single SCF reference. Martin and Davidson[6, 28] used a 2h1p CI approach in which the CI expansion for each of the cationic states is based on a closed-shell SCF reference. The excitation operators used in creating the ionized wavefunction are identical to those used in the EOM method, but the reference is the SCF wavefunction. The ionized wavefunctions thus may be very different from the corresponding EOMIP wavefunction. Also, the $\omega^{\mathcal{K}}_{\mathrm{2hpCI}}$ energy will be the difference, between the correlated energy of the ionized state and

the SCF energy of the reference state. This means that only the differences between the ionization energies are considered "good", and it is common practice to offset the entire calculated spectrum by a constant energy in order to match one theoretical peak (typically the lowest ionization energy) to its experimental value.

6.2.2 Spin-Adapted Cluster Methods

The Symmetry Adapted Clusters (SAC) method of Nakatsuji[7, 39] is similar in most respects to the CC method presented in this work. The important features of this approach are the explicit spin adaptation of the excitation operators and the projection of the final wavefunction by a spin projection operator. The result, though requiring fewer independent variables, has a much more complicated algorithmic expression, a necessity to customizing the program for each type of spin function, and a proliferation of terms to be coded. As a practical matter, the developer found it necessary to truncate the exponential expansion to no more than quadratic terms. For open shell references, this is not quite equivalent to truncation of the CC equations to T^2 terms as it includes some higher spin-flip terms as a consequence of the spin adaptation.

The SAC- configuration interaction (SAC-CI) method[7, 8] is very much akin to the EOM approach, but using explicitly symmetry-adapted EOM-type operators, and based on a SAC rather than a CC reference, resulting in a slightly different $\bar{H}$, which is further altered by the neglect of certain contributions to $\bar{H}$ elements. In addition,

implementations of SAC-CI have also employed configuration selection procedures similar to those used by CI practitioners to limit the size of the matrices that must be diagonalized, unlike the EOMCC implementation presented here.

6.3 Eclectic Approaches

When the most straightforward methods fail, it is possible to approach a difficult state from an unusual direction. For example, inner valence ionization states can be accessible as excitations from an outer valence ionized reference, or as electron attached states from a di-ionized reference. Bernholdt [40], finding that the structures of the low-lying Σ states of the C_5^+ were difficult to impossible to converge using QRHF at the CCSD level of theory as well as evidence of discontinuities in the $^2\Sigma_u^+$ state, was able to use the FSCC(0,1) approach with the well-behaved, closed-shell C_5 as the starting point, in order to examine portions of the potential energy surfaces of all three ionized states.

CHAPTER 7

COUPLED-CLUSTER LINEAR-RESPONSE THEORY

The formalism developed by Koch and Jørgensen[16] for coupled-cluster linear response functions may be as easily applied to ionization potentials as to excitation energies. All that is required is to construct a perturbation operator capable of causing an "excitation" from the occupied to "free-electron" space, and a new wavefunction of the appropriate form. In the following sections, a linear response theory formalism, based on the time-dependent perurbation theory (TDPT) approach of Koch and Jørgensen, will be developed.

7.1 Perturbation Applied to the CC Hamiltonian

An RSPT approach is used, with the usual coupled-cluster quantities defined as the zeroth-order solutions, and the full wavefunction expanded in terms of corrections to the coupled-cluster T operator. Although there is a single zeroth order expression, a spectrum of solutions to the full Hamiltonian will be sought, the maximum number of which can be determined from the form of the corrections to T. The definitions to be used are:

1. H_{SCF}, the zeroth order approximation to the Hamiltonian, is the usual Fock operator. The perturbation is a first-order correction to the Hamiltonian, V^{IP}. The full Hamiltonian becomes

$$H_{\mathsf{SCF}} + \beta V^{IP}. \tag{7.1}$$

2. The zeroth order wavefunctions and energies are those from the coupled-cluster and Λ solutions;

$$\begin{aligned}
\left|\mathcal{K}^{(0)}\right\rangle &\equiv |0\rangle = \left|CC^0\right\rangle = e^{T_{\mathcal{K}}^{(0)}}|0\rangle && (7.2)\\
E_0^{(0)} &\equiv E_{CC} && (7.3)\\
H_{\mathsf{SCF}}\left|\mathcal{K}^{(0)}\right\rangle &= E_0^{(0)}\left|\mathcal{K}^{(0)}\right\rangle \equiv E_{CC}\left|\mathcal{K}^{(0)}\right\rangle && (7.4)\\
\left\langle\mathcal{L}^0\right| &\equiv \langle 0|\,(1+\Lambda_{\mathcal{K}}^0)e^{-T_{\mathcal{K}}^{(0)}} && (7.5)\\
\left\langle\mathcal{L}^0\right| H_{\mathsf{SCF}} &= \left\langle\mathcal{L}^0\right| E_{CC}. && (7.6)
\end{aligned}$$

3. The T operator for the state labeled $\mathcal{K}$ is written as the zeroth order T plus a sum of perturbative corrections:

$$\begin{aligned}
T_{\mathcal{K}} &\equiv T_{\mathcal{K}}^{(0)} + T_{\mathcal{K}}^{(1)} + T_{\mathcal{K}}^{(2)} + \cdots \\
&= T^{(0)} + T_{\mathcal{K}}^{(1)} + T_{\mathcal{K}}^{(2)} + \cdots . && (7.7)\\
& && (7.8)
\end{aligned}$$

The full wavefunction can be written as

$$\begin{aligned}
|\mathcal{K}\rangle &\equiv e^{T_{\mathcal{K}}}|\mathsf{HF}\rangle && (7.9)\\
&= \left(e^{T_{\mathcal{K}}^{(0)}} * e^{T_{\mathcal{K}}^{(1)}} * e^{T_{\mathcal{K}}^{(2)}} * \cdots\right)|\mathsf{HF}\rangle \\
&= e^{T_{\mathcal{K}}^{(0)}} * \left((1 + T_{\mathcal{K}}^{(1)} + \frac{1}{2}T_{\mathcal{K}}^{(1)^2} + \cdots) * (1 + T_{\mathcal{K}}^{(2)} + \frac{1}{2}T_{\mathcal{K}}^{(2)^2} + \cdots) * \cdots\right)|\mathsf{HF}\rangle ,
\end{aligned}$$

which works out the zeroth order wavefunction plus a sum of perturbative corrections

$$\begin{aligned} |\mathcal{K}\rangle &= \left|\mathcal{K}^{(0)}\right\rangle + \left|\mathcal{K}^{(1)}\right\rangle + \left|\mathcal{K}^{(2)}\right\rangle + \cdots \\ &= |CC\rangle + \left|\mathcal{K}^{(1)}\right\rangle + \left|\mathcal{K}^{(2)}\right\rangle + \cdots \end{aligned} \tag{7.10}$$

$$\left|\mathcal{K}^{(1)}\right\rangle = T_{\mathcal{K}}^{(1)}\left|\mathcal{K}^{(0)}\right\rangle \tag{7.11}$$

$$\left|\mathcal{K}^{(2)}\right\rangle = \left(T_{\mathcal{K}}^{(2)} + \frac{1}{2}T_{\mathcal{K}}^{(1)^2}\right)\left|\mathcal{K}^{(0)}\right\rangle \tag{7.12}$$

etc.

The Λ operator can also be expanded in a perturbation series

$$\Lambda_{\mathcal{K}} = \Lambda^{(0)} + \Lambda_{\mathcal{K}}^{(1)} + \cdots,$$

so that the full wavefunction is

$$\langle\mathcal{L}_{\mathcal{K}}| = \langle 0|\left(1 + \Lambda_{\mathcal{K}}^{(0)} + \Lambda_{\mathcal{K}}^{(1)} + \cdots\right) e^{-(T^{(0)} + T_{\mathcal{K}}^{(1)} + \cdots)}, \tag{7.13}$$

a sum of the zeroth order wavefunction and perturbative corrections:

$$\left\langle\mathcal{L}_{\mathcal{K}}^{(1)}\right| = \langle 0|\left[\Lambda_{\mathcal{K}}^{(1)} + \left(1 + \Lambda_{\mathcal{K}}^{(0)}\right) T_{\mathcal{K}}^{(1)}\right] e^{-T_{\mathcal{K}}^{(0)}} \tag{7.14}$$

$$\left\langle\mathcal{L}_{\mathcal{K}}^{(2)}\right| = \langle 0|\left[\Lambda_{\mathcal{K}}^{(2)} - \Lambda_{\mathcal{K}}^{(1)} T_{\mathcal{K}}^{(1)} + (1 + \Lambda_{\mathcal{K}}^{(0)})(\frac{1}{2}T_{\mathcal{K}}^{(1)^2} - T_{\mathcal{K}}^{(2)})\right] e^{-T_{\mathcal{K}}^{(0)}} \tag{7.15}$$

etc.

4. The perturbation operator, V^{IP}, must allow first-order corrections to T and Λ to be defined as follows:

$$T_{\mathcal{K}}^{(0)} \equiv \sum_{ai} t_i^a a^\dagger i + \frac{1}{4}\sum_{ijab} t_{ij}^{ab} a^\dagger i b^\dagger j + \cdots \tag{7.16}$$

$$= \sum_{\mu} t^{(0)}_{\mathcal{K}\mu}\,\tau^0_\mu,$$

$$T^{(1)}_{\mathcal{K}} \equiv \sum_i t(1)^{\mathcal{K}}_i \chi^\dagger_{\mathcal{K}} i + \frac{1}{2}\sum_{ija} t(1)^{\mathcal{K}a}_{i\ j} \chi^\dagger_{\mathcal{K}} i a^\dagger j + \cdots \tag{7.17}$$

$$= \sum_{\mu} t^{(1)}_{\mathcal{K}\mu}\,\tau^1_\mu$$

$$\Lambda^{(0)}_{\mathcal{K}} \equiv \sum_{\mu} \lambda^{(0)}_{\mathcal{K}\mu} (\tau^0_\mu)^\dagger \tag{7.18}$$

$$\Lambda^{(1)}_{\mathcal{K}} \equiv \sum_{\mu} \lambda^{(1)}_{\mathcal{K}\mu} (\tau^1_\mu)^\dagger. \tag{7.19}$$

Here, as expected, is where the treatment of the IP problem is different from that of the EE problem. Although the $T^{(0)}_{\mathcal{K}}$ amplitudes have nonzero contributions only to the usual excitations from occupied to virtual space, a single excitation to a "free-electron" function $\chi_{\mathcal{K}}$ must be introduced in the first order to describe an ionization process while preserving the number of electrons. In the limit where the "escaping" electron has zero kinetic energy, this form of $T^{(1)}_{\mathcal{K}}$ allows the the first-order corrections to the wavefunctions, $\left|\mathcal{K}^{(1)}\right\rangle$ and $\left\langle\mathcal{L}^{(1)}\right|$, to be represented as $(N-1)$–electron eigenfunctions of the zeroth-order Hamiltonian. Keeping in mind that in the zeroth-order wavefunction coefficients to the $\tau^1_\mu \backslash (\tau^1_\mu)^\dagger$ operators are zero, while in the first-order correction the coefficients to the $\tau^0_\mu \backslash (tau^0_\mu)^\dagger$ operators are zero, it is possible to treat the perturbation problem in a manner analogous to that of Koch and Jørgensen.

So far, the only assumption made in this development of a perturbation theory is that the only processes initiated by the perturbing operator, V^{IP}, are electron detachment type processes. This is justified in describing, for example, a photodetachment process where there is a sizable gap between the frequencies of light which

will cause electron detachment and those which cause excitations. One does not expect excitations and ionizations to occur at the same frequency.

7.2 coupled-cluster Response Theory

7.2.1 Time Dependent Perturbation on a Coupled-Cluster Reference

With these definitions, the coupled-cluster response theory for electron detachment processes can be developed in a manner analogous to that of Koch and Jørgensen. Although the determination of the energies requires only the $T_{\mathcal{K}}^{(0)}$ amplitudes, the formation of the linear response function requires the calculation of the first-order corrections to the wavefunction.

Once the CC solution is found, an operator $\bar{H}_N \equiv e^{-T_{\mathcal{K}}^{(0)}} H_{\mathsf{SCF}} e^{T_{\mathcal{K}}^{(0)}}$ is defined, which has right and left eigenfunctions $|0\rangle$ and $\langle 0|\,(1+\Lambda_{\mathcal{K}}^0)$

$$\bar{H}_N |0\rangle = E_{CC} |0\rangle \tag{7.20}$$

$$\langle 0|\,(1+\Lambda_{\mathcal{K}}^0)\,\bar{H}_N = \langle 0|\,(1+\Lambda_{\mathcal{K}}^0)\,E_{CC}, \tag{7.21}$$

or

$$H_{\mathsf{SCF}} e^{T_{\mathcal{K}}^{(0)}} |0\rangle = E_{CC} e^{T_{\mathcal{K}}^{(0)}} |0\rangle \tag{7.22}$$

$$\langle 0|\,(1+\Lambda_{\mathcal{K}}^0) e^{-T_{\mathcal{K}}^{(0)}} H_{\mathsf{SCF}} = \langle 0|\,(1+\Lambda_{\mathcal{K}}^0) e^{-T_{\mathcal{K}}^{(0)}} E_{CC}. \tag{7.23}$$

The next step is to find the response of both the left and right eigenfunctions. Projecting the Schrödinger equation

$$i\frac{d}{dt}|CC(t)\rangle = H\,|CC(t)\rangle \tag{7.24}$$

by $\langle\mu|\, e^{-T_\mathcal{K}}$ and collecting terms by order in β leads to the following expressions for the time evolution of $T_\mathcal{K}$:

$$\begin{aligned}
\frac{dT_\mathcal{K}}{dt}\,|CC\rangle &= -i(H_{\mathsf{SCF}} + V^{IP})\,|CC\rangle\,; && (7.25)\\
\frac{dt^{(0)}_{\mathcal{K}\mu}}{dt} &= -i\left\langle\bar{\mu}^0\right| H_{\mathsf{SCF}}\left|CC^0\right\rangle = -i\left\langle\mu^0\right|\bar{H}_N\,|0\rangle = 0; && (7.26)\\
\frac{dT^{(1)}_\mathcal{K}}{dt}\left|CC^0\right\rangle &= i\left[T^{(1)}_\mathcal{K}\frac{dT^{(0)}_\mathcal{K}}{dt} - H_{\mathsf{SCF}}\,T^{(1)}_\mathcal{K} - V^{IP}\right]\left|CC^0\right\rangle\\
\frac{dt^{(1)}_{\mathcal{K}\mu}}{dt} &= -\left\langle\bar{\mu}^1\right| T^{(1)}_\mathcal{K}\,H_{\mathsf{SCF}}\left|CC^0\right\rangle + \left\langle\bar{\mu}^1\right| H_{\mathsf{SCF}}\,T^{(1)}_\mathcal{K}\left|CC^0\right\rangle + \left\langle\bar{\mu}^1\right| V^{IP}\left|CC^0\right\rangle\\
&= -i\left[\left\langle\mu^1\right|\left[\bar{H}_N, T^{(1)}_\mathcal{K}\right]|0\rangle + \left\langle\bar{\mu}^1\right| V^{IP}\left|CC^0\right\rangle\right]; && (7.27)
\end{aligned}$$

where $\langle\bar{\mu}| \equiv \langle\mu|\, e^{-T^{(0)}_\mathcal{K}}$, $\bar{H}_N \equiv e^{-T^{(0)}_\mathcal{K}} H_{\mathsf{SCF}} e^{T^{(0)}_\mathcal{K}}$. The response of the λ amplitudes,

$$\begin{aligned}
-i\,\langle\mathcal{L}(t)|\left(\frac{d}{dt}\right)^\dagger e^{T_\mathcal{K}} &= \langle\mathcal{L}(t)|\,He^{T_\mathcal{K}} && (7.28)\\
\langle\mathsf{HF}|\left[(1+\Lambda_\mathcal{K})\frac{-dT_\mathcal{K}}{dt} + \frac{d\Lambda_\mathcal{K}}{dt}\right] &= i\,\langle\mathsf{HF}|\,(1+\Lambda_\mathcal{K})\,e^{-T_\mathcal{K}}(H_{\mathsf{SCF}} + V^{IP})e^{T_\mathcal{K}},
\end{aligned}$$

can be derived with the help of equation 7.25

$$\begin{aligned}
\langle 0|\frac{d\Lambda_\mathcal{K}}{dt}\,|\nu\rangle &= i\,\langle\mathcal{L}|\,(H_{\mathsf{SCF}} + V^{IP})\,\tau_\nu\,|CC\rangle - i\,\langle 0|\,(1+\Lambda_\mathcal{K})\,e^{-T_\mathcal{K}}\,\tau_\nu\,(H_{\mathsf{SCF}} + V^{IP})\,|CC\rangle\\
&= i\,\langle 0|\,(1+\Lambda_\mathcal{K})\,e^{-T_\mathcal{K}}\left[(H_{\mathsf{SCF}} + V^{IP}), \tau_\nu\right]e^{T_\mathcal{K}}\,|0\rangle\,, && (7.29)
\end{aligned}$$

$$\begin{aligned}
\frac{d\lambda^{(0)}_{\mathcal{K}\mu}}{dt} &= i\,\langle 0|\,(1+\Lambda^{(0)}_\mathcal{K})\left[\bar{H}_N, \tau^0_\mu\right]|0\rangle = 0, && (7.30)\\
\frac{d\lambda^{(1)}_{\mathcal{K}\mu}}{dt} &= i\,\langle 0|\,(1+\Lambda^{(0)}_\mathcal{K})\left[\left[\bar{H}_N, \tau^1_\mu\right], T^{(1)}_\mathcal{K}\right]|0\rangle + i\,\langle 0|\,\Lambda^{(1)}_\mathcal{K}\left[\bar{H}_N, \tau^1_\mu\right]|0\rangle\\
&\quad + i\,\langle 0|\,(1+\Lambda^{(0)}_\mathcal{K})\,e^{-T^{(0)}_\mathcal{K}}\left[V^{IP}, \tau^1_\mu\right]e^{T^{(0)}_\mathcal{K}}\,|0\rangle\,. && (7.31)
\end{aligned}$$

7.2.2 The Linear Response Function

Following the development of Olsen and Jørgensen[41], as applied by Koch and Jørgensen to the coupled-cluster reference[16], we define the operator perturbation operator, V^{IP}. Assuming the perturbation vanishes at $t = -\infty$, it can be written as

$$V^{IP} = \int_{-\infty}^{\infty} d\omega \, V^w e^{(-i\omega+\alpha)t}, \tag{7.32}$$

where a real, positive, and small α ensures that V^{IP} is zero at $t = -\infty$, and $V^w e^{\alpha t}$ is assumed to reach a finite value at non-infinite times. If V^w contains one constant frequency component ω_b, this becomes

$$\begin{aligned} V^{IP} &= \int_{-\infty}^{\infty} d\omega \, \vec{r} \left[\delta(\omega - \omega_b) + \delta(\omega + \omega_b)\right] V(\omega) e^{(-i\omega+\alpha)t} && (7.33) \\ &= \left(V(\omega_b)\, e^{(-i\omega+\alpha)t} + V(-\omega_b)\, e^{(i\omega_b+\alpha)t}\right) \vec{r}, && (7.34) \end{aligned}$$

which could describe the amplitude of a periodic electric or magnetic field of frequency ω_b.

The expectation value of an operator $O(t)$ is $\langle \mathcal{L}(t)| \, O(t) \, |CC(t)\rangle$ and can be written as a perturbation expansion of $\mathcal{L}$ and $|CC\rangle$

$$\begin{aligned} \langle \mathcal{L}| \, O \, |CC\rangle &= \left\langle \mathcal{L}^0 \middle| \, O \, \middle| CC^0 \right\rangle \\ &\quad + \left\langle \mathcal{L}^1 \middle| \, O \, \middle| CC^0 \right\rangle + \left\langle \mathcal{L}^0 \middle| \, O \, \middle| CC^1 \right\rangle \\ &\quad + \left\langle \mathcal{L}^2 \middle| \, O \, \middle| CC^0 \right\rangle + \left\langle \mathcal{L}^1 \middle| \, O \, \middle| CC^1 \right\rangle + \left\langle \mathcal{L}^0 \middle| \, O \, \middle| CC^2 \right\rangle + \cdots, && (7.35) \\ & && (7.36) \end{aligned}$$

Or, in response function notation,

$$\left\langle \mathcal{L}^0 \middle| \, O \, \middle| CC^0 \right\rangle + \int_{-\infty}^{\infty} d\omega_1 \, e^{(-i\omega_1+\alpha)t} \, \langle\langle O; V^{\omega_1} \rangle\rangle_{\omega_1}$$

$$+\frac{1}{2}\int_{-\infty}^{\infty}d\omega_1\int_{-\infty}^{\infty}d\omega_2\, e^{(-i\omega_1+\alpha)t}\, e^{(-i\omega_2+\alpha)t}\, \langle\langle O;V^{\omega_1};V^{\omega_2}\rangle\rangle_{\omega_1;\omega_2}+\cdots. \quad (7.37)$$

So that

$$\left\langle \mathcal{L}^1\middle|\, O\,\middle|CC^0\right\rangle+\left\langle \mathcal{L}^0\middle|\, O\,\middle|CC^1\right\rangle=\int_{-\infty}^{\infty}d\omega_1\, e^{(-i\omega_1+\alpha)t}\, \langle\langle O;V_1^{\omega}\rangle\rangle_{\omega_1} \quad (7.38)$$

The t and λ amplitudes can also be written in terms of their Fourier transforms:

$$t_{\mathcal{K}\mu}^{(1)} = \int_{-\infty}^{\infty}d\omega_1\, X_{\mathcal{K}\mu}^{(1)}(\omega_1+i\alpha)\, e^{(-i\omega_1+\alpha)t}, \quad (7.39)$$

$$\lambda_{\mathcal{K}\mu}^{(1)} = \int_{-\infty}^{\infty}d\omega_1\, Y_{\mathcal{K}\mu}^{(1)}(\omega 1+i\alpha)\, e^{(-i\omega_1+\alpha)t}. \quad (7.40)$$

Substituting these expressions into equations 7.27 and 7.31 gives

$$X_{\mathcal{K}\mu}^{(1)}(\omega_1+i\alpha) = \sum_{\nu}(-A+(\omega_1+i\alpha)\,\mathrm{I})_{\mu\nu}^{-1}\,\xi_{\nu}^{\omega_1} \quad (7.41)$$

$$Y_{\mathcal{K}\mu}^{(1)}(\omega_1+i\alpha) = -\sum_{\nu}\left(\eta_{\nu}^{\omega_1}(\omega_1)+\sum_{\gamma}F_{\nu\gamma}\,X_{\mathcal{K}\gamma}^{(1)}(\omega_1+i\alpha)\right)\times (A+(\omega_1+i\alpha)\,\mathrm{I})_{\nu\mu}^{-1} \quad (7.42)$$

where

$$A_{\mu\nu} = \langle\mu|\left[\bar{H}_N,\tau_{\nu}\right]|0\rangle,$$

$$\xi_{\nu}^{\omega_1} = \langle\nu|\, e^{-T_{\mathcal{K}}^{(0)}}V^{\omega_1}e^{T_{\mathcal{K}}^{(0)}}\,|0\rangle,$$

$$F_{\nu\gamma} = \langle 0|\,(1+\Lambda^0)\left[\left[\bar{H}_N,\tau_{\nu}\right],\tau_{\gamma}\right]|0\rangle.$$

Now the linear response function can be written in terms of the Fourier transform of the first-order perturbed wavefunction:

$$\langle\langle O;V_1^{\omega}\rangle\rangle_{\omega_1} = \sum_{\mu}Y_{\mathcal{K}\mu}^{(1)}(\omega_1)\,\langle\bar{\mu}|\,O\,\left|CC^0\right\rangle+\sum_{\mu}\left\langle\mathcal{L}^0\middle|\,[O,\tau_{\mu}]\,\middle|CC^0\right\rangle\,X_{\mathcal{K}\mu}^{(1)}(\omega_1) \quad (7.43)$$

$$= \sum_{\mu}\left\{\left\langle\mathcal{L}^0\middle|\,[V^{\omega_1},\tau_{\mu}]\,\middle|CC^0\right\rangle+\sum_{\gamma}F_{\mu\gamma}\sum_{\nu}(-A+\omega_1 I)_{\gamma\nu}^{-1}\,\xi_{\nu}^{\omega_1}\right\}\times$$

$$\sum_{\sigma}(-A-\omega_1\mathbf{I})^{-1}_{\mu\sigma}\left\langle\bar{\sigma}\right|O\left|CC^0\right\rangle$$
$$+\sum_{\mu}\left\langle\mathcal{L}^0\right|[O,\tau_\mu]\left|CC^0\right\rangle\sum_{\nu}(-A+\omega_1\mathbf{I})^{-1}_{\mu\nu}\,\xi^{\omega_1}_{\nu} \tag{7.44}$$

7.2.3 Energies and Transition Intensities

The transition energies are found at the poles of the linear response function, which are found at $+/-$ the eigenvalues of the matrix A. This matrix,

$$A_{\mu\nu}=\langle\mu|\left[\bar{H}_N,\tau_\nu\right]|0\rangle\,,$$

is exactly the matrix derived in the coupled-cluster Equation of Motion method, by a completely different route. The τ_k operators are the EOMIP wavefunctions. There is no quantity analogous to the $T^{(1)}_{\mathcal{K}}$ amplitudes. What the LRT provides, from the EOM practitioner's point of view, is an unambiguous definition of the transition intensities.

$$I=\lim_{\omega_1\to\omega_k}(\omega_1-\omega_k)\left\langle\left\langle O;V^t\right\rangle\right\rangle_{\omega_1} \tag{7.45}$$

where ω_k is a simple pole of $\langle\langle O;V^t\rangle\rangle$, an eigenvalue of the matrix A. If

$$(S^{-1}AS)_{nm}=\mathcal{W}_{nm}=\delta_{nm}\omega_n, \tag{7.46}$$

the bra and ket functions can be transformed:

$$\begin{aligned}\langle k| &= \sum_{\mu}S^{-1}_{k\mu}\langle\mu|\\ \tau_k &= \sum_{\mu}\tau_\mu S_{\mu k}.\end{aligned}$$

The $X^{(1)}$ and $Y^{(1)}$ vectors can also be transformed:

$$\begin{aligned}
\mathcal{X}_{\mathcal{K}}^{(1)}(\omega_1) &= S^{-1}X_{\mathcal{K}}^{(1)}(\omega_1) = S^{-1}(-A+\omega_1\mathbf{I})^{-1}S\,S^{-1}\,\xi^{\omega_1}(\omega_1) \\
&= (-\mathcal{W}+\omega_1\mathbf{I})^{-1}\,V^{\omega_1} \qquad (7.47) \\
\mathcal{X}_{\mathcal{K}k}^{(1)}(\omega 1) &= \frac{V_k^{\omega_1}}{(\omega_1-\omega_k)} \qquad (7.48)
\end{aligned}$$

$$\begin{aligned}
\mathcal{Y}_{\mathcal{K}}^{(1)} &= Y^{(1)}(\omega_1)S = -\eta^{\omega_1}S\,S^{-1}(A+\omega_1\mathbf{I})^{-1}S \\
&\quad - X^{(1)^\dagger}S^{-1\dagger}\,S^\dagger F^\dagger S\,S^{-1}(A+\omega_1\mathbf{I})^{-1}S \\
&= \mathcal{V}^{\omega_1}(\mathcal{W}+\omega_1\mathbf{I})^{-1} - V^{\omega_1\dagger}\,(-\mathcal{W}+\omega_1)^{-1\dagger}\,G\,(\mathcal{W}+\omega_1\mathbf{i})^{-1} \qquad (7.49) \\
\mathcal{Y}_{\mathcal{K}k}^{(1)}(\omega_1) &= -\frac{\mathcal{V}^{\omega_1}}{(\omega_k+\omega_1)} - \sum_n V_n^{\omega_1}\frac{G_{nk}}{(\omega_1-\omega_k)(\omega_n+\omega_1)} \qquad (7.50)
\end{aligned}$$

where

$$\begin{aligned}
V_n^{\omega_1} &= \sum_\mu S_{n\mu}^{-1}\xi_\mu^{\omega_1} = \left\langle \bar{k}\right| V^{\omega_1}\left|CC^0\right\rangle, \\
\mathcal{V}_n^{\omega_1} &= \sum_\mu \eta_\mu^{\omega_1}S_{\mu n}^{-1} = \left\langle \mathcal{L}^0\right|\left[V^{\omega_1},\tau_k\right]\left|CC^0\right\rangle, \\
G_{mn} &= \sum_{\mu\nu} F_{\nu\mu}S_{\mu m}S_{\nu n} = \langle 0|\,(1+\Lambda^0)\left[\left[\bar{H}_N,\tau_n\right],\tau_m\right]|0\rangle\,.
\end{aligned}$$

The linear response function can now be written

$$\begin{aligned}
\langle\langle O;V^{\omega_1}\rangle\rangle_{\omega_1} &= \sum_n \mathcal{Y}_{\mathcal{K}n}^{(1)}(\omega_1)\,\langle\bar{n}|\,O\left|CC^0\right\rangle + \sum_m \langle 0|\left[\bar{H}_N,\tau_m\right]|0\rangle\,\mathcal{X}_{\mathcal{K}m}^{(1)} \\
&= -\sum_n \frac{\mathcal{V}_n^{\omega_1}\,\langle\bar{n}|\,O\left|CC^0\right\rangle}{(\omega_n+\omega_1)} - \sum_m \frac{V_m^{\omega_1}}{(\omega_1-\omega_m)}\sum_n \frac{G_{mn}\,\langle\bar{n}|\,O\left|CC^0\right\rangle}{(\omega_1+\omega_n)} \\
&\quad + \sum_m \left\langle \mathcal{L}^0\right|\left[O,\tau_m\right]\left|CC^0\right\rangle \frac{V^{\omega_1}}{(\omega_1-\omega_m)}\,,
\end{aligned}$$

and the transition intensity as

$$\lim_{\omega_1\to\omega_k}(\omega_1-\omega_k)\left[\sum_n \frac{-\mathcal{V}_n^{\omega_1}\,\langle\bar{n}|\,O\left|CC^0\right\rangle}{(\omega_n+\omega_1)}\right.$$

$$+\sum_m \left(\left\langle \mathcal{L}^0 \right| [O, \tau_m] \left| CC^0 \right\rangle - \sum_n \frac{G_{mn} \langle \bar{n}| O \left| CC^0 \right\rangle}{(\omega_1 + \omega_n)} \right) \frac{V_m^{\omega_1}}{(\omega_1 - \omega_m)} \Bigg]$$

$$= \Gamma^O_{0\to k} \times \Gamma^{V^{\omega_k}}_{k\to 0} \tag{7.51}$$

where

$$\begin{aligned} \Gamma^O_{0\to k} &= \left(\left\langle \mathcal{L}^0 \right| [O, \tau_k] \left| CC^0 \right\rangle - \sum_n \frac{\langle \mathcal{L}^0 | \left[[O, \tau_n], \tau_k \right] \left| CC^0 \right\rangle \langle \bar{n}| O \left| CC^0 \right\rangle}{(\omega_k + \omega_n)} \right) \\ &= \Big(\langle 0| (1 + \Lambda^0)(\bar{O}\tau_k)_c |0\rangle \\ &\quad - \sum_n \frac{\langle 0| (1 + \Lambda^0) (\bar{O}\tau_n\tau_k)_c |0\rangle \langle n| \bar{O} |0\rangle}{(\omega_k + \omega_n)} \Big), \end{aligned} \tag{7.52}$$

and

$$\begin{aligned} \Gamma^{V^{\omega_k}}_{k\to 0} &= \left\langle \bar{k} \right| V^{\omega_k} \left| CC^0 \right\rangle \\ &= \langle k| \bar{V}^{\omega_k} |0\rangle, \end{aligned} \tag{7.53}$$

are referred to as the transition matrix elements and

$$\begin{aligned} \bar{O} &= e^{-T^{(0)}_\kappa} O\, e^{T^{(0)}_\kappa} = (O\, e^{T^{(0)}_\kappa})_c \\ \bar{V}^{\omega_k} &= e^{-T^{(0)}_\kappa} V^{\omega_k}\, e^{T^{(0)}_\kappa} = (V^{\omega_k}\, e^{T^{(0)}_\kappa})_c. \end{aligned}$$

In the usual propagator approach to transition expectation values, an expression of the form $\langle 0| O |k\rangle\langle k| V^{\omega_k} |0\rangle$ would be expected. The expression given above does not have the same symmetric appearance because of the difference between the right- and left-hand solutions. The calculation of the transition expectation value is more complicated because of this asymmetry.

CHAPTER 8

METHODS FOR TRANSITION MOMENTS IN THE EOMIP APPROACH

For an experiment in which it is proposed to observe an absorption spectrum, the dipole operator $\vec{r}$ is the appropriate choice for O. However, in the case of photoelectron experiments, it is the electron momentum which is observed. The proper choice of O must be $\vec{p}$, the momentum operator for the outgoing electron. In either of these cases, O is a one-body operator. The second term of $\Gamma^{O}_{0\to k}$ contains the integral

$$\langle 0| \left(1 + \Lambda^0\right) \left(\bar{O}\tau_n\tau_k\right)_c |0\rangle ,$$

which includes a product of two one-body excitation operators (τ_n and τ_k) contracted with a one-body operator (O). If the outgoing electron functions are orthogonal to the occupied and virtual orbitals, there is no contraction of these three operators which can survive the left projection by $\langle 0| \left(1 + \Lambda^0\right)$, so that term becomes zero and the transition matrix element becomes

$$\Gamma^{O}_{0\to k} = \langle 0| \left(1 + \Lambda^0\right) \left(\bar{O}\tau_k\right)_c |0\rangle . \tag{8.1}$$

No matter what is used for O, the nature of the outgoing one-electron function must be known in order to calculate $\Gamma^{O}_{0\to k}$ and $\Gamma^{V^{\omega_k}}_{k\to 0}$. Free-electron functions are dependent on the experimental method and not included in the basis sets for standard electronic structure methods; integrals of $\vec{r}$ and $\vec{p}$ involving these functions are not

readily available. Therefore, it is usual to make some kind of approximation for both $\Gamma^{O}_{0\to k}$ and $\Gamma^{V^{\omega}k}_{k\to 0}$. The most common approximation is the so-called monopole approximation as developed by, for example, Martin and Shirley in 1976[4].

8.1 The Monopole Approximation

A symmetric Hamiltonian is assumed, and the dipole approximation to the cross section for photoemission by an incident photon field is employed:

$$\sigma_{DA} \propto (\hbar\omega_1)^{-1} \left[\vec{\mathbf{r}} \cdot \langle \psi_f(N) | \vec{\mathbf{p}} | \psi_i(N) \rangle\right]^2 \rho(E_f), \tag{8.2}$$

where $\rho(E_f)$ is the density of states in the continuum at the final energy. The authors proposed to determine the intensities of the shakeup satellite peaks relative to the related principal core ionization potentials, introducing two important approximations.

1. The principal ionizations are characterized by annihilation of an electron from a single orbital, and the satellites also have a non-negligible contribution from this annihilation. Therefore the momentum operator, acting on an initial state dominated by an ionization from orbital i, is approximated as:

$$\sum_m \langle m | \vec{\mathbf{p}} | \chi \rangle \, m^{\dagger} \chi \, | \psi_f(N) \rangle \approx i^{\dagger} \chi \, | \psi_f(N) \rangle \, \langle i | \vec{\mathbf{p}} | \chi \rangle \, . \tag{8.3}$$

2. Both ρ and the momentum integrals $\langle i | \vec{\mathbf{p}} | \chi \rangle$ are approximately constant over the range of energies spanned by the principal and its satellites.

This means that the ratio of the intensity of the nth satellite peak, $I(n)$, to its principal, $I(0)$, is

$$\begin{aligned} \frac{I(n)}{I(0)} &= \frac{|\langle\chi_n|\,\vec{\mathbf{p}}\,|i\rangle|^2}{|\langle\chi_0|\,\vec{\mathbf{p}}\,|i\rangle|^2}\frac{|\langle\psi_n|\,i^\dagger\chi_n\,|0\rangle|^2}{|\langle\psi_0|\,i^\dagger\chi_0\,|0\rangle|^2}\frac{\rho(E_n)}{\rho(E_0)} \\ &\approx \frac{\langle\psi_n|\,i^\dagger\chi_n\,|0\rangle^2}{\langle\psi_0|\,i^\dagger\chi_0\,|0\rangle^2} \end{aligned} \tag{8.4}$$

And the calculation of the intensities is reduced to the calculation of transition density matrix elements for the principal and its satellites.

Further simplifications are possible. In 1977, Martin and Davidson[6] employed a simplification which included only final state correlation and only one term from the resulting transition density matrix. For the ionized states, they used a (1h, 2h1p) CI calculation and argued that, for the principal and its satellites, only one contribution was important -- that hole state which dominates both. So for a CI wavefunction of the form

$$\psi_n = \sum_i C_i^{\mathbf{n}}\Phi_i + \sum_{ija} C^{\mathbf{n}a}_{ij}\Phi^a_{ij} \tag{8.5}$$

they approximated the ratio of intensities as

$$I(n)/I(0) \approx \frac{\langle\psi_n|\,i^\dagger\,|0\rangle^2}{\langle\psi_0|\,i^\dagger\,|0\rangle^2} \approx \frac{(C_i^{\mathbf{n}})^2}{\left(C_i^{\mathbf{0}}\right)^2}\ . \tag{8.6}$$

In a 1992 paper by Murray and Davidson[28], the same features were calculated with a multi-reference CI approach, and the same expression was used for the relative intensities. The authors report good agreement with experiment.

8.2 Transition Moment Expression for Non-Symmetric Eigenstates

For the non symmetric eigenvalue problem, there are two different approximations to the wavefunction in the full space. Equation 8.2 must be modified to recognize that the left- and right- handed wavefunctions are not identical. This results in

$$\sigma_{DA} \propto (\hbar\omega_1)^{-1} \left[\vec{\mathbf{r}} \cdot \left\langle \psi_i^L(N) \right| \vec{\mathbf{p}} \left| \psi_f^R(N) \right\rangle\right] \left[\vec{\mathbf{r}} \cdot \left\langle \psi_f^L(N) \right| \vec{\mathbf{p}} \left| \psi_i^R(N) \right\rangle\right] \rho(E_f), \qquad (8.7)$$

which yields, under the same set of approximations as was made above,

$$\begin{aligned} \frac{I(n)}{I(0)} &= \frac{|\langle \chi_n | \vec{\mathbf{p}} | i \rangle|^2}{|\langle \chi_0 | \vec{\mathbf{p}} | i \rangle|^2} \frac{\left\langle 0^L \right| i^\dagger \chi_n \left| \psi_n^R \right\rangle \left\langle \psi_n^L \right| i^\dagger \chi_n \left| 0^R \right\rangle}{\langle 0^L | i^\dagger \chi_0 | \psi_0^R \rangle \langle \psi_0^L | i^\dagger \chi_0 | 0^R \rangle} \frac{\rho(E_n)}{\rho(E_0)} \\ &\approx \frac{\left\langle 0^L \right| i^\dagger \chi_n \left| \psi_n^R \right\rangle \left\langle \psi_n^L \right| i^\dagger \chi_n \left| 0^R \right\rangle}{\langle 0^L | i^\dagger \chi_0 | \psi_0^R \rangle \langle \psi_0^L | i^\dagger \chi_0 | 0^R \rangle}. \end{aligned} \qquad (8.8)$$

In this case, the Murray and Davidson approximation gives

$$I(n)/I(0) \approx \frac{\left\langle 0^L \right| i^\dagger \left| \psi_n^R \right\rangle \left\langle \psi_n^L \right| i^\dagger \left| 0^R \right\rangle}{\langle 0^L | i^\dagger | \psi_0^R \rangle \langle \psi_0^L | i^\dagger | 0^R \rangle} \approx \frac{(D_i^{\mathbf{n}} C_i^{\mathbf{n}})}{\left(D_i^{\mathbf{0}} C_i^{\mathbf{0}}\right)} \quad . \qquad (8.9)$$

In cases where $\bar{H}_N$ is close to being symmetric, there is some justification, considering the number of approximations already made, in reducing this back to equation 8.6. This approximation can, of course, only be applied to those cases where one of the states of interest is a principal ionization state.

8.3 Transition Moment Expression for the EOMIP problem

For the EOMIP case, the expressions for the transition matrix elements are:

$$\Gamma^O_{0\to k} = \langle 0 | (1+\Lambda) e^{-T} O e^T \chi^\dagger \Omega^K | 0 \rangle$$

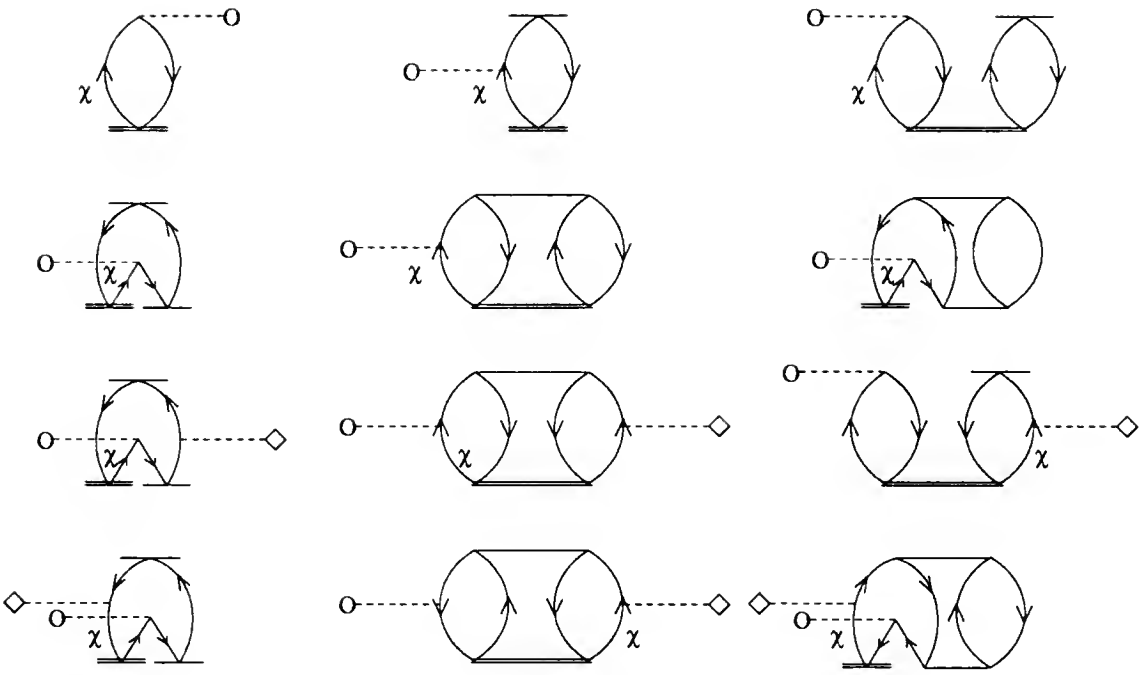

Figure 8.1: Diagrammatic expression of $\Gamma^{O}_{0\to k}$ terms

$$= \sum_i \langle i|\, O\, |\chi\rangle\, D_{i\chi} + \sum_a \langle a|\, O\, |\chi\rangle\, D_{a\chi} \tag{8.10}$$
$$+ \sum_a \langle a|\, \chi\rangle \left(\sum_{ib} \langle i|\, O\, |b\rangle\, \Gamma_{iba\chi} + \sum_{ij} \langle i|\, O\, |j\rangle\, \Gamma_{ija\chi} + \sum_{bc} \langle b|\, O\, |c\rangle\, \Gamma_{bca\chi} \right)$$

where

$$\begin{aligned}
D_{i\chi} &= c_i^{\mathcal{K}} - \sum_{me} \left(c_{mi}^{\mathcal{K}e} + c_m^{\mathcal{K}} t_i^e \right) \lambda_m^e - \frac{1}{2} \sum_{menf} c_j^{\mathcal{K}} t_{in}^{ef} \lambda_{mn}^{ef} \\
D_{a\chi} &= \sum_i c_m^{\mathcal{K}} \lambda_m^a + \frac{1}{2} \sum_{mne} c_{mn}^{\mathcal{K}e} \lambda_{mn}^{ae} \\
\Gamma_{iba\chi} &= \sum_m \lambda_m^a \left(c_{mi}^{\mathcal{K}b} - c_i^{\mathcal{K}} t_m^b \right) - \frac{1}{2} \sum_{mne} \lambda_{mn}^{ae} c_i^{\mathcal{K}} t_{mn}^{be} \\
\Gamma_{ija\chi} &= \lambda_j^b c_i^{\mathcal{K}} - \sum_{me} \lambda_{jm}^{ae} c_{im}^{\mathcal{K}e} \\
\Gamma_{bca\chi} &= -\frac{1}{2} \sum_{mn} \lambda_{mn}^{bc} c_{mn}^{\mathcal{K}c}.
\end{aligned}$$

The other matrix element is:

$$\Gamma^{V^{\omega_k}}_{k\to 0} = \langle 0|\, Y^{\mathcal{K}\dagger} \chi e^{-T} O e^{T}\, |0\rangle$$

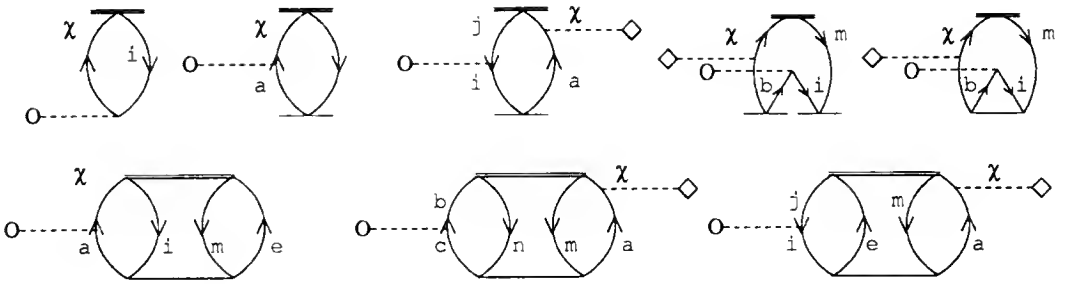

Figure 8.2: Diagrammatic expression of $\Gamma^{V^{\omega}k}_{k\to 0}$ terms

$$= \sum_i \langle\chi|\, O\,|i\rangle\, D_{\chi i} + \sum_a \langle\chi|\, O\,|a\rangle\, D_{\chi a} \tag{8.11}$$
$$+ \sum_a \langle\chi|\, a\rangle \left(\sum_{ib} \langle i|\, O\,|b\rangle\, \Gamma_{ib\chi a} + \sum_{ij} \langle i|\, O\,|j\rangle\, \Gamma_{ij\chi a} + \sum_{bc} \langle b|\, O\,|c\rangle\, \Gamma_{bc\chi a} \right)$$

where

$$\begin{aligned}
D_{\chi i} &= y_i^{\mathcal{K}*} \\
D_{\chi a} &= \sum_m y_i^{\mathcal{K}*} t_m^a - \frac{1}{2} \sum_{mne} y_{mn}^{\mathcal{K}e\,*} t_{mn}^{ae} \\
\Gamma_{ib\chi a} &= \sum_m \left(y_m^{\mathcal{K}*} t_{im}^{ab} + \frac{1}{2} y_m^{\mathcal{K}*} t_i^a t_m^b \right) \\
\Gamma_{ij\chi a} &= \sum_{me} y_{ij}^{\mathcal{K}e*} t_{im}^{ae} - y_j^{\mathcal{K}*} t_i^a \\
\Gamma_{bc\chi a} &= \frac{1}{2} \sum_{mn} y_{mn}^{\mathcal{K}b\,*} t_{mn}^{ac}.
\end{aligned}$$

In cases where the outgoing electron function is orthogonal to the virtual orbitals, all Γ terms, which involve $\langle\chi|\, p\rangle$ or $\langle p|\, \chi\rangle$ will disappear, leaving the much simpler D expressions in terms of $\langle p|\, O\,|\chi\rangle$ and $\langle\chi|\, O\,|p\rangle$. Using the approximations of Martin and Shirley, these expressions reduce to

$$\Gamma^{O}_{0\to k} \approx \langle i|\, O\,|\chi\rangle\, D_{i\chi} \tag{8.12}$$

$$\Gamma^{V^{\omega}k}_{k\to 0} \approx \langle\chi|\, O\,|i\rangle\, D_{\chi i}, \tag{8.13}$$

where i is the occupied orbital which dominates the ionization event.

That means that the ratio of intensities of satellite state $\mathcal{N}$ and its principal state $\mathcal{K}$ is approximated as.

$$\begin{aligned}\frac{I(\mathcal{N})}{I(\mathcal{K})} &\approx \frac{D^{\mathcal{N}}_{\chi i} D^{\mathcal{N}}_{i\chi}}{D^{\mathcal{K}}_{\chi i} D^{\mathcal{K}}_{i\chi}} \\ &= \frac{y_i^{\mathcal{N}*}\left(c_i^{\mathcal{N}} + \sum_{me}\left(c_{im}^{\mathcal{N}e} - c_m^{\mathcal{N}} t_i^e\right)\lambda_m^e - \frac{1}{2}\sum_{menf} c_m^{\mathcal{N}} t_{in}^{ef}\lambda_{mn}^{ef}\right)}{y_i^{\mathcal{K}*}\left(c_i^{\mathcal{K}} + \sum_{me}\left(c_{im}^{\mathcal{K}e} - c_m^{\mathcal{K}} t_i^e\right)\lambda_m^e - \frac{1}{2}\sum_{menf} c_m^{\mathcal{K}} t_{in}^{ef}\lambda_{mn}^{ef}\right)}.\end{aligned} \tag{8.14}$$

Because $Y^{\mathcal{K}}$ is, to first order, identical to $C^{\mathcal{K}}$, one can make the further approximation

$$\frac{I(\mathcal{N})}{I(\mathcal{K})} \approx \frac{c_i^{\mathcal{N}}\left(c_i^{\mathcal{N}} + \sum_{me}\left(c_{im}^{\mathcal{N}e} - c_m^{\mathcal{N}} t_i^e\right)\lambda_m^e - \frac{1}{2}\sum_{menf} c_m^{\mathcal{N}} t_{in}^{ef}\lambda_{mn}^{ef}\right)}{c_i^{\mathcal{K}}\left(c_i^{\mathcal{K}} + \sum_{me}\left(c_{im}^{\mathcal{K}e} - c_m^{\mathcal{K}} t_i^e\right)\lambda_m^e - \frac{1}{2}\sum_{menf} c_m^{\mathcal{K}} t_{in}^{ef}\lambda_{mn}^{ef}\right)}. \tag{8.15}$$

The simplest possible approximation, then, to EOMIP relative intensities is

$$\frac{I(\mathcal{N})}{I(\mathcal{K})} \approx \frac{c_i^{\mathcal{N}2}}{c_i^{\mathcal{K}2}}, \tag{8.16}$$

and the next simplest approximation is:

$$\frac{I(\mathcal{N})}{I(\mathcal{K})} \approx \frac{c_i^{\mathcal{N}}\left(c_i^{\mathcal{N}} + \sum_{me}\left(c_{im}^{\mathcal{N}e} - c_m^{\mathcal{N}} t_i^e\right)\lambda_m^e\right)}{c_i^{\mathcal{K}}\left(c_i^{\mathcal{K}} + \sum_{me}\left(c_{im}^{\mathcal{K}e} - c_m^{\mathcal{K}} t_i^e\right)\lambda_m^e\right)}. \tag{8.17}$$

One more approach is simply to use the approximations to the transition matrix elements directly, as electron propagator practitioners often use pole strengths to approximate intensities. This procedure is most defensible when the pole strengths are compared to low-incident energy photoelectron spectra.

$$I(\mathcal{N}) \approx c_i^{\mathcal{N}}\left(c_i^{\mathcal{N}} + \sum_{me}\left(c_{im}^{\mathcal{N}e} - c_m^{\mathcal{N}} t_i^e\right)\lambda_m^e\right). \tag{8.18}$$

CHAPTER 9

IMPLEMENTATION

The EOMIP equations have been implemented in the ACESII framework, using the direct product decomposition approach of Stanton, Gauss, and Bartlett. Rather than explicitly forming the matrix defined by equations 3.20 and 3.21, the non-symmetric generalization of the Davidson[24] method developed by Hirao and Nakatsuji[42] for eigenvector extraction has been used. In this approach, matrix-vector products are formed and stored on disk, and only a smaller, projected "mini-matrix" is kept in memory.

It is computationally convenient to form a small matrix in memory and diagonalize it to recover all the eigenvectors and eigenvalues. But in many cases, only a few of these solutions are of interest, and the diagonalization becomes increasingly expensive. Therefore, it is advantageous to use methods in which the matrix to be diagonalized is never formed explicitly, or at least never held in memory, and the matrix is never diagonalized. All of these large matrix methods depend on the fact that the Raleigh quotient of a non-symmetric matrix A

$$\rho(y,x) = \frac{y^{\dagger}Ax}{y^{\dagger}x} \tag{9.1}$$

is stationary with respect to variation of the elements of x and y if and only if these vectors are corresponding left and right eigenvectors of A.

Davidson's method, like many other large matrix methods, uses a variation on the Lanczos method. In both these methods, the nonsymmetric eigenvalue problem

$$AX_i = X_i\lambda_i \tag{9.2}$$

$$Y_i^\dagger A = \lambda_i Y_i^\dagger \tag{9.3}$$

is solved by projecting the nonsymmetric matrix A into a smaller space spanned by a set of trial vectors B. Since the matrix is nonsymmetric, it is formally correct to use two different bi-orthogonal trial spaces, B and L. The projected "minimatrix"

$$M = L^\dagger AB \tag{9.4}$$

$$L^\dagger B = \mathbf{I} \tag{9.5}$$

is diagonalized to yield approximate eigenvalues and eigenvectors which are expansion coefficients to approximate eigenvectors of A

$$D^\dagger MC = d \tag{9.6}$$

$$X_i = \sum_k C_{ik}B_k \tag{9.7}$$

$$Y_i = \sum_k D_{ik}L_k. \tag{9.8}$$

Residual vectors $\mathcal{X}$ and $\mathcal{Y}$ are a measure of the error in the approximate eigenvector. These error vectors are defined to satisfy

$$(A - d_i)(X_i - \mathcal{X}_i) \equiv 0 \tag{9.9}$$

$$(A - d_i)(Y_i - \mathcal{Y}_i) \equiv 0. \tag{9.10}$$

It is the method of approximating the residual vector which characterizes these methods. The Davidson method approximates these as

$$\mathcal{X}_{ji} = (d_i - A_{jj})^{-1}\left[(AX)_{ji} - d_i X_{ji}\right] \tag{9.11}$$

$$y_{ji} = (d_i - A_{jj})^{-1} \left[(A^{\dagger} Y)_{ji} - d_i Y_{ji} \right]. \tag{9.12}$$

These new correction vectors are then bi-orthonormalized and added to the B and L spaces, after which the entire procedure is repeated.

If only the right-hand eigenvectors, X, are required, there is another approach which can be used to save computational time. The right-hand projection space B can be used in place of the L space, and the method becomes almost identical to the symmetric Davidson method except that the algorithm for diagonalization of the minimatrix M must be suitable for nonsymmetric matrices. By the time convergence is reached, B generally spans a space sufficient to represent, to a good approximation, the left-hand eigenvectors of A. In test calculations, these two approaches have been shown to have very similar convergence properties[42].

At each iteration, it is necessary to choose some subset of roots of the minimatrix to be improved. There are several approaches. If one is interested in the N lowest roots of the matrix A, one can simply always choose the lowest roots of the minimatrix. If, however, it is desired to converge directly to higher roots, some other approach must be used.

Because the principal IP eigenvectors are, in almost all cases, dominated by the annihilation of an electron from a single occupied molecular orbital, it is useful to "pre-load" the B space with guess vectors having $C_k^{\mathcal{K}} = 1$ for each root $\mathcal{K}$ desired corresponding to the ionization of the electron in orbital k. Then, at each iteration, those minimatrix roots which are most similar to the original guess vector are chosen for improvement until convergence is reached. Alternatively, those roots which are

most similar to roots saved from the previous iteration can be chosen, but the author has found that the use of this approach can lead to choosing the wrong root, as the desired root may be poorly represented in the first few iterations, and the algorithm may follow several different roots successively, finally settling on an unexpected solution.

Shakeup roots which are characterizable as satellites of a particular principal ionization are still dominated by the annihilation of a single electron, but also contain large contributions from one or several excitations of the ionized species. These solutions are more difficult to characterize for two reasons: 1) it is not always known ahead of time which excitations are most important to the desired shakeups, and 2) even in cases where the important excitations are known, the unoccupied orbitals available from a typical Hartree-Fock calculation in a larger than minimal basis set are not useful in a "molecular orbital" analysis of the system being studied – they have very little correspondence to the orbitals which would be produced in an excited-state or N+1 (or more) electron calculation which occupied portions of the desired orbital space. In this case, it is useful, once the principal root is found, to specify an energy range which removes the principal root from consideration, and then converge all roots found within that range, or impose the additional constraint that chosen roots should have a significant overlap with the principal root of which they are satellites. In the author's experience that first converging the principal roots in question results in a B space containing significant contributions to the space of shakeup roots. Several of these satellites near in energy to the principal may be selected within the first few shakeup iterations, especially in cases where these shakeups are large compared

to the "principal", and the two wavefunctions are similar. In other cases, the author uses other procedures to load the B space with relevant vectors, such as relaxing energy range restrictions for a few iterations, even choosing random vectors.

CHAPTER 10

APPLICATION OF THE EOMIP METHOD TO SMALL MOLECULES

10.1 A Survey of FSCCSD and EOMCCSD Calculations

Table 10.1 is a survey of FSCCSD for the ionization of a range of small molecules. Bernholdt [40] reported results differing by almost zero to approximately .6 eV from experiment for valence ionizations of a range of molecules, mostly in DZP basis sets, mostly at experimental geometries. There are a few general trends.

- Energies in a larger basis at the same geometry are larger.
- DZP ionization energies are generally smaller than experimental energies.
- For well-behaved closed-shell molecules, the first ionization energy, even at the DZP level is generally within .2 eV or so of experiment. A notable exception to this rule is the *s*-tetrazine example.
- In the larger basis sets, there is a trend for higher-energy EOMIP ionizations to be increasingly high relative to their corresponding experimental energies.
- Increasing the basis set size, as in the cases of the Stanton, Bartlett, and Rittby O_2 study and the Pal *et al.* study of formaldehyde, improves agreement with experiment.

Table 10.1: A survey of FSCCSD results

Molecule	Basis	Final State	Energy (eV) Theory	Expt.
CH_2NH	DZP[i]	$^2A'$	10.34	10.52, 10.70, 10.56
		$^2A''$	12.29	12.43, 12.48, 12.44
		$^2A'$	15.08	15.13, 15.11, 15.00
		$^2A'$	17.19	17.04, 17.07, 17.00
s-tetrazine	DZP[h]	$^2B_{3g}$	9.20	9.7
		$^2B_{1u}$	11.87	11.9
		$^2B_{2g}$	12.12	12.1
		^2A_g	12.69	12.8
		$^2B_{2u}$	13.01	13.3
		$^2B_{1g}$	13.52	13.5
H_2CO	$[5s3p1d/2s1p]$[a]	$^2B_2$	10.51	10.88
		$^2B_1$	14.36	14.38
		$^2A_1$	15.75	16.00
H_2CO	$[5s3p/2s]$[d]/	$^2B_2$	10.07[d], 10.43[h]	10.88
	$[5s3p1d/2s1p]$[e]	$^2B_1$	14.14[d], 14.13[h]	14.38
		$^2A_1$	15.20[d], 15.67[h]	16.00
CH_2	DZP[c]	$^2A_1$	10.20	10.26 (DZP-FCI)
		$^2B_2$	14.91	14.85 (DZP-FCI)
		$^2A_1$	22.55	22.14 (DZP-FCI)
CH_2PH	DZP[i]	$^2A''$	10.08	10.30
		$^2A'$	10.28	10.70
		$^2A'$	13.17	13.20
$^3\Sigma_g^-$ O_2	DZP[a]/PVQZ++[g]	$^2\Pi_g$	11.76[a], 12.39[g]	12.35
		$^4\Pi_u$	16.40[a], 16.76[g]	16.85
		$^4\Sigma_g^-$	17.75[a], 18.26[g]	18.33
		$^4\Sigma_u^-$	24.58[a], 24.82[g]	24.66
N_2	$[5s4p1d]$[a]	$^2\Sigma_g$	15.44	15.6[b]
		$^2\Pi_u$	17.14	16.88[b]
		$^2\Sigma_u$	18.64	18.6[b]
ketene	DZP[a]	$^2B_1$	9.40	9.64(a)
		$^2B_2$	14.26	13.84(a)
H_2O	DZP[c]	$^2B_1$	11.97	12.61
		$^2A_1$	14.28	14.73
		$^2B_2$	18.75	18.55
diazomethane	DZP[a]	$^2B_1$	8.60	9.00(a)
		$^2B_2$	13.79	14.13(v)
HF	$[5s3p/3s]$[f]	$^2\Pi$	15.08	16.1
		$^2\Sigma$	19.43	19.9
		$^2\Sigma$	39.75	39.7

[a] Bernholdt [40]; [b] Experimental results [34] [c] Vaval, Ghose, Pal, and Mukherjee [43]
[d] Pal, Rittby, Bartlett, Sinha, Mukherjee [44], $[5s3p/2s]$ basis; [e] *ibid*, $[5s3p1d/2s1p]$ basis
(a) and (v) indicate adiabatic/vertical ionizations of ketene and diazomethane
[f] Sinha et al. [45]
[g] Stanton, Bartlett, and Rittby [46]
[h] Rittby and Bartlett [13]
[i] Watts, Rittby, and Bartlett [47]

These results are encouraging; it is easy to surmise that the EOMIP approach can be applied to a variety of molecules with very good results. In addition, the EOMIP method can be used to examine shake-up states, and is not plagued (as is FSCC) by intruder-state problems in the inner-valence region.

The EOMIP approach is conceptually well suited to the study of ionic spectra, including first, principal, and shakeup ionization energies and intensities. For N_2, for example, there are six molecular orbitals (five σ and one π) to be explored. Using a well-correlated single-state method such as CCSD or CCSD(T) would require one calculation for the neutral N_2, and a separate calculation for each of the N_2^+ states. All the N_2^+ calculations would have to be open-shell, doubling the effective size of the orbital space involved in the SCF and correlated calculations. In addition, it is not easy to obtain a suitable set of molecular orbitals for every open-shell state. While it is a simple matter to remove an electron from the highest-energy orbital of any symmetry, it requires a bit of trickery and a few more SCF iterations to converge on a core-hole state. And it is generally impossible to converge an SCF state with an electron removed from an inner-valence orbital. The QRHF reference, a non-SCF state can be used in this case. There is no reliable way to describe a state corresponding to a shakeup peak, and no way to specify which of the two $2\sigma_g$ nitrogen peaks (table 10.4 and figure 10.1) will be found in this approach. When the EOMIP approach is used, only one CCSD calculation, on the closed-shell state, is required. The EOMIP calculations which follow are considerably less expensive in terms of computer time. And shakeup peaks can be specified in terms of energy ranges and the molecular orbitals with with they are associated. The equation-of-motion

excitation energy (EOMEE) approach can also be used as a route to finding ionization states in the excitation spectrum of N_2^+ species. There are two disadvantages to this approach. First, not all of the desired ionization states can be described primarily as a single excitation from one reference. Multiple references, and thus multiple CCSD calculations must be employed. Secondly, although the linear form of the EOMEE equations makes iteration less computationally demanding than CCSD iterations, EOMEE is still more demanding than EOMIP – there are more amplitudes and more and bigger terms to calculate in EOMEE.

What follows in this chapter is an EOMIP study of the ionization spectra of several well-understood molecules, using large basis sets, with attention to prominent shakeup features. All calculations were performed with the ACES II program system[1] and the author's ACES II-based CC EOMIP program[2].

The EOMIP intensities which appear in this and the following chapter were calculated using the approximation of equation 8.18, except where principal peak intensities have been scaled to experimental intensities, as noted. For the figures, Lorentzian functions were applied to the theoretical transition energy/intensity information in order to simulated the degree of experimentally-observed broadening. In some cases, the experimental curves were also created from available energy/intensity data by

[1]ACES II is a quantum chemical program package especially designed for CC and MBPT energy and gradient calculations. Elements of this package are: the SCF, integral transformation, correlation energy, and gradient codes written by J. F. Stanton, J. Gauss, J. D. Watts, W. J. Lauderdale, and R. J. Bartlett; the VMOL integral and VPROPS property integral programs written by P. R. Taylor and J. Almlöf; a modified version of the integral derivative program ABACUS written by T. Helgaker, H. J. Aa. Jensen, P. Jørgensen, J. Olsen, and P. R. Taylor[48]

[2]CCEOMIP is a quantum chemical program designed to calculate vertical electron detachment energies and intensities, written by Renée Peloquin Mattie. It requires ACES-II CCSD T and $\bar{H}$ lists [49]

application of Lorentzian lineshapes. In the carbon cluster plots, the experimental curves were created by digitization of experimental plots provided by Yang et al[35].

10.2 Unsaturated Molecules

10.2.1 Nitrogen

Nitrogen presented one of the earliest challenges to theoreticians. The ionization energies obtained from Koopmans' theorem are not predictive the observed spectrum, and are in fact incorrectly ordered (table 10.3). Self-consistent field calculations do not order these ionizations properly. Correlated calculations are necessary, and highly correlated calculations are needed to describe the breakdown of the molecular orbital picture in the inner-valence region correctly.

Two basis sets were used in the nitrogen calculations. The smaller basis was based on the triple-zeta plus polarization basis set of Dunning[50], with the innermost p orbital uncontracted, as was used by Rittby and Bartlett[34]. The larger is the Dunning pVTZ+ basis set [51], a polarized-valence triple-zeta basis set which includes diffuse s,p,d and f functions . Here, however, the CCSD optimized internuclear separation, R = 2.0778 was used rather than the experimentally-obtained geometry R = 2.0693 used by Rittby and Bartlett.

In the smaller basis set (table 10.2), results show agreement with experimental results to within .2 eV for the outer-valence region. The $2\sigma_g$ inner valence hole state, however, shows an error of 1.3 eV and the $1\sigma_g$ core hole state is in error by .7 eV.

Table 10.2: N_2 in 5s4p1d basis at $R = 1.09898$ Å

N_2	N_2^+	Reference	EOMIP	(I_{theo})	Exp[a]	
$X\,^1\Sigma_g^+$		RHF -109.358913 au				
	$X\,^2\Sigma_g^+$	$3\sigma_g$	15.376 eV		15.5 eV	
	$^2\Pi_u$	$1\pi_u$	17.022 eV		16.8 eV	
	$^2\Sigma_u^+$	$2\sigma_u$	18.607 eV		18.6 eV	
					25.0 eV	(shakeup)
					28.2 eV	(shakeup)
					31.5 eV	(shakeup)
	$^2\Sigma_g^+$	$2\sigma_g,\ 1\bar{\pi}_g^\dagger 1\bar{\pi}_u 2\sigma_u$	32.153 eV	(.5[b])		
	$^2\Sigma_g^+$	$2\sigma_g$	38.616 eV	(1.0[b])	37.3 eV	
	$^2\Sigma_g^+$	$2\sigma_g,\ 5\bar{\sigma}_g^\dagger 3\bar{\sigma}_g 3\sigma_g$	42.543 eV	(.2[b])		
	$^2\Sigma_g^+$	$1\sigma_g$	410.623 eV		409.9 eV	

[a] Banna and Shirley [52]

[b] Simple approximation relative to $2\sigma_g$ principal

Moving the the larger pVTZ+ basis seems to afford no improvement of the valence and core peaks, in fact shifting each peak toward higher energies by an amount which increases with the transition energy. As shown in table 10.3, the valence σ_g and σ_u holes are still within .2 eV of experiment, but the energy of the $1\pi_u$ hole seems to have gotten worse – it is not quite within .5 eV of experiment. However, the inner valence region is now much more similar to the experimental spectrum. The inner valence $2\sigma_g$ hole ionization is characterized experimentally by a fairly broad peak, relative to the outer valence or core ionization. In this region, the simple MO picture breaks down, and it is difficult to speak of a single line corresponding to the ejection of the $2\sigma_g$ electron. The calculations show two lines of similarly large intensity, one near 33 and one near 39 eV. Vibrational and vibronic effects can be expected to be quite strong in this region [31] as well.

Table 10.3: N_2, pVTZ+ basis

Ionization energy eV (Intensity)							
Koop.	EOMIP				Other[a]	Exp	Orbital
approx	CLOSED		CORE				Assignment
17.277	15.683	(.931)	15.499	(.880)	15.666[b]	15.5	$3\sigma_g$
16.793	17.332	(.958)	17.159	(.918)	17.227	16.8	$1\pi_{ux}$
16.793	17.332	(.961)	17.159	(.964)	17.227	16.8	$1\pi_{uy}$
21.147	18.888	(.895)	18.674	(.858)	18.908	18.6	$2\sigma_u$
						25.0	
—	29.887	(.02)	28.917	(.026)		28.2	$2\sigma_u$, $2\pi_g^\dagger 3\sigma_g 1\pi_u$
—	32.679	(.320)	31.983	(.284)	29.0734	31.5	$2\sigma_g$, $2\pi_g^\dagger 2\sigma_u 1\pi_u$
—	33.319	(0.004)					$1\pi_u$, $3\pi_g^\dagger 1\sigma_u 3\sigma_g$
40.189	38.695	(.518)	38.106	(.470)		37.3	$2\sigma_g$
—	39.307	(.002)					$2\sigma_g$, $4\sigma_g^\dagger 3\sigma_g 3\sigma_g$
—	42.400	(.034)					$2\sigma_g$, $4\overline{\sigma}_g^\dagger 3\overline{\pi}_u 3\pi_u$
—	42.519	(.001)					$2\sigma_g$, $5\overline{\sigma}_g^\dagger 3\overline{\sigma}_g 3\sigma_g$
—	43.030	(.045)					$2\sigma_g$, $2\overline{\pi}_u^\dagger 3\overline{\sigma}_g 2\pi_u$
—	43.461	(.067)					$2\sigma_g$, $4\overline{\sigma}_g^\dagger 3\overline{\pi}_u 3\pi_u$
—	44.566	(.067)					$2\sigma_g + 3\sigma_g$, $2\overline{\pi}_u^\dagger 1\overline{\pi}_u 3\sigma_g$
—	45.452	(.001)					$2\sigma_u$, $6\overline{\sigma}_u^\dagger 1\overline{\pi}_u 1\pi_u$
—	46.919	(.005)					$2\sigma_u$, $5\overline{\sigma}_u^\dagger 3\overline{\sigma}_g 3\sigma_g$
426.723	410.587	(.806)	409.609	(.753)		409.9	$1\sigma_u$
426.623	410.768	(.807)	409.799	(.755)			$1\sigma_g$

[a] EOMEE, except where otherwise noted

[b] ΔCCSD

In the plots in figure 10.1, Lorentzian lineshapes have been applied to the EOMIP peaks to simulate the line broadening found in low-resolution experimental spectra. Each EOMIP plot is superimposed on a plot of an experimentally-derived photoemission spectrum based on MgKα [52] and YMζ [53] experiments. Peak positions were taken from the YMζ experiment (at 1253.6 eV), which provided much better resolution in the region between 20 and 45 eV, while relative peak intensities were taken from the MgKα experiment (at 132.3 eV) , which is more suitable for comparison to EOMIP intensities, as they should most resemble threshold photodetachment intensities.

The simulated spectra in figure 10.1 indicate a good match between the experimental peaks at 28.2 and 31.5 eV and the $2\sigma_u$ peaks at 29.9 and 32.7 eV with pVTZ+ closed shell orbitals and 28.9 and 31.9 eV with pVTZ+ core hole orbitals. The core hole orbitals give somewhat better agreement over the entire spectrum, especially at higher energies. In the inner-valence region and for the core peaks, improvement becomes notable, as seen in table 10.5 No peaks were found which can reasonably be assigned to the 25.0 eV experimental peak. Schirmer, Cederbaum, Domke, and von Niessen, in their 1977 paper, saw a peak right at 25 eV, but they were using a much smaller basis set (11s 7p/5s 3p), which is lacking in polarization functions compared to the pVTZ+ (11s 6p 3d 2f/5s 4p 3d 2f). The author's experience and that of others indicates that this means some larger shakeup peaks in the smaller basis set, and Schirmer *et al.* show more shakeup peaks than are perhaps indicated by the experimental spectra, making a doublet-with-a-shoulder of the 37 eV $2\sigma_g$ ionization, and giving them a significant $2\sigma_g$ peak at about 40 eV, similar to the appearance of

Table 10.4: Summary of N_2 EOMIP ionization calculations

	Energies eV		
5S4P1D	*p*VTZ+		
	C.S.	C.H.	Exp
15.376	15.683	15.499	15.5
17.002	17.332	17.159	16.8
18.607	18.888	18.674	18.6
			25.0
	29.887	28.917	28.2
32.153	32.679	31.983	31.5
	33.319		
38.616	38.695	38.106	37.3
	39.307		
	42.400		
	42.519		
	43.030		
	43.461		
	44.566		
	45.452		
	410.587	409.609	409.9
410.623	410.768	409.799	

Table 10.5: N_2 EOMIP error, 5s4p1d and *p*VTZ+ bases. Energies and errors are in eV.

Expt.	5s4p1d	*p*VTZ+	
		closed	core
15.5	-0.1	0.2	0.0
16.8	0.2	0.5	0.4
18.6	0.0	0.3	0.1
28.2	—	1.0	0.7
31.5	0.6	1.2	0.4
37.3	1.3	1.4	0.8
409.9	0.7	0.8	0.2

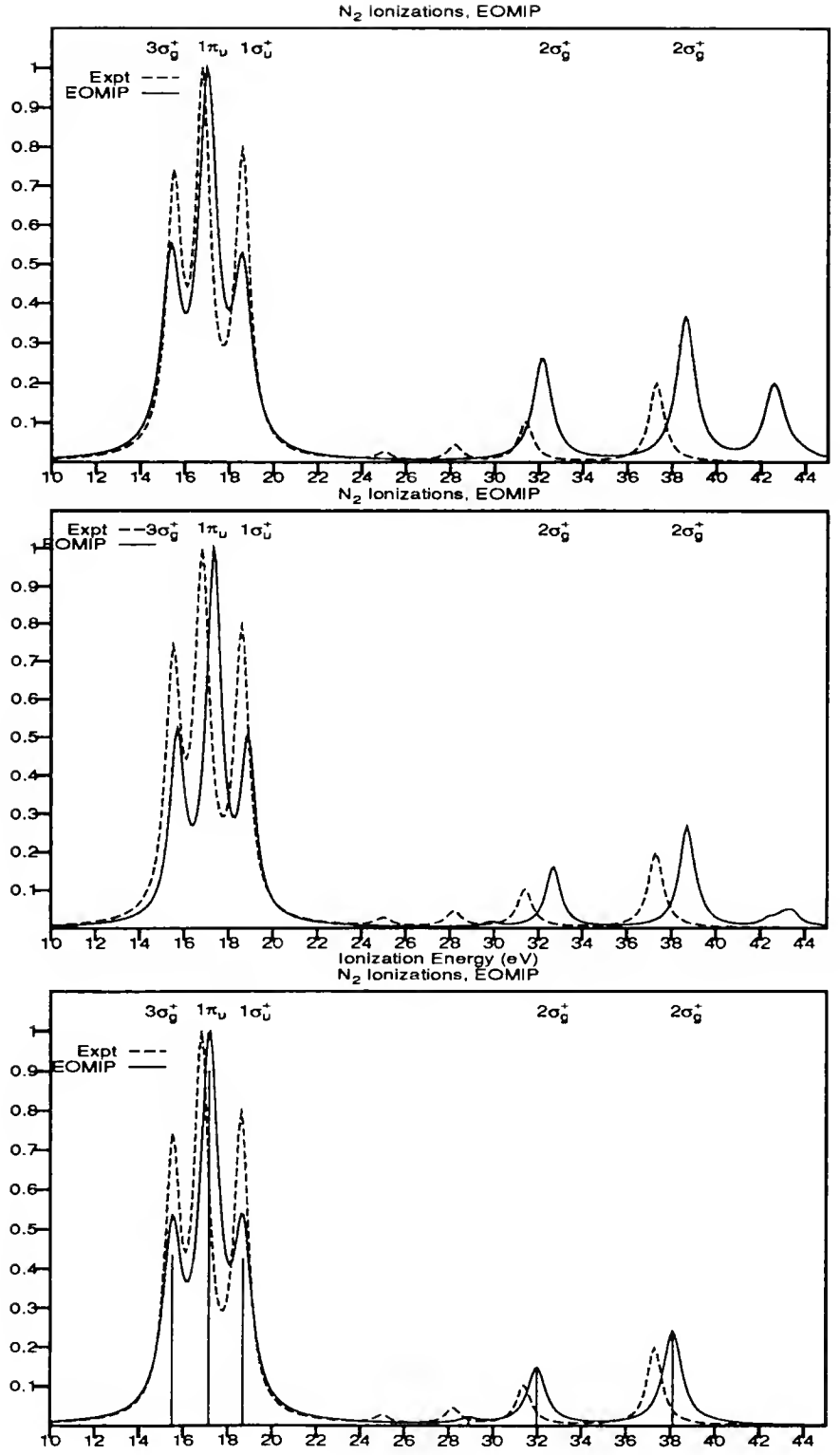

Figure 10.1: N2 ionizations in three MO sets

significant EOMIP peak at 38.6 eV when the 5s4p1d basis is used. This region shows much less intensity in the pVTZ+ closed-shell or core-hole orbital calculations, in agreement with experiment. In the core-hole orbital set, the largest of the $2\sigma_g$ peaks has moved .8 eV closer to the experimental peak, while its companion peak has moved .3 eV closer to experiment and the ratio of the two peaks is more similar to that in the experimental spectrum. In the core region, the $1\sigma_u$ and $1\sigma_g$ peaks have both moved slightly closer to the experimental value. In general, the energies of all the major peaks are reduced in the core-hole basis, moving closer to experiment. Interestingly, core-hole orbitals do not improve the performance of EOMIP by decreasing the size of correlation corrections to the wavefunction. The sizes of the EOMIP doubles contributions in the two cases are similar, although there is some difference in the ordering of these contributions because the largest T1 amplitudes are approximately twice as large (.075 versus .015) in the core-hole as in the closed-shell basis.

10.2.2 Ethylene

Ethylene has been studied in two different basis sets – Nakatsuji's Basis I[54] and the Dunning pVTZ+ basis[51]. In the smaller basis, the Herzberg[55] ground state geometry was used and relative intensities were calculated using the simple approximation of equation 8.16. For the larger basis set study, the geometry was optimized at the CCSD level in the pVTZ basis set, and the improved approximation to relative intensities from equation 8.17 was used.

The inner- and outer-valence region of the ethylene ionization spectrum has been studied before, with an eye toward the assignment of the strong satellite peak at 27.4 eV[6, 28, 56, 54]. The valence ionizations, as well as the strongest of the related shake-ups, are given in table 10.6 along with the experimental numbers and the theoretical results of Nakatsuji in the same basis set. The outer-valence results show excellent agreement with experiment, while the inner-valence principle peak at $\approx$ 24 eV, like the SAC-CI, appears at a slightly higher energy. The shakeup at 27.4 eV appears in the experimental spectrum as a strong, somewhat broad satellite. Cederbaum[56] implies that this peak should be assigned to a $2a_g$ shakeup, and in this Davidson[28] concurs. Nakatsuji attributes this peak to a sum of the nearby $1b_{2u}$ and $2b_{1u}$ shake-ups. The difference in the ordering of the $1b_{2u}$ and $2a_g$ peaks just below the the experimental peak is puzzling for two methods which are apparently so similar, but there are several other theoretical shakeup peaks with very small intensity in the same region. It would seem that the nearby $2a_g$ shakeup is another likely candidate.

It is interesting to note that both Cederbaum and Davidson report significantly greater relative intensities for the shakeup peaks than have been obtained from either the EOMIP or SAC-CI calculations. Davidson has noted that the satellite intensities decreased as the virtual space size was increased, so that the addition of Rydberg orbitals to relatively small basis sets such as the Nakatsuji basis I could be a significant effect.

To clear up some of the questions raised, the study was repeated using the larger, Dunning pVTZ+ basis[51], which includes more diffuse s,p,d and f functions. The pVTZ, CCSD optimized geometry is R_{CC} = 1.327Å, R_{CH} = 1.077Å,

Table 10.6: Ionization spectrum of ethylene, 10-30 eV

Ionization energy eV (Intensity)				
EOMIP		SAC-CI[a]	Experiment[b]	Orbital Assignment
*p*VTZ+	BASIS I			
10.72 (.95)	10.39 (.95)	10.25 (.95)[c]	10.51 (.95)	$1b_{3u}$
13.14 (.93)	12.85 (.93)	12.78 (.93)[c]	12.85 (.93)	$1b_{3g}$
14.97 (.92)	14.59 (.92)	14.50 (.92)[c]	14.66 (.92)	$3a_g$
16.37 (.88)	16.03 (.88)	15.93 (.88)[c]	15.87 (.88)	$1b_{2u}$
19.65 (.85)	19.36 (.85)	19.32 (.85)[c]	19.1 (.85)	$2b_{1u}$
24.52 (.007)	23.55 (.008)	23.45 (.01)		$2b_{1u}$, $2b_{2g}^{\dagger}1b_{3u}1a_g$
24.51 (.74)	24.25 (.74)	24.37 (.74)[c]	23.7 (.74)	$2a_g$
		25.86 (.04)		$1b_{2u}$, $2b_{2g}^{\dagger}1b_{3g}1b_{3u}$
	26.13 (.015)			$2a_g$, $7a_g^{\dagger}1b_{3u}1b_{3u}$
	26.16 (.052)			$1b_{2u}$, $3b_{2g}^{\dagger}1b_{3g}1b_{3u}$
26.73 (.052)				$1b_{2u}$, $2b_{2g}^{\dagger}$ $1b_{3g}$ $1b_{3u}$
26.81 (.006)		26.97 (.01)		$2a_g$, $5a_g^{\dagger}$ $1b_{3u}1b_{3u}$
			27.4 (.29)	
28.18 (.001)				$2b_{1u}$, $3b_{1u}^{\dagger}$ $1b_{3u}$ $1b_{3u}$
28.6 (.017)				$2a_g$, $7a_g^{\dagger}$ $1b_{3u}1b_{3u}$
29.26 (.044)				$2b_{1u}$, $2b_{2g}^{\dagger}$ $3a_g$ $1b_{3u}$
	29.76 (.010)	29.28 (.02)		$1b_{3g}$, $2b_{2g}^{\dagger}$ $1b_{2u}$ $1b_{3u}$
30.03 (.012)				$1b_{3g}$, $3b_{3g}^{\dagger}$ $1b_{3u}$ $1b_{3u}$
	30.06 (.094)			$2a_g$, $1b_{2g}^{\dagger}$ $1b_{3u}$ $2b_{1u}$
		30.15 (.09)		$2a_g$, $6a_g^{\dagger}$ $1b_{3u}1b_{3u}$, $2b_{2g}^{\dagger}$ $2b_{1u}$ $1b_{3u}$
30.77 (.075)				$2a_g$, $2b_{2g}^{\dagger}$ $2b_{1u}$ $1b_{3u}$
			31.2 (.1)[d]	

[a] Nakatsuji [54]

[b] Banna and Shirley [52], Gelius [57]

[c] Theoretical intensities of principal peaks scaled to experimental data

[d] Energy and intensity from Weigold [58]

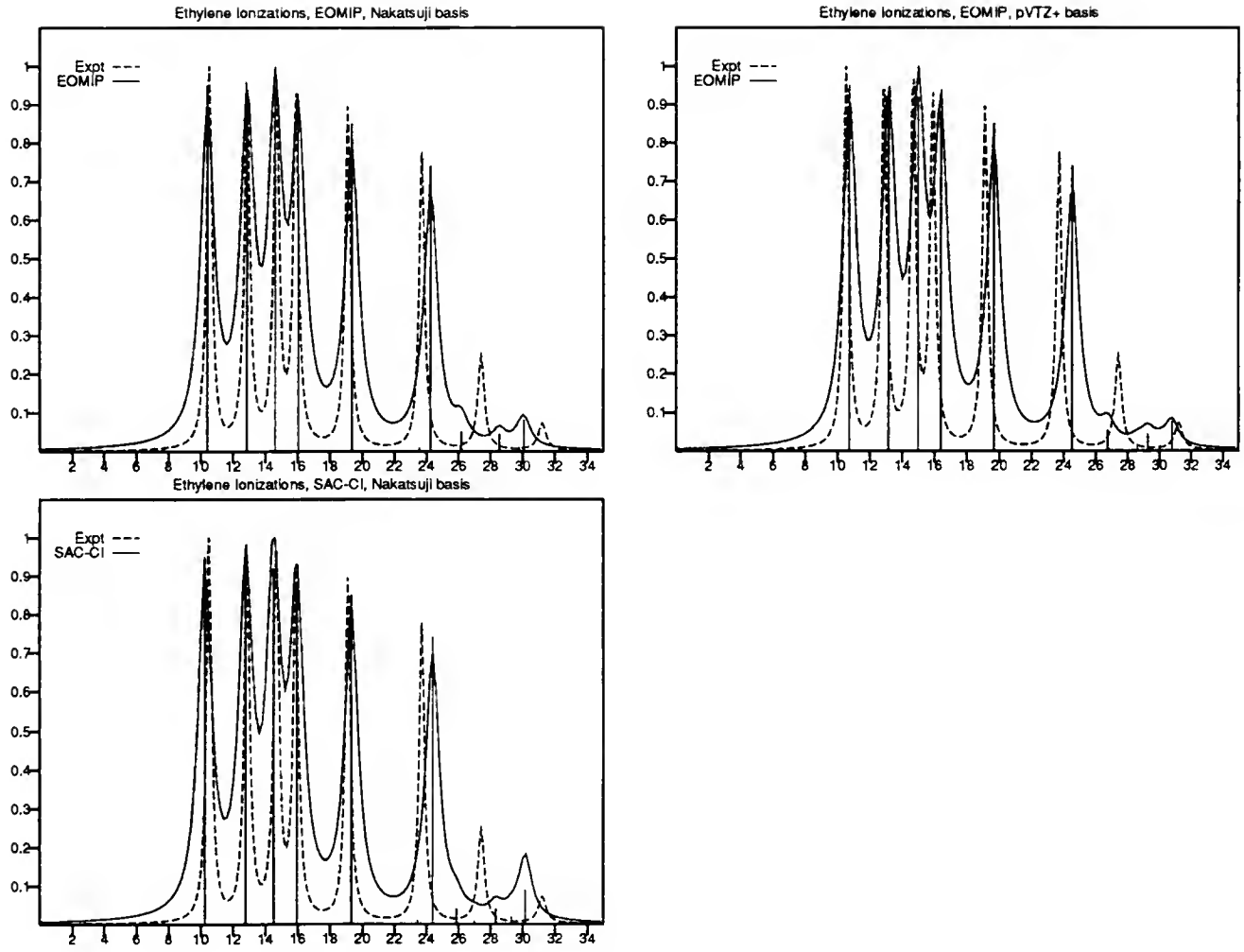

Figure 10.2: EOMIP and SAC-CI ionization spectra of ethylene

$\angle_{HCH} = 121.459°$. The virtual space is significantly larger, but the diffuse functions less so than those in the Rydberg-supplemented basis used by Nakatsuji. It was anticipated that this basis set would represent an improvement over the smaller basis and, since ethylene is well represented at the CCSD level of theory, the end result would be improved ionization energies. Instead, what is observed is a spectrum of ionized functions which are generally similar to those obtained in the smaller basis (allowing for the presence of diffuse orbitals in the low-lying virtual space), but with ionization energies which grow progressively larger than the experimental energies and those calculated in the smaller basis.

A small study of the effects of basis set choice and orbital relaxation on the $3a_g$ ionization (table 10.7) reveals that removing the diffuse functions or replacing them with Nakatsuji's molecule-centered Rydberg set has little discernible effect on the ionization energies calculated by the CCSD, CCSD(T), or EOMIP methods. It is apparent, however, that orbital relaxation is an important effect. The ΔCC (QRHF calculations for the cation) and EOMIP results in the C_2H_4 orbitals over-estimate the energy by about .19 to .34 eV, while in the $C_2H_4^+$ ROHF orbitals, ΔCC (QRHF calculations for the neutral) methods actually underestimate the energy by over 1 eV, and the EOMIP overestimates it by a similar amount. In the more natural calculation – both neutral and cation correlated calculations are based on the appropriate SCF calculation – both of the CC methods perform well, within .2 eV of experiment in either basis set. The problem for the CC calculations is apparently in large part one of orbital relaxation. Neither set of orbitals provides a reasonable starting point for both the neutral and the cation. The coupled-cluster triples correction can hardly be

said to be much help in improving either of the semi-QRHF calculations. In the pVTZ closed-shell orbitals, triples lower the energy of the neutral by .42 and the cation by .38 eV. In the pVTZ cation orbitals, triples lower the neutral by .47 and the cation by .44 eV.

Table 10.7: Effect of orbital choice on ethylene $3a_g$ ionization

basis	MOs	Energy eV		
		ΔCCSD	ΔCCSD(T)	EOMIP
pVTZ	C_2H_4	14.846	14.877	14.935
	$C_2H_4^+$	13.458	13.486	15.902
	MIXED	14.879	14.855	
pVTZ	C_2H_4	14.847	14.880	14.936
+Rydberg	$C_2H_4^+$	13.669	13.752	15.886
	MIXED	14.881	14.858	
Basis I	C_2H_4	14.610	14.627	14.686
	$C_2H_4^+$	13.491	13.533	15.660
	MIXED	14.640	14.604	

[a]ROHF performed with $3a_g$ orbital half filled.

[b]Neutral in Neutral orbitals, cation in ROHF orbitals

The difference between the ΔCC and EOMIP calculations in either set of orbitals are largely attributable to spectator triples – excitations which are CC doubles but EOMIP triple excitations. In the CCSD calculation on the neutral in these orbitals, there is a large T_2 amplitude (-.14272) describing the excitation of both $1b_{1u}$ (π_{CC}) HOMO electrons to a $1b_{2u}$ (π^*_{CC}) orbital, followed by another double excitation π to π^*(-.05468). The EOMIP wavefunction is dominated by the annihilation of the $3a_g$ electron, with other contributions from the $\pi \rightarrow \pi^*$ double excitation, followed by a single excitation from the $1b_{3u}$ HOMO to the $2b_{3u}$ virtual orbital and one from the

$1b_{2u}$ to $2b_{2u}$, giving a wavefunction dominated by the action of

$$-.143\ 2b^{\dagger}_{2g}2\overline{b}^{\dagger}_{2g}1b_{3u}1\overline{b}^{\dagger}_{3u}3a_g + .0953\ 2b^{\dagger}_{3u}1b_{3u}3a_g + .0839\ 2b^{\dagger}_{2u}1b_{2u}3a_g.$$

For the cation in these orbitals, the largest amplitude is again the T_2 providing the double excitation from the $1b_{3u}$ π_{CC} bonding HOMO to the $2b_{3u}$ π_{CC} anti bonding orbital, followed by a double excitation from the bonding to the anti bonding orbital, combined with an excitation from the half-full $3a_g$ orbital to the empty $4a_g$

$$(-.127\ 2b^{\dagger}_{2g}2\overline{b}^{\dagger}_{2g}1b_{3u}1\overline{b}^{\dagger}_{3u} - .0701\ 3a^{\dagger}_{g}2b_{1u}2\overline{b}^{\dagger}_{2g}1\overline{b}_{3u} - .0547\ 2b^{\dagger}_{2g}3\overline{b}^{\dagger}_{2g}1b_{3u}1\overline{b}^{\dagger}_{3u})3a_g$$

It is the second term here that is missing from the EOMIP wavefunction expression above, where it contributes as a T_2 * C_1 term, and has an amplitude of less than .001 relative to the principal ionization. EOMIP-SD has no way to recover this determinant. Strangely enough, the same phenomenon is observed in the C_2H_4 orbitals, but the effect on the energy is not nearly as large. The ΔCC results are much closer to the "mixed" results (around .2 eV) and the EOMIP is closer as well (within .1 eV of the ΔCCSD, and within .3 eV of either "mixed' result).

In Nakatsuji's Basis I, the very same kind of behavior is again observed. In the closed-shell orbitals, the largest contributors to EOMIP wavefunction are

$$3\overline{a}_g + .098\ 3b^{\dagger}_{3u}1b_{3u}3\overline{a}_g + .0531\ 4\overline{b}^{\dagger}_{2g}1\overline{b}_{3u}3b^{\dagger}_{2g}1b_{3u}3\overline{a}_g - .0525\ 3b^{\dagger}_{2g}1b_{3u}3\overline{a}_g - .0489\ 4b^{\dagger}_{2u}1b_{2u}3\overline{a}_g,$$

while the largest contributors to $C_2H_4^+$ CCSD wavefunction are

$$3\overline{a}_g + .143\ 3\overline{b}^{\dagger}_{2g}1\overline{b}_{3u}3b^{\dagger}_{2g}1b_{3u}3\overline{a}_g - .103\ 3b^{\dagger}_{3u}1b_{3u}3\overline{a}_g - .078\ 2b^{\dagger}_{3u}1b_{3u}3\overline{a}_g - .076\ 1b^{\dagger}_{2g}3a_g2\overline{b}_{1u}.$$

The first three determinants are the same in either case, but with very different relative weights. Still, the EOMIP energy is very slightly closer to the ΔCCSD energy

than is the case in the pVTZ basis, with or without Rydberg orbitals. Going from the small BASIS I to the larger pVTZ basis lowers the energy of the closed-shell ethylene more than it does the cation, which means that all the calculated ionization energies are lower in the Nakatsuji basis. The ΔCC energies in the closed-shell orbitals are actually below the experimental value of 14.66 eV, and the EOMIP value is a very good match to experiment.

Because Nakatsuji's basis I lowers C_2H_4 ionization energies relative to more complete basis sets it manages, without improving the agreement between EOMIP and ΔCC methods, to provide a very good match between SAC-CI or CC EOMIP calculations and the experiment.

10.2.3 Butadiene

As the experimental spectrum in figure 10.3 indicates, there is noticeably more complexity in the butadiene than in the ethylene valence spectrum. The broadening of the peaks in the region above 20 eV indicates the possibility of shakeup peaks as well as the onset of shake-off effects – double ionizations. Because the PS (photoemission spectroscopy) experiment was performed in the x-ray region, at 1487 eV, the experimental intensities are not directly comparable to those obtained using the formula in equation 8.18. However, there appears to be good correlation between the positions of experimental and theoretical peaks. The tendency of higher energy peaks to be increasingly higher in energy than experiment is consistent with the trends observed at this level of theory for large basis sets with several polarization functions.

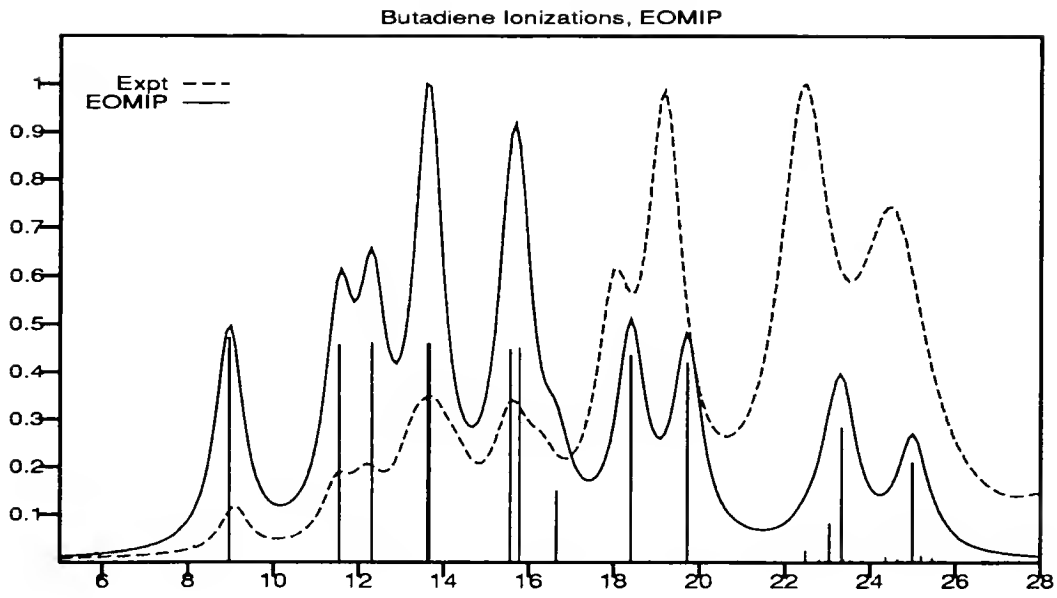

Figure 10.3: Ionization spectrum of 1,3 *trans*-butadiene
Simulated experimental spectrum from 1487 eV XPS, reference [59]. Theoretical peaks are convoluted with Lorentzian functions with FWHM of 1eV.

Table 10.8: Ionization of 1,3 *trans*-butadiene, DZP+sp basis. Energies reported in eV

EOMIP	Expt	Orb
8.968 (0.946)	9.09 (0.06)	1bg
11.552 (0.917)	11.49 (0.07)	1au
12.320 (0.925)	12.19 (0.09)	7ag
13.621 (0.925)	13.29 (0.11)	6bu
13.675 (0.920)	13.76 (0.13)	6ag
	14.29 (0.07)	
15.573 (0.897)	15.59 (0.17)	5ag
15.786 (0.904)		5au
16.651 (0.298)	16.29 (0.08)	1au
18.396 (0.873)	18.00 (0.33)	4bu
18.854 (0.007)		1bg
19.724 (0.839)	19.19 (0.64)	4ag
19.816 (0.005)		4bu
20.903 (0.007)		2ag
21.479 (0.003)		4bu
21.796 (0.003)		5ag
22.172 (0.003)		4bu
22.483 (0.047)		3bu
22.892 (0.004)		1bg
22.974 (0.009)		3ag
23.052 (0.161)		3bu
23.191 (0.004)		3bu
23.191 (0.002)		3ag
23.335 (0.567)	22.44 (0.93)	3bu
23.374 (0.016)		5ag

EOMIP	Expt	Orb
23.537 (0.011)		3bu
23.678 (0.006)		3ag
23.807 (0.007)		3bu
22.815 (0.012)		3bu
23.808 (0.007)		3bu
23.888 (0.005)		4ag
24.366 (0.020)		5bu
24.367 (0.002)		1au
24.640 (0.012)		2bu
24.687 (0.009)		3ag
24.696 (0.001)		1au
24.944 (0.003)		3bu
24.991 (0.419)	24.53 (1.00)	3ag
25.061 (0.006)		3bu
25.194 (0.026)		3bu
25.447 (0.019)		3ag
25.501 (0.007)		1au
25.527 (0.002)		3ag
25.660 (0.001)		3ag
25.728 (0.008)		3ag
	28.29 (0.13)	
293.332 (0.809)		2ag
293.332 (0.809)		2bu
293.707 (0.816)		1bu
293.731 (0.816)		1ag

One interesting feature of this conjugated molecule is the relatively large shakeup peak which appears among strong principal ionization at 16.65 eV. This does not occur in the case of ethylene (section 10.2.2), where the first strong shakeup appears slightly higher in energy than all the valence principal peaks. In addition, the ethylene peak shakeup is a $1b_{2u}$ satellite of a peak more than 10 eV lower in energy, and has an intensity less than 6% that of the principal peak. The butadiene $1a_u$ shakeup, however, appears only 5 eV above, and has an intensity nearly a third that of the principal. Lisini, Fronzoni, and DeCleva [60] do not find this strong shakeup using the 2h1p CI method.

There are a couple of noticeable discrepancies between the experiment and theory. Keane *et al.* find 3 peaks in the structure centered around 14 eV, and two in the structure near 16 eV. The EOMIP calculation gave only two peaks near 14 eV, and 3 near 16 eV. Of the three near 16 eV, the EOMIP peak at 16.65 appears to be assignable to the experimental 16.29 eV peak, leaving the pair at 15.57 and 15.79 eV to be assigned to the 15.59 eV experimental peak. The nearly-degenerate pair at about 13.6 eV can be assigned to the experimental structure centered around the 13.76 eV peak. These are all strong principal ionizations, as evidenced by the pole strengths given in table 10.8, and it is difficult to conceive of the energies being improperly ordered at this level of theory. The energy is too low for double ionization processes to play an important role. The only remaining possibility is that of relatively strong shakeup peak in near 14 eV. Still, this would not account for the "extra" peak found in the EOMIP calculation near 16 eV. A lower-energy, UPS (ultraviolet photoemission spectroscopy) experiment or an electron momentum experiment would give different

relative intensities between states of different symmetries, yielding more information about the composition of these two structures.

10.3 Saturated Molecules

10.3.1 Ammonia

ACESII calculations on NH_3 are carried out in the C_s symmetry point group, the largest Abelian subgroup of the full C_{3v} point group to which NH_3 belongs. The C_{3v} electronic configuration is written as $1a_1^2 2a_1^2 1e^4 3a_1^2$, while the computational C_s configuration is $1a'^2 2a'^2 1a''^2 3a'^2 4a'^2$, where the degenerate pair ($2a'$, $1a''$) is equivalent to the $1e$ orbital in the C_{3v} representation.

Table 10.9: NH_3 EOMIP error vs. experiment

Expt.	EOMIP	Expt.	EOMIP
10.85	0.05	27.6	0.30
16.50	0.16		

The calculated outer-valence EOMIP energies (10.94 and 16.62 eV) are in good agreement with experimental results (10.85 and 16.5 eV, references [61, 62, 63]). The experimental peak at 27.6 eV is matched to .3 eV by the EOMIP result of 27.91 eV, and the shakeup roots on the high-energy end of this peak are in qualitative agreement with the "tail" on the experimental peak. The researchers in reference [61] fit the shape of this undulating tail to 4 wide Lorentzian lineshapes (see table 10.10).

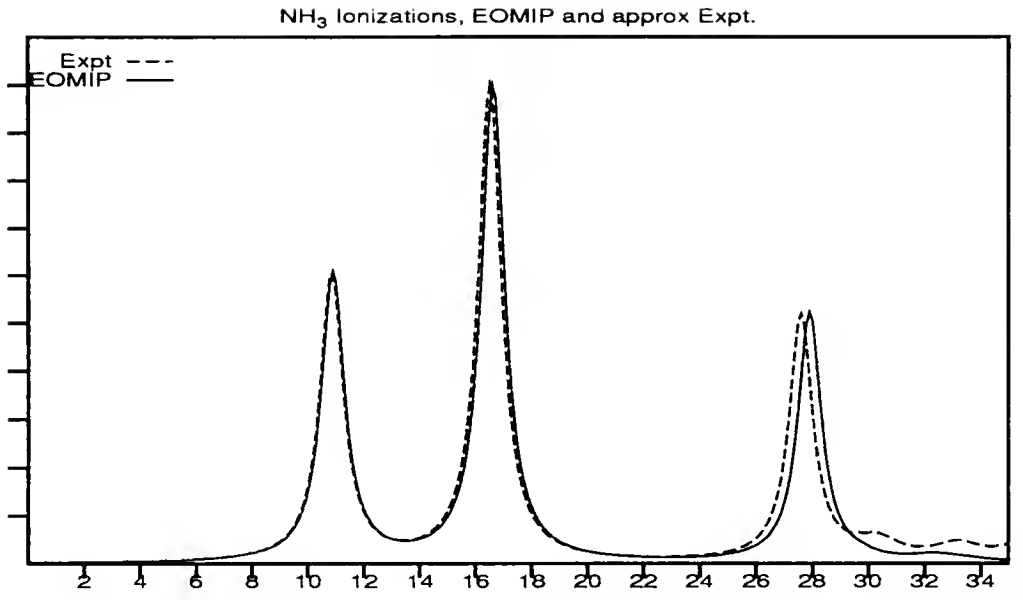

Figure 10.4: NH_3 Ionization Spectrum. Lorentzian lineshapes applied to reported experimental energies and intensities.

In the current study, the structure found in this region was qualitatively similar in appearance but smaller in intensity.

The trend of higher-energy ionizations to be progressively further from the experimental values is consistent with results for ethylene and N_2 (section 10.2).

10.3.2 Water

Compared to ammonia, water shows a much richer inner-valence structure, with several shakeup peaks surrounding the inner valence peak structure between 32 and 35 eV. The EOMIP calculation shows good agreement with experiment in the valence region, including the $2a_1$ shakeup peaks, but does not reproduce the amount of intensity in the weak satellites near 27 and 38 eV. Bawagan and Davidson, in reference [64], found more shakeup intensity, using a 109 Gaussian function basis and a 2h1p CI

Table 10.10: NH_3, pVTZ+ basis

Energy eV (Intensity) EOMIP	Experiment[a]	Orbital Assignment
10.902(.941)	10.85(.956)	$4a'$
16.616(1.56)	16.5 (1.58)	1e
27.907(.813)	27.6(.813)	$2a'$
29.709(.009)		$2a'$ $8\overline{a}'^{\dagger}3\overline{a}'3a'$
	30.3(.13)	
30.628(.0005)		$2a'$ $10\overline{a}'^{\dagger}3\overline{a}'3a'$
32.361(.003)		$1a'$ $7\overline{a}'^{\dagger}3\overline{a}'3a'$
	33.2(.11)	
33.453(.016)		$2a'$ $7\overline{a}'^{\dagger}3\overline{a}'3a'$,
33.639(.0005)		$1a''$ $8\overline{a}'^{\dagger}1\overline{a}''4a'$
35.252(.0002)		$1a''$ $3\overline{a}''^{\dagger}4\overline{a}'4a'$
34.631(.0002)		$1a''$ $3\overline{a}''^{\dagger}4\overline{a}'4a'$
35.074(.0004)		$1a''$ $(10\overline{a}'^{\dagger}1\overline{a}''4a' - 3\overline{a}''^{\dagger}3\overline{a}'4a')$
	35.5(.11)	
37.595(.0008)		$1a''$ $8\overline{a}\prime^{\dagger}1\overline{a}''3a'$
37.939(.0003)		$1a''$ $(3\overline{a}''^{\dagger}4\overline{a}'3a' + 9\overline{a}'^{\dagger}4\overline{a}'1a'')$
	41.8(.08)	

[a] Davidson et al. [61]

Table 10.11: H_2O EOMIP error vs. experiment

Expt.	EOMIP	Expt.	EOMIP
12.61	0.00	32.30	0.46
14.73	0.13	34.90	0.19
18.55	0.38	539.70	1.36

Table 10.12: Ionization of H_2O

Koopmans' theorem	Ionization energy eV (Intensity) EOMIP		Exp		Orbital Assignment
13.884	12.609	(.940)	12.61	(1.0)	$1b_1$
15.935	14.858	(.940)	14.73	(0.8)	$3a_1$
19.432	18.925	(.950)	18.55	(0.6)	$1b_2$
			27.0	(0.02)	
36.786	32.760	(.707)	32.30	(0.44)	$2a_1$, $5\overline{a}_1^\dagger 1\overline{b}_2 1b_2$
—	35.092	(.160)	34.90	(0.15)	$2a_1$, $5\overline{a}_1^\dagger 1\overline{b}_2 1b_2$
—	37.828	(.006)			$2a_1$, $5\overline{a}_1^\dagger 1\overline{a}_1 1a_1$
			37.8	(0.078)	
—	40.421	(.007)			$2a_1$, $2\overline{b}_2^\dagger 3\overline{a}_1 1b_2$
—	40.609	(.001)			$8\overline{a}_1^\dagger 1\overline{b}_2 1b_2$
—	41.524	(.001)			$2\overline{b}_2^\dagger 1\overline{b}_2 3a_1$
—	41.759	(.002)			$7\overline{b}_1^\dagger 3\overline{a}_1 1b_1$, $2a_1$
—	44.758	(.001)			$2\overline{b}_1^\dagger 1\overline{b}_2 1b_2$, $2a_1$
—	45.117	(.0007)			$4\overline{a}_1^\dagger 1\overline{b}_2 1b_2$, $3a_1$
—	45.496	(.001)			$8\overline{a}_1^\dagger 1\overline{b}_2 1b_2$, $2a_1 + 3a_1$
—	46.348	(.003)			$7\overline{a}_1^\dagger 3\overline{a}_1 3a_1$, $2a_1 + 3a_1$
—	46.749	(.001)			$7\overline{a}_1^\dagger 3\overline{a}_1 3a_1$, $3a_1$
—	47.077	(.012)			$5\overline{a}_1^\dagger 3\overline{a}_1 3a_1$, $3a_1$
—	47.256	(.002)			$3\overline{b}_1^\dagger 3\overline{a}_1 1b_1$, $3a_1$
—	48.713	(.003)			$3\overline{b}_1^\dagger 1\overline{b}_1 3a_1$, $2a_1$
—	48.728	(.002)			$9\overline{a}_1^\dagger 1\overline{b}_2 1b_2$, $2a_1$
—	49.243	(.0004)			$8\overline{a}_1^\dagger 3\overline{a}_1 1a_1$, $2a_1 - 3a_1$
—	50.069	(.001)			$2b_1^\dagger 3a_1 1b_1$, $3a_1$
—	50.119	(.003)			$10a_1^\dagger 3b_2 3b_2$, $2a_1$
—	50.936	(.0004)			$5a_1^\dagger 3b_1 3b_1$
—	51.077	(.0004)			$4b_2^\dagger 3a_1 1b_2$
559.638	541.062	(.830)	539.7		$1a_1$, $42a_1^\dagger 2a_1 2a_1$

approach. However, they report energies of 33.1 and 33.6 eV for the $2a_1$ ionizations, an average of about .6 eV in error compared to the average of .3 eV in error for the EOMIP calculation on the same two peaks.

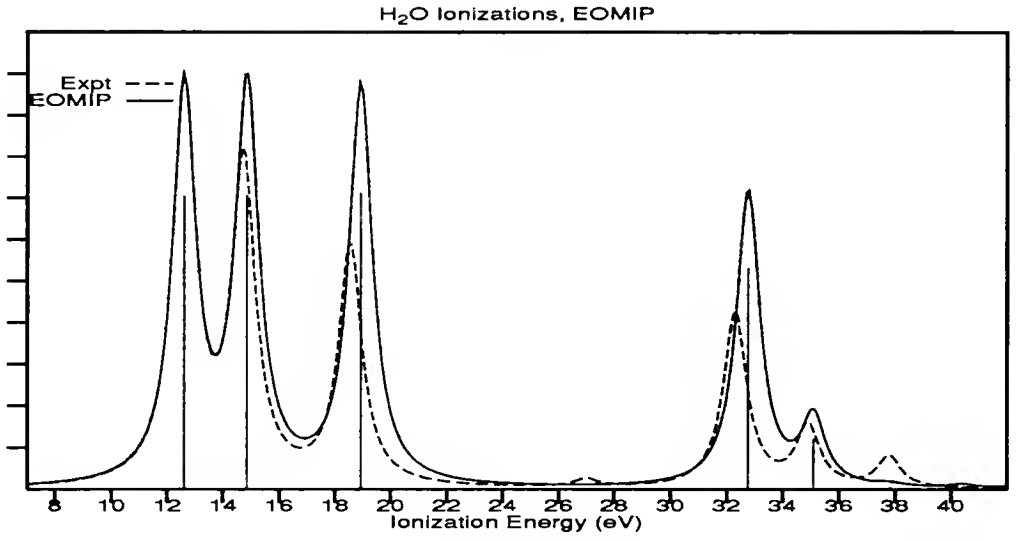

Figure 10.5: H_2O EOMIP ionization spectrum. Lorentzian lineshapes applied to reported experimental energies and intensities.

10.4 Nitrogen and C_2: A study in contrasts

10.4.1 Single-Determinant and Multideterminant References

The $C_2X^1\Sigma_g^+ \rightarrow C_2^+a^2\Pi_u$ transition is a difficult test for any method because both species have significant multireference character. The C_2 $X^1\Sigma_g^+$ ground state is characterized by two electronic configurations, $1\sigma_g^2 1\sigma_u^2 2\sigma_g^2 2\sigma_u^2 1\pi_u^4$ and $1\sigma_g^2 1\sigma_u^2 2\sigma_g^2 3\sigma_g^2 1\pi_u^4$. The C_2^+ state is dominated by the $1\sigma_g^2 1\sigma_u^2 2\sigma_g^2 2\sigma_u^2 1\pi_u^3$ configuration, with a major contribution from $1\sigma_g^2 1\sigma_u^2 2\sigma_g^2 3\sigma_g^2 1\pi_u^4$, and smaller contributions from $1\sigma_g^2 1\sigma_u^2 2\sigma_g^2 2\sigma_u^2 1\pi_u^1 1\pi_g^2$ and other electronic configurations. The $N_2X^1\Sigma_g^+ \rightarrow N_2^+X^2\Sigma_g$ problem, by contrast, is

computationally much less demanding. The N_2 neutral state is well characterized by only one electronic configuration, and the $N_2^+ X^2\Sigma_g$ ionized state has a much smaller multi-reference character than $C_2^+ a^2\Pi_u$, with $1\sigma_g^2 1\sigma_u^2 2\sigma_g^2 2\sigma_u^1 3\sigma_g^2 1\pi_u^3 1\pi_g^1$ weighted only one tenth of the major configuration in the wavefunction. A comparison of the CCSD, CCSD(T), and EOMIP energies and wavefunctions of these two molecules near their minima should provide some insight into the nature of the EOMIP solution at these two extremes. A *p*VTZ+*sp* basis was chosen for all calculations, and the optimum geometries of the molecules and the studied cations were determined in that basis at the CCSD level of theory.

The EOMIP energy calculated for N_2^+ differed from the CCSD energy by an average of .011 eV over the range shown in table 10.13, with a maximum of .03 eV at the longest bond length, 1.150 Å. The difference between EOMIP and CCSD energies of C_2^+ over the range 1.180 to 1.360 Å, shown in table 10.14, differ by an average of .025 eV, over twice as large. The EOMIP and ΔCCSD(T) electron detachment energies for N_2 differ by an average of .12 eV, while for C_2 these differ by an average of .55 eV.

For both molecules, EOMIP state energies (CCSD energy of the neutral + EOMIP electron detachment energy) were closer to the CCSD than to CCSD(T). In figure 10.6a, the N_2^+ EOMIP and CCSD curves appear nearly superimposed, about .02 au (.5 eV) removed from the CCSD(T) curve. In figure 10.6b, the EOMIP and ΔCCSD energies again track closely, differing from the ΔCCSD(T) energies by about .01 eV. Although the EOMIP electron detachment energies for C_2 are closer to the ΔCCSD (figure 10.6d), than to the ΔCCSD(T) energies, they cannot be said to be particularly

close to either, differing by about .5 eV from the ΔCCSD energies, which in turn were separated from the ΔCCSD(T) energies by about .15 eV.

As a general rule of thumb, CCSD underestimates the stability of multiconfiguration references, while CCSD(T) might overestimate it, relative to Full CI (FCI)[65]. For the simple case of N_2, where the reference state is very much a single configu-

Table 10.13: N_2 $X^1\Sigma_g$ and N_2^+ $X^2\Sigma_g$ in pVTZ+sp basis

	N_2 $X^1\Sigma_g^+$		N_2^+ $X^2\Sigma_g^+$			Ionization		
R_{NN}	CCSD	CCSD(T)	EOMIP	CCSD	CCSD(T)	EOMIP	CCSD	CCSD(T)
Å	-109. (au)			-108. (au)			(eV)	
1.040	.398 874	.416 579	.818 616	.817 765	.839 868	15.790	15.813	15.693
1.060	.404 342	.422 754	.825 668	.825 069	.847 923	15.747	15.763	15.642
1.080	.406 948	.426 097	.829 808	.829 505	.853 123	15.705	15.713	15.592
1.090	.407 296	.426 825	.830 905	.830 766	.854 771	15.685	15.723	15.566
1.091[a]	.407 299	.426 862	.830 974	.830 851	.854 891	15.683	15.686	15.564
1.100	.407 066	.426 982	.831 411	.831 449	.855 844	15.665	15.663	15.542
1.107[b]	.406 511	.426 736	.831 422	.831 605	.856 307	15.649	15.644	15.522
1.110	.406 297	.426 610	.831 367	.831 593	.856 382	15.645	15.639	15.517
1.130	.403 295	.424 423	.829 781	.830 422	.856 006	15.606	15.590	15.468
1.150	.398 570	.420 545	.826 428	.827 536	.853 928	15.569	15.539	15.419
AEA						15.671[c]	15.666	15.526

[a]VEDE

[b]VEA

[c]Calculated as CCSD(N_2, 1.107) - CCSD(N_2, 1.091) + EOMIP(1.107)

ration function and the ionized state is very slightly multiconfigurational, it is easy to conclude that the ΔCCSD(T) energy will be lowered relative to the ΔCCSD energy. And this is the case. The energy of the cation is generally expected to be more stabilized than the energy of the neutral by higher excitations (such as the triples approximation), lowering the ionization energy. The EOMIP energies closely follow the ΔCCSD energies, which seems reasonable.

The C_2 case is different, however. For C_2 the triples are more important in the neutral than in the ionized state. The CCSD and CCSD(T) energies of the $C_2X^1\Sigma_g^+$

Table 10.14: C_2 $X^1\Sigma_g^+$ and C_2^+ $a^2\Pi_u$ in pVTZ+sp basis

	C_2 $X^1\Sigma_g^+$		C_2^+ $a^2\Pi_u$			Ionization		
R_{CC}	CCSD	CCSD(T)	EOMIP	CCSD	CCSD(T)	EOMIP	CCSD	CCSD(T)
Å	-75. (au)			-75. (au)			(eV)	
1.180	.767 465	.801 316	.279 333	.304 090	.333 627	13.283	12.609	12.727
1.200	.771 083	.805 085	.286 498	.311 277	.340 748	13.186	12.512	12.635
1.220	.773 176	.807 351	.291 977	.316 807	.346 242	13.094	12.419	12.548
1.240	.773 918	.808 287	.295 954	.320 863	.350 286	13.006	12.328	12.463
1.242[a]	.773 924	.808 313	.296 268	.321 185	.350 608	12.998	12.320	12.455
1.260	.773 467	.808 048	.298 598	.323 610	.353 041	12.922	12.200	12.347
1.280	.771 965	.806 774	.300 061	.325 199	.354 657	12.841	12.157	12.303
1.300	.769 544	.804 595	.300 481	.325 766	.355 265	12.764	12.076	12.227
1.302[b]	.769 220	.804 298	.300 469	.325 772	.355 276	12.755	12.067	12.219
1.320	.766 319	.801 624	.299 984	.325 437	.354 988	12.690	11.997	12.154
1.340	.762 399	.797 969	.298 684	.324 322	.353 936	12.618	11.921	12.083
1.360	.757 878	.793 723	.296 683	.322 524	.352 209	12.550	11.847	12.014
AEA						12.883[c]	12.187	12.328

[a]VEDE

[b]VEA

[c]Calculated as CCSD(C_2, 1.302) - CCSD(C_2, 1.242) + EOMIP(1.302)

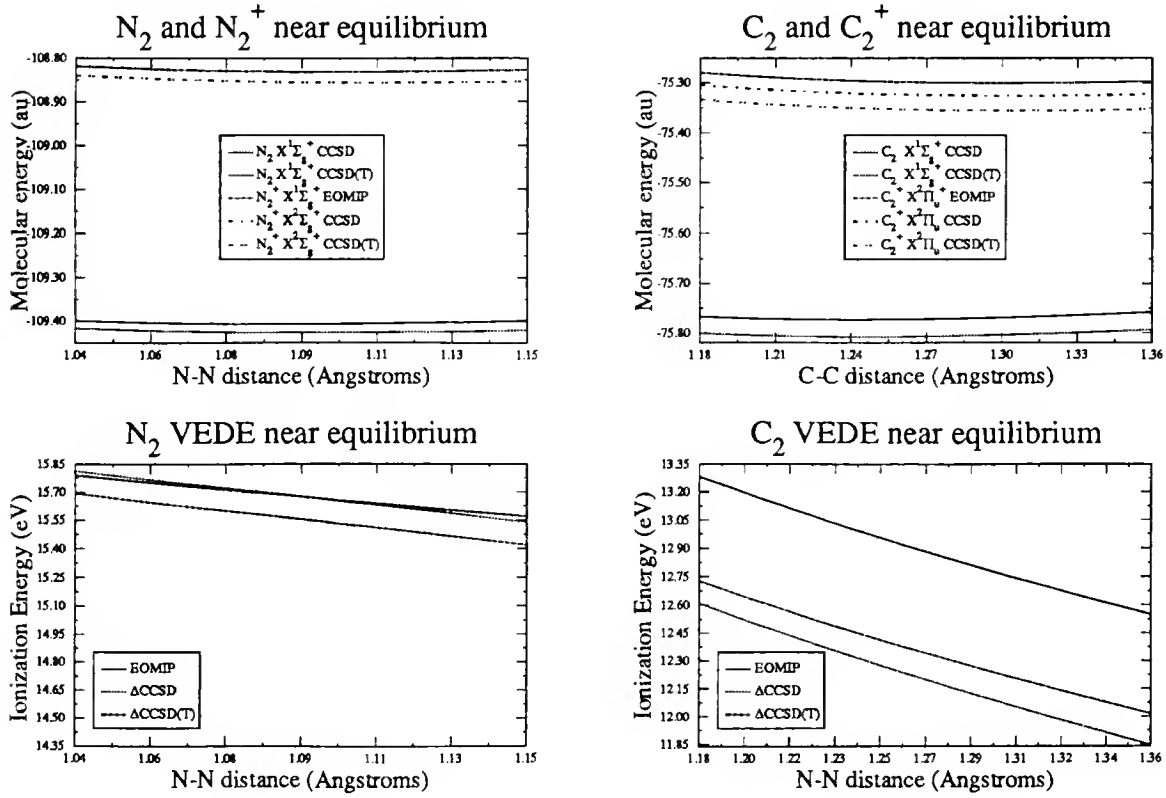

Figure 10.6: N_2 and C_2 potentials and ionization

neutral, are further apart than those for N_2, but those for the $C_2^+ a^2\Pi_u$ state, which has even more multiconfiguration character, are closer together. Thus, the ΔCCSD(T) is greater than ΔCCSD. And the EOMIP is now greater than ΔCCSD(T). It is apparent that this example defeats simple rules of thumb. The EOMIP energy is in fact worse than the Koopmans' approximation of 12.45 eV.

For the N_2 ionization, the experimental vertical electron-detachment energy (VEDE) is 15.5 eV. The CCSD(T) VEDE energy is in error by less than a tenth of an eV, while the CCSD(T) AEA result is in error by about a quarter of that. Any of the EOMIP results differ by between .1 and .2 eV, still within "experimental" accuracy, and accurate enough to interpret with confidence the doublet ionization spectrum of $N_2 X^1\Sigma_g^+$ (table 10.3).

For the C_2 ionization, ionization peaks have not been experimentally assigned, but according to Watts' best calculations[66], the EOMIP calculation is not accurate enough to distinguish between the $C_2 X^1\Sigma_g^+ \rightarrow C_2^+ a^2\Pi_u$ (at 12.51 eV) and $C_2 X^1\Sigma_g^+ \rightarrow C_2^+ X^4\Sigma_g^-$ (at 12.60 eV) transitions. The EOMIP calculation of the former weighs in at 12.998 eV, hardly within "experimental error" of either peak. The latter transition, of course, is fundamentally 2h1p, which means there is no relaxation at all to be provided by a EOMIP-SD calculation. The test calculation provided a VEDE of over 15 eV (table 11.1)– not useful to this task (there is, however, another approach to the EOMIP calculation of the energy, which will be presented in section 11.1).

At the equilibrium distance for the neutral species, the most important configurations in the N_2^+ CCSD and EOMIP wavefunction are $1\sigma_g^2 1\sigma_u^2 2\sigma_g^2 2\sigma_u^1 3\sigma_g^2 1\pi_u^4$ and $1\sigma_g^2 1\sigma_u^2 2\sigma_g^2 2\sigma_u^1 3\sigma_g^2 1\pi_u^3 1\pi_g^1$, with coefficients in the ratio 1:-0.1 for CCSD, and 1:-.077 for EOMIP:

$$\left|N_2^+ X^2\Sigma_g^+\right\rangle = \left(1 + C_{1\pi_u 2\overline{\sigma}_g}^{1\pi_g 3\overline{\sigma}_g}\ 1\pi_g^\dagger 3\overline{\sigma}_g^\dagger 2\overline{\sigma}_g 1\pi_u + \cdots\right) 3\overline{\sigma}_g \left|N_2 X^1\Sigma_g^+\right\rangle.$$

There is qualitative agreement in the general form of the wavefunction. In the CCSD calculation, the second determinant is created by the T_2 element associated with $t_{1\pi_u 2\overline{\sigma}_g}^{1\pi_g 3\overline{\sigma}_g}$ operating on the cation reference determinant $3\overline{\sigma}_g \left|N_2 X^1\Sigma_g^+\right\rangle$, while in the EOMIP calculation it is created by the action of the $C_{1\pi_u 2\overline{\sigma}_u}^{1\overline{\pi}_g}$ operator – double excitations for both methods.

For the C_2^+ CCSD wavefunction, the major components are

$$\begin{aligned}\left|C_2^+ a^2\Pi_u\right\rangle = \Big(1 &+ t_{2\sigma_u 2\overline{\sigma}_u}^{3\sigma_g 3\overline{\sigma}_g} 3\sigma_g^\dagger 3\overline{\sigma}_g^\dagger 2\overline{\sigma}_u 2\sigma_u \\ &+ t_{1\pi_u 1\overline{\pi}_u}^{1\pi_g 1\overline{\pi}_g} 1\pi_g^\dagger 1\overline{\pi}_g^\dagger 1\overline{\pi}_u 1\pi_u + t_{1\overline{\pi}_g 2\sigma_u}^{1\overline{\pi}_u 3\sigma_g} 1\overline{\pi}_u^\dagger 3\sigma_g^\dagger 2\sigma_u 1\overline{\pi}_g \\ &+ t_{2\sigma_u}^{3\sigma_g} 3\sigma_g^\dagger 2\sigma_u + t_{2\overline{\sigma}_u}^{3\overline{\sigma}_g} 3\overline{\sigma}_g^\dagger 2\overline{\sigma}_u\Big)\ 1\overline{\pi}_u \left|C_2 X^1\Sigma_g^+\right\rangle\end{aligned}$$

with the determinants in the ratios 1:-.351:-.106:.098:-.083:-.081, resulting from the action of the wave reaction operator $(1 + T_1 + T_2 + \cdots)$ on the N-1 electron reference $1\overline{\pi}_u \left|C_2 X^1\Sigma_g^+\right\rangle$. In the EOMIP wavefunction, these determinants appear in the ratio 1:−.278:

(< .06):−.078:−.119:−.046. In addition, there are three more determinants:

$$\left(.081\ 1\pi_u^\dagger 1\pi_u 1\overline{\pi}_u + .075\ 3\pi_u^\dagger 1\pi_u 1\overline{\pi}_u + .072\ 3\overline{\pi}_u^\dagger 1\overline{\pi}_u 1\overline{\pi}_u\right)\left|C_2X^1\Sigma_g^+\right\rangle$$

which are at least as important to the EOMIP wavefunction as some of the determinants above, but which are not as important to the C_2^+ CCSD wavefunction. The most striking difference between the CCSD and EOMIP wavefunctions is the coefficient to the $1\pi_g^\dagger 1\overline{\pi}_g^\dagger 1\overline{\pi}_u 1\pi_u$ determinant. It appears in the EOMIP wavefunction as a product of the C_2 CCSD $t_{1\pi_u 1\overline{\pi}_u}^{1\pi_g 1\overline{\pi}_g}$ coefficient (|amplitude| <.06) and the EOMIP $t_{\overline{\pi}_u}$ coefficient. The difference between the sizes of this t amplitude in the two CCSD calculations is quite large, and could only be made up by the EOMIP calculation if it included the $t_{1\overline{\pi}_u 1\pi_u 1\overline{\pi}_u}^{1\pi_g 1\overline{\pi}_g}$ operator, a triple excitation in EOMIP parlance. In FSIP parlance, triples of the form $S_{1\overline{\pi}_u 1\pi_u 1\overline{\pi}_u}^{1\overline{\pi}_u 1\pi_g 1\overline{\pi}_g}$ are commonly referred to as *spectator triples* because an active hole is both annihilated and created, and therefore appears as a sort of "spectator" line to a double excitation process. As discussed in chapter 4.2, there is a simple correspondence between the FS S and the EOMIP t amplitudes which, in cases like this where only one of the EOMIP T_1 amplitudes is important, is nearly identity. The desired $t_{1\overline{\pi}_u 1\pi_u 1\overline{\pi}_u}^{1\pi_g 1\overline{\pi}_g}$ is therefore the EOMIP equivalent of the FSIP spectator triple excitation. A perturbation theory analysis of the EOMIP equations indicates that EOMIP triples contributions, which appear at third order in W (appendix B) are possibly more important in cases like this than triples corrections to the CCSD energy. This is borne out by the importance of the spectator triples to the description of the C_2^+ wavefunction. It is clear that the absence of the spectator triples is principally responsible in this case for the inability of the EOMIP wavefunction to

mimic qualitatively the C_2^+ CCSD wavefunction, and the author asserts that the attempt to reproduce the proper wavefunction in the absence of this important part of the manifold space also results in the relatively large weights of the three odd EOMIP determinants which are not important to the C_2^+ CCSD wavefunction. Attempts to improve FSIP energies by adding triples approximations have had mixed results[40], but it would be an interesting course of extended further study to examine the effects of various levels of approximation to the addition of spectator triples effects to the wavefunction.

For the single-reference N_2 case, of course, the spectator triples do not make an important contribution, and the EOMIP calculation does a good job of reproducing the CCSD result.

CHAPTER 11

LINEAR CARBON CLUSTER ANION PHOTOELECTRON SPECTRA

Carbon clusters have been found in interstellar space, where they are suspected of being important in the formation of many carbon-containing compounds [67, 68], and in hydrocarbon flames, where they are important in the formation of soot particles [69]. They can be created in the laboratory by super heating graphite, separated by mass spectrometry, and the smaller clusters have been studied with more and more exacting techniques in recent years [70, 71, 35, 72, 36]. Moving from larger to larger clusters, researchers hope to observe the transition from cluster to extended material. Yet there are still many questions about the structure and properties of small clusters. State-of-the art quantum theory, employing high-level *ab initio* methods, permits accurate predictions of the properties observed in spectroscopic experiments. Matching theoretical calculations of vibrational, excitation, and ionization energies to experimentally obtained spectra can and has provided information about the structure of the species in question. Early experimental analyses of carbon clusters produced in hot carbon vapors [73] and among molecular dissociation products [74] were invariably complicated by the mixture of electronic and vibrational states produced by such methods. Early theoretical approaches based on MO theory or low-level correlation approaches [75] yielded energies roughly in agreement with the experiments, but

electronic configuration assignments which have been discounted by more recent experimental and theoretical results. Thirty years of improved results from increasingly sophisticated experimental and theoretical designs, laid out in Weltner and Van Zee's 1989 review [70], led to the present situation. During an extended debate between experimentalists and theoreticians [76, 77, 78, 79, 80], a picture began to form of the structures of the small carbon clusters. Recent photoionization experiments, involving the separation by time-of-flight mass spectrometry of a beam of mixed carbon cluster anions, have produced some very high quality spectra of the small carbon clusters [71, 35, 72, 36]. These have been followed up by some very high-level theoretical calculations on the geometries and electronic structures of the neutral and anionic clusters [66, 65, 81, 82, 83, 84], in which the geometries and ground electronic states of the neutral carbon clusters C_2 – C_{10} and their anions have been calculated very accurately [65]. The vibrationally resolved spectra from Neumark's group [72, 36, 85] are highly resolved, revealing vibrational and electronic structure of the transition within a window of 2 to 3 eV above the first ionization energy of each cluster anion, C_2^- – C_9^-, with which the results of Watts [66] are in very good agreement. The spectra of C_2^- – C_{30}^- produced in Smalley's group, while much less resolved, reveal a wealth of structure in a range of 3 to 5 eV above the first ionization. C_3^- in particular exhibits a very rich structure, and the other small linear species display several broad features. Most of these peaks are as yet unassigned; many must be due to transitions to excited states of the neutral clusters. Considering the main strength of the EOMIP method – an economical and conceptually simple approach to calculating several ionizations at

once – the author has applied the method to the interpretation of the photoelectron spectra of these novel molecules.

Anions of linear carbon clusters present a challenge to any theoretician. For chains of three carbons and longer, the valence orbitals of the neutral are of π symmetry. The anions involve either one or three electrons in a π orbital. With a code that is limited to Abelian symmetries, there are plenty of opportunities for both spin contamination and symmetry breaking at the Hartree-Fock level. C_2 exhibits significant multireference character. While the CCSDT approach can be expected to overcome these defects of the reference determinant, and has been shown, in large basis sets, to yield good agreement with experiment [65, 66], the CCSD method cannot be expected to do so well. This has been demonstrated with the odd-numbered neutral chains, where there is the indication that non-iterative triples corrections are not sufficient to describe the wavefunction [65]; some type of iterative triples approach is indicated.

Despite these difficulties Watts and Bartlett reported ΔCCSD calculations within .2 eV of the experiments for the first ionizations of the linear carbon clusters C_2^- through C_9^-, using DZP+*sp* or DZP+*p* bases and UHF orbitals. Since EOMIP results can come very close to reproducing CCSD energies in many cases, it is not unreasonable to apply the EOMIP method to the study of the outer valence spectra of these carbon clusters.

11.1 C_2, C_2^+, and C_2^-

Recent coupled-cluster studies of C_2 and its anion have demonstrated good agreement with experimental results when pVTZ and pVQZ basis sets were used at the CCSD(T) level of theory and higher[66, 65]. Here, the pVTZ basis set is used, and geometry is optimized at the CCSD level for both the neutral and the anion. These CCSD geometries are quite close to that obtained at the CCSD(T) level although the reference energies differ somewhat.

11.1.1 Ionization of C_2

A detailed study of the C_2 $X^1\Sigma_g^+$ and C_2^+ $a^2\Pi_u$ transition in the pVTZ+sp basis was presented in table 10.14. Here, that ionization is presented again, along with some 2h1p transitions, in table 11.1.

These vertical detachment energies from the ground state of C_2 are not experimentally verified, but the comparison to calculations of Watts and Bartlett[66] indicate that EOMIP has not done especially well in this very difficult case. Especially difficult are the $^4\Sigma_g^-$ and $^2\Sigma_g^-$ calculations. These fundamentally 2h1p transitions cannot be very well represented at the CC EOMIP-SD level of theory except in the most fortuitous of circumstances.

The C_2 $a^3\Pi_u \rightarrow C_2^+$ $X^4\Sigma_g^-$ transition should be much more amenable to EOMIP treatment. The neutral is well characterized by the single ROHF determinant $1\sigma_g^2 1\sigma_u^2 2\sigma_g^2 2\sigma_u^2 1\pi_u^3 3\sigma_g^1$n and the cation by $1\sigma_g^2 1\sigma_u^2 2\sigma_g^2 2\sigma_u^2 1\pi_u^2 3\sigma_g^1$, the result is an energy

Table 11.1: Ionization of C_2. Energies reported in eV

C_2	C_2^+	Reference	EOMIP pVTZ	EOMIP pVTZ+sp	CCSD(T) pVTZ[a]
$X^1\Sigma_g^+$					
	$a^2\Pi_u$	$1\pi_u$	12.991	12.998	12.45
	$^4\Sigma_g^-$	$3\sigma_g^\dagger 1\pi_{ux} 1\pi_{uy}$	15.366		12.51
	$^2\Sigma_g^-$	$3\sigma_g^\dagger 1\pi_{ux} 1\pi_{uy}$	16.961		
$a^3\Pi_u$					
	$X^4\Sigma_g^-$	$1\overline{\pi}_u$		12.231	11.67
	$a^2\Pi_u$	$3\sigma_g$, $3\overline{\sigma}_g^\dagger 2\overline{\sigma}_u 2\sigma_u$		12.506	12.23

[a] Watts and Bartlett [66]

.56 eV greater than the CCSD(T) result, which is itself perhaps an overestimation of the true value[66]. The case of the transition to $a^2\Pi_u$ state of the cation should be a more difficult one. With significant contribution from the a doubly-excited determinant (.27 in $1\sigma_g^2 1\sigma_u^2 2\sigma_g^2 1\pi_u^3 3\sigma_g^2$), it would be expected that the EOMIP energy, like the ΔCCSD, would overestimate the ionization energy, while the ΔCCSD(T) should underestimate it. This is consistent with the results, but here the EOMIP energy is only about .3 eV from the ΔCCSD energy, apparently better performance than that obtained from the seemingly more tractable C_2 $a^3\Pi_u \rightarrow C_2^+$ $a^4\Sigma_g^-$ transition.

11.1.2 Ionization of C_2^-

The most accurate experimental[36, 71] results for the photodetachment of C_2^- indicate that the EOMIP value of the $X\,^2\Sigma_g^+ \rightarrow X\,^1\Sigma_g^+$ vertical electron detachment energy falls within .3 eV of the experimental result (see table 11.2). Previous, highly accurate theoretical results [66, 65] indicate that better agreement with experiment is

Table 11.2: Ionization of C_2^- in pVTZ+sp basis, UHF orbitals. Energies reported in eV.

	C_2	Reference	EOMIP	ΔCCSD(T)[a]	Experiment
$X^2\Sigma_g^+$		UHF/CCSD	-75.900280 au		
	$X^1\Sigma_g^+$	$3\sigma_g^+$	3.529	3.115	3.273[b]
	$^1\Pi_u$[b]	$1\pi_u$	4.019		
	$^1\Sigma_u^+$[b]	$2\sigma_g$	5.500		
	$^1\Sigma_g^+$[b]	$2\sigma_g^+$	15.752		
	$^1\Sigma_g^+$[b]	$1\sigma_g^+$	285.167		
	$a^3\Pi_u$	$1\overline{\pi}_u$	3.627		3.351[c]
					$\approx$4.3?[c]
	$^3\Sigma_u^+$	$2\overline{\sigma}_g^+$	4.761		

[a] Watts and Bartlett [66], in pVQZ basis

[b] Arnold et al. [36]; [c] Yang et al. [35]

possible, but that the results are affected both by increasing the basis set from pVTZ to pVQZ, and by the inclusion of triples in the coupled-cluster calculation (both cause changes to the energy on the order of .1eV) . As a rule, CCSD underestimates the stability of a multi-configuration reference relative to the FCI result, while CCSD(T) overestimates it. Therefore, it is not surprising that the EOMIP result (which should, except in pathological cases, be quite close to the ΔCCSD result) is greater than the experimental energy, while the ΔCCSD(T) result is lower. Simulated C_2^- spectra are found in section 11.4

11.2 Ionization of C_3^-

Electron detachment energy calculations on C_3^- were performed using 3 different sets of orbitals – orbitals from a C_3^- UHF calculation, from a C_3 RHF calculation, and from a C_3^{4-} RHF calculation. While the UHF calculation is expected to reproduce

the energy of the anion fairly well, the calculation on a non symmetric wavefunction produces both a poor approximation to the true spin eigenfunction – the average multiplicity at the UHF level is 2.117 – and a set of π orbitals in which the x and y (B_{3u} and B_{2u} in the D_{2h} Abelian subgroup in which the computations were performed) components differed significantly. Although the approximate spin multiplicity is 2.092 at the MBPT(2) level and 2.013 when the CCSD calculation converges, it might be expected that the UHF orbitals are unsuited to represent the closed-shell C_3. While

Table 11.3: $C_3^- X\,^2\Pi_u \rightarrow C_3 X\,^1\Sigma_g^+$ in pVTZ+sp basis.

Method	E(C_3^-) Hartrees	VEDE eV	Source
ΔCCSD	-113.915414534294	2.038	
EOMIP, C_3^- orbitals	-113.915414534294	2.157	
EOMIP, C_3^{4-} orbitals	-113.915428019063	-1.133	
EOMIP, C_3 orbitals	-113.913530561817	1.989	
ΔCCSD(T)		1.61	Watts and Bartlett [65]
Experiment		1.98 $\pm$ 0.02	Arnold et al. [36]

a restricted open-shell Hartree-Fock (ROHF) calculation in the Abelian subgroup D_{2h} provides a spin eigenfunction, it cannot provide π_x and π_y orbitals of the proper symmetry. Therefore, quasi-restricted Hartree-Fock (QRHF) calculations were attempted, one using the orbitals from the C_3 RHF calculation, and one from C_3^{4-}, the next $^1\Sigma_g^+$ species, which has a filled π_g. While the C_3^{4-} orbitals reproduce the C_3^- CCSD energy, there are several large T amplitudes in the CCSD wavefunction, indicating these orbitals are not suitable for the EOMIP CCSD calculation. The result is a negative electron detachment energy. The C_3 orbitals gave, to within .002%, the

same C_3^- CCSD energy, an electron detachment energy within .05 eV of the ΔCCSD value, and fortuitously closer to the experimental energy.

11.3 First Ionization Energies

The carbon clusters were studied in several different basis sets as a preliminary to the study of their full spectra. These preliminary results indicate considerable effects of orbital choice. The orbitals from the restricted Hartree-Fock calculation on the neutral (RHF in the cases of C_2, C_3, and C_5, ROHF in the cases of the open-shell neutral carbon clusters) seemed to give results closest to the ΔCCSD energies, and so were initially selected for the extended studies of the ionization spectra. But these were not, in all cases, the choices which best reproduced the experimental spectra, as can be seen from the simulated ionization spectra presented in section 11.4.

11.4 Interpretation of Spectra

Lorentzian line shapes were used to simulate ionization spectra, with a FWHM of .25eV used in all cases except for the C_2^- spectra, for which a FWHM of .2eV was used.

Table 11.4: C_n/C_n^-.

Method		Orbitals	C_n^- CCSD (au)	VEDE (eV)	Source
$C_3^-\ ^2\Pi_g/C_3\ ^1\Sigma_g^+$					
*p*VTZ+*sp*	EOMIP	C_3^- UHF	-113.915415	2.157	
*p*VTZ+*sp*	EOMIP	C_3 RHF	-113.913530	1.989	
*p*VTZ+*sp*	CCSD	C_3^- UHF	-113.915415	2.05	Watts and Bartlett [82]
*p*VTZ+*sp*	CCSD(T)	C_3^- UHF		1.88	Watts and Bartlett [82]
*p*VTZ+*sp*	CCSD	C_3^- ROHF		1.90	Watts and Bartlett [82]
Experiment				1.98± 0.02	Arnold et al. [36]
$C_4^-\ ^2\Pi_g/C_4\ ^3\Sigma_g^-$					
DZP+*sp*	EOMIP	C_4^{2-} RHF	-151.758857	4.55	
DZP+*sp*	EOMIP	C_4^{2+} RHF	-151.756564	2.08	
DZP+*sp*	EOMIP	C_4 ROHF	-151.756460	2.78	
DZP+*sp*	EOMIP	C_4^- ROHF	-151.757755	3.47	
DZP+*sp*	EOMIP	C_4^- UHF	-151.758929	3.43	
DZP+*sp*	CCSD			3.73	Watts and Bartlett [65]
DZP+*sp*	CCSD(T)			3.76	Watts and Bartlett [65]
*p*VTZ+*sp*	EOMIP	C_4^- ROHF	-151.875081	3.66	
*p*VTZ+*sp*	EOMIP	C_4^- UHF	-151.876304	3.63	
*p*VTZ+*sp*	EOMIP	C_4 ROHF	-151.873807	3.51	
*p*VTZ+	CCSD	ROHF		3.91	
*p*VTZ+	CCSD(T)	ROHF		3.95	
Experiment				3.882±0.01	Arnold et al. [36]
$C_5^-\ ^2\Pi_u/C_5\ ^1\Sigma_g^+$					
DZP+*sp*	EOMIP	C_5^- UHF	-189.732655	2.91	
DZP+*sp*	EOMIP	C_5^- ROHF	-189.731051	2.83	
DZP+*sp*	EOMIP	C_5 RHF	-189.730180	2.71	
DZP+*sp*	CCSD			2.79	Watts and Bartlett [65]
DZP+*sp*	CCSD(T)			2.50	Watts and Bartlett [65]
*p*VTZ+*sp*	EOMIP	C_5^- UHF	-189.885918	3.14	
*p*VTZ+*sp*	EOMIP	C_5^- ROHF	-189.884250	3.06	
*p*VTZ+*sp*	EOMIP	C_5 RHF	-189.883307	2.93	
*p*VTZ+*sp*	CCSD	UHF		3.02	Watts and Bartlett [82]
*p*VTZ+*sp*	CCSD(T)	UHF		2.74	Watts and Bartlett [82]
*p*VTZ+*sp*	CCSD	ROHF		2.97	Watts and Bartlett [82]
*p*VTZ+*sp*	CCSD(T)	ROHF		2.78	Watts and Bartlett [82]
Experiment				2.839±0.008	Arnold et al. [36]

Table 11.4: C_n/C_n^- (*Continued*)

Method	Orbitals	C_n^- CCSD (au)	VEDE (eV)	Source
$C_6^- \ ^2\Pi_u/C_6 \ ^3\Sigma_g^-$				
DZP+sp EOMIP	C_6 ROHF	-227.706504	5.99	
DZP+sp EOMIP	C_6^{2+} RHF	-227.706974	5.63	
DZP+sp EOMIP	C_6^- ROHF	-227.707420	4.35	
DZP+sp EOMIP	C_6^- UHF	-227.708828	4.31	
DZP+sp EOMIP	C_6 UHF	-227.708080	4.14	
DZP+sp CCSD			4.17	Watts and Bartlett [65]
DZP+sp CCSD(T)			4.15	Watts and Bartlett [65]
Experiment			4.185±0.006	Arnold et al. [36]
$C_7^- \ ^2\Pi_g/C_7 \ ^1\Sigma_g^+$				
DZP+sp EOMIP	C_7 RHF	-265.661618	3.31	
DZP+sp EOMIP	C_7^- UHF	-265.693376	3.56	
DZP+sp EOMIP	C_7^- ROHF	-265.692714	3.43	
DZP+sp CCSD			3.4	Watts and Bartlett [65]
DZP+sp CCSD(T)			3.01	Watts and Bartlett [65]
Experiment			3.538±0.014	Arnold et al. [36]
$C_8^- \ ^2\Pi_g/C_8 \ ^3\Sigma_g^-$				
DZP+sp EOMIP	C_8 ROHF	-303.633302	4.50	
DZP+sp EOMIP	C_8^- ROHF	-303.635412	4.63	
DZP+sp EOMIP	C_8^- UHF	-303.637055	4.59	
DZP+p CCSD			4.45	Watts and Bartlett [65]
DZP+p CCSD(T)			4.39	Watts and Bartlett [65]
Experiment			4.379±0.006	Arnold et al. [36]
$C_9^- \ ^2\Pi_u/C_9 \ ^1\Sigma_g^+$				
DZP+sp EOMIP	C_9^- UHF	-341.589514	4.04	
DZP+sp EOMIP	C_9^- ROHF	-341.587993	3.85	
DZP+sp EOMIP	C_9 RHF	-341.586665	3.76	
DZP+sp CCSD	UHF	-341.589514	3.83	
DZP+p CCSD			3.80	Watts and Bartlett [65]
DZP+p CCSD(T)			3.31	Watts and Bartlett [65]
Experiment			3.684±0.01	Arnold et al. [36]
$C_{10}^- \ ^2\Pi_u/C_{10} \ ^3\Sigma_g^-$				
DZP+sp EOMIP	C_{10}^- ROHF	-379.558974	4.88	
DZP+sp EOMIP	C_{10}^- UHF	-379.560459	4.80	
DZP+sp EOMIP	C_{10}^- ROHF	-379.557551	4.73	
DZP+sp MBPT(2)	UHF	-379.520429	4.72	
DZP+sp CCSD	UHF	-379.560459	4.68	
DZP+p CCSD			4.71	Watts and Bartlett [65]
DZP+p CCSD(T)			4.59	Watts and Bartlett [65]

11.4.1 Odd-Length Chains

For the odd clusters C_5^- and C_7^-, and C_9^-, where there is only one electron in an open-shell π orbital, the QRHF orbitals based on the closed shell give very good results for the first ionization, as might be expected. Where QRHF or ROHF orbitals were used for the C_5^- and C_7^-, spectra, the EOMIP results are a good match to the experimental spectrum. Anion UHF orbitals, used in C_9^- gave decidedly poorer results. So selection of appropriate orbitals is important. Large T amplitudes and large correlation energies indicate that the orbitals are poorly chosen, and that the EOMIP results will be poor as well.

11.4.2 C_3^-

The experimental ionization spectrum of C_3^- is very rich. The two main features (the peaks at 1.95 and 4.3 in the Smalley C_3^- spectrum, 1.995 and 4.113 in the Neumark spectrum) are easily assigned to the $X^1\Sigma_g^+$ and $a^3\Pi_u$ states of C_3, in agreement with the assignment in Neumark. The feature at about 5.0 eV seems to be well matched to the $^3\Pi_g$ state at about the same energy, with the succeeding gap and calculated $^3\Sigma_u^+$ peak at 5.286 eV relatively well matched to the gap and peak in the Smalley spectrum at about that frequency. The complicated feature at about 6.0 eV in the Smalley spectrum is difficult to assign. There are a number of large peaks in the region which may all contribute. Chief among these is the $^1\Sigma_u^-$ peak at 5.6 eV.

Table 11.5: Ionization of C_3^- $X^2\Pi_g$ in pVTZ+sp basis, QRHF reference

		Energy eV (Intensity)			
C_3 State	Reference	EOMIP		Other	Experiment
$X^1\Sigma_g^+$	$1\pi_g$	1.989	(.883)	1.90[a]	1.98 ± 0.02[b]
					1.95[c]
$^3\Pi_u$	$3\overline{\sigma}_u^+$	4.172	(.879)		
					≈4.113[b]
					≈4.3[c]
$^1\Pi_u$	$3\overline{\sigma}_u^+$	4.616	(.842)		
$^3\Pi_g$	$4\overline{\sigma}_g^+$	5.056	(.848)		
$^3\Sigma_u^+$	$1\overline{\pi}_{ux}$	5.286	(.903)		
$^1\Pi_g$	$4\sigma_g^+$	5.560	(.805)		
$^3\Sigma_u^-$	$1\overline{\pi}_{uy}$	5.595	(.758)		
					≈5.1 - 6.0[c]
$^1\Sigma_u^-$	$1\pi_{uy}$	5.683	(.907)		
$^1\Sigma_u^+$	$1\pi_{ux}$	5.821	(.835)		
$^3\Pi_g$	$2\overline{\sigma}_u^+$, $6\sigma_g^{+\dagger}1\sigma_g^+1\overline{\sigma}_u^+$	15.163	(.224)		
$^3\Pi_u$	$3\overline{\sigma}_g^+$, $4\overline{\sigma}_u^{+\dagger}3\overline{\sigma}_u^+4\overline{\sigma}_g^+$	17.498	(.325)		
$^3\Pi_u$	$3\sigma_g^+$, $4\pi_{ux}^{\dagger}4\sigma_g^+1\pi_{ux}$	17.541	(.495)		

[a] Watts and Bartlett [82] ROHF-CCSD(T)/PVTZ+sp;
[b] Arnold et al. [36]; [c] Yang et al. [35]

Because the EOMIP code used is not spin-adapted, open-shell singlets such as this one are not properly represented, and it is expected that the singlet-triplet splitting is under-represented by a factor on the order of $2^{\frac{1}{2}}$ (cf. work by Nooijen et al.). It is reasonable to expect that the $^1\Sigma_u^-$ peak as well as the nearby $^1\Sigma_u^+$ at 5.8 eV will contribute to this feature.

It is important to note that all of the calculated transitions in this range are very strongly dominated by a single 1-hole process. Significant calculated shakeup peaks first appear in the 15-18 eV region.

Because the EOMIP program lacks explicit spin adaptation, the only open-shell wavefunctions which are properly spin adapted are those with all parallel spins in the half-filled orbitals. This means that the open-shell singlet states of C_3 (all but

Table 11.6: Ionization of $X^2\Pi_g$ C_3^- in pVTZ+sp basis, UHF basis

C_3 State	Reference	Energy eV (Intensity) EOMIP		Experiment
$X^1\Sigma_g^+$	$1\pi_g$	1.989		1.98 ± 0.02^b
				1.95^c
$^3\Pi_u$	$3\sigma_u^+$	4.172		
				$\approx 4.113^b$
				$\approx 4.3^c$
$^1\Pi_u$	$3\sigma_u^+$	4.616		
$^3\Pi_g$	$4\sigma_g^+$	5.056	(1.000^d)	
$^3\Sigma_u^+$	$1\pi_{ux}$	5.286		
$^1\Pi_g$	$4\sigma_g^+$	5.559		
$^3\Sigma_u^-$	$1\pi_{uy}$	5.595		
$^1\Sigma_u^-$	$1\pi_{uy}$	5.638		
$^1\Sigma_u^+$	$1\pi_{ux}$	5.821		
				≈ 5.1 - 6.0^c
$^1\Sigma_g^+$	$1\pi_g$, $1\overline{\pi}_u^\dagger$ $1\overline{\pi}_g$ $3\sigma_g^+$	10.351	(0.002^d)	
$^3\Pi_u$	$2\sigma_u^+$	15.163		
$^3\Pi_g$	$3\sigma_g^+$	17.541		

[a] Watts and Bartlett [82] UHF-CCSD(T)/PVTZ+sp;
[b] Arnold et al. [36]; [c] Yang et al. [35]; [d] Relative to $^3\Pi_g$ state at 5.056 eV

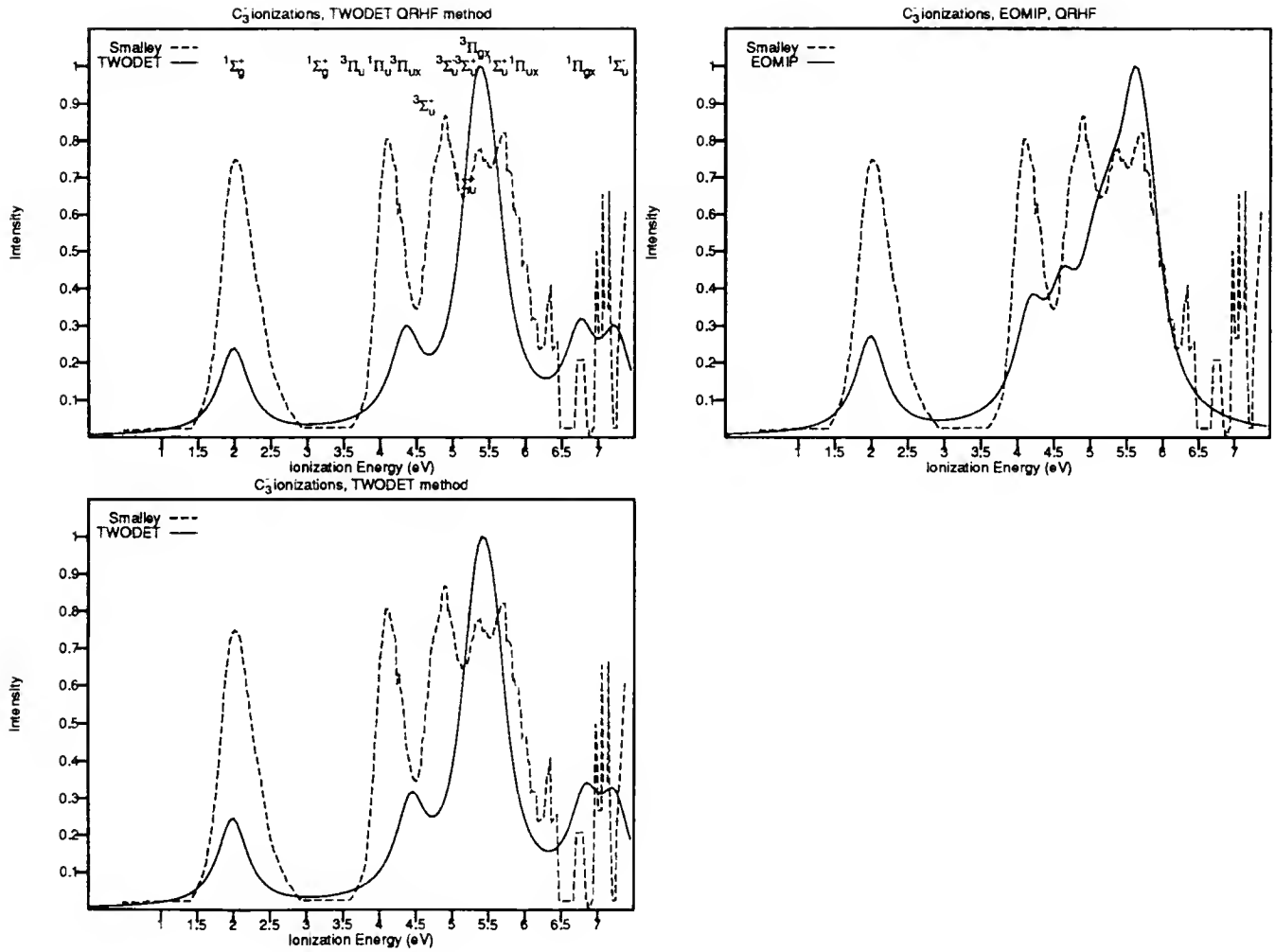

Figure 11.1: Ionization spectrum of C_3^-, pVTZ+sp basis

the lowest-energy, closed-shell $X^1\Sigma_g^+$ state) are spin-contaminated. For example, if the $X^2\Pi_u$ state has one unpaired electron in the $1\pi_g$ orbital of beta spin, the EOMIP open-shell singlet wavefunction describing the $^1\Pi_u$ wavefunction is dominated by the annihilation of the $3\overline{\sigma}_u$ beta electron, leaving an open-shell $1\overline{\pi}_g\ 3\sigma_u$ configuration. But the proper representation of the spin state demands that the spin-flipped configuration $1\pi_g\ 3\overline{\sigma}_u$ be represented with equal weight in the wavefunction. Because this state can be reached via the EOMIP doubles operator $c_{1\overline{\pi}_g 3\sigma_u}^{1\pi_g} 1\pi_g^\dagger 3\sigma_u 1\overline{\pi}_g$, it does appear in the final wavefunction. But correlation of this 2-configuration reference requires excitations from both configurations, and the required triple excitation operators are not present in the EOMIP operator. This lack of balance – essentially treating two equally important configurations at different levels of theory – makes it impossible to correlate the state while at the same time maintaining a spin eigenfunction. Inclusion of triple excitations in the method would improve the situation by pushing the problem back one level of theory, where correlation contributions will be smaller, in all but very unusual cases. For larger molecules, the error induced in the energy by the incomplete treatment of spin adaptation may be barely significant compared to experimental errors, but molecules as small as C_3 are known to exhibit larger singlet-triplet splittings.

Two sets of two-determinant MRCCSD calculations were performed – one using QRHF orbitals from the closed-shell C_3 SCF calculation, and the other using orbitals chosen to be more suited to each ionization. An important feature of the two-determinant calculations (figure 11.1) is the very close grouping of ionization energies in the 5.0 to 5.6 eV region. This results in one tall peak at around 5.5 eV rather

than several maxima in the 4.5 to 6eV region. The EOMIP spectrum, although it has similar difficulties, seems to represent the spectrum slightly more realistically, with a better matching of triplet peaks to the experimental features. Too-small singlet-triplet splittings might be held responsible for the very close spacing of IEs in the 5.5 to 6 eV region. It is not easy to account for the lack of any calculated peak corresponding to the feature above 7 eV.

11.4.3 C_5^-

The calculated peaks in figure 11.2 are offset slightly from the experimental in a manner consistent with results for small closed-shell molecules.

The rising section at the high-energy end of the spectrum is explained by energies which fall outside the 0-7.5 eV window observed in the Smalley experiment.

In table 11.7, the first ionization energy is within .2 eV of the experimental results, and the theoretical states between 5.3 and 6.0 eV result, after the application of Lorenz broadening, in a peak at 5.46 eV, within 1 eV of the experimental peak at 5.39 eV.

11.4.4 C_7^-

Like C_5, C_7 is a closed-shell species, and again the calculated spectrum bears a distinct resemblance to experiment. Peak shapes suggest that IEs greater than 5.5 eV are too large.

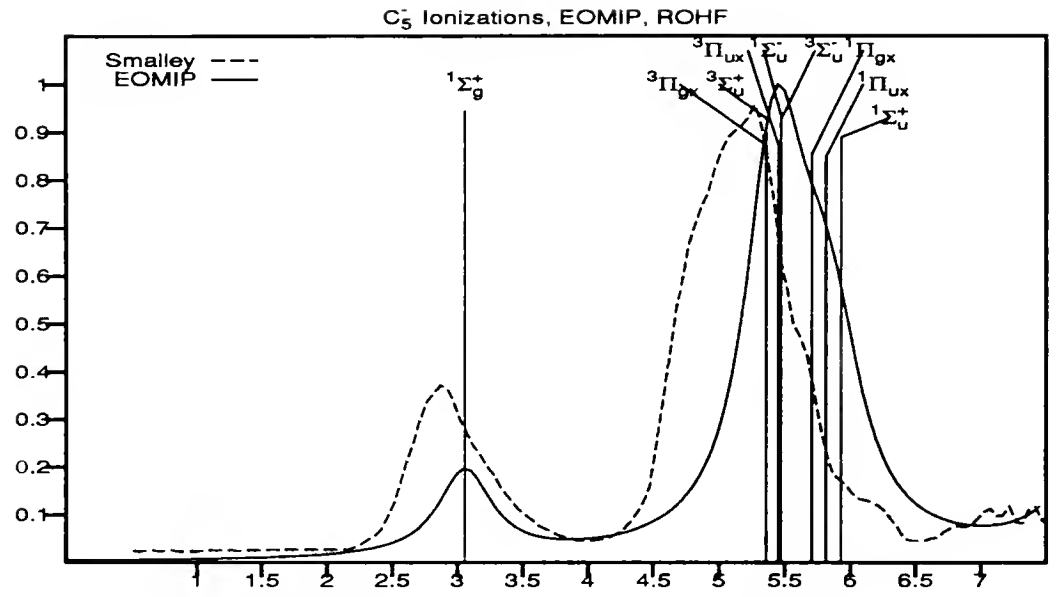

Figure 11.2: Ionization of C_5^-, ROHF basis

Table 11.7: C_5^- Ionization, ROHF orbitals

	Energy eV (Intensity)		
C_5 State	EOMIP		Expt.
$1\Sigma_g^+$	3.058	(0.945)	2.839±0.008[a] 2.8[b]
$^3\Pi_{gx}$	5.359	(0.873)	
$^3\Sigma_u^+$	5.362	(0.928)	
$^3\Pi_{ux}$	5.455	(0.872)	5.29[c]
$^1\Sigma_u^-$	5.473	(0.934)	
$^3\Sigma_u^-$	5.476	(0.928)	
$^1\Pi_{gx}$	5.708	0.854	
$^1\Pi_{ux}$	5.816	0.849	
$^1\Sigma_u^+$	5.932	0.889	
$^3\Sigma_g^+$	7.860	0.898	

[a] As reported by Arnold et al. [36]

[b] As reported by Yang et al.[35]; [c] Maxima observed in plots by Yang et al. [35]

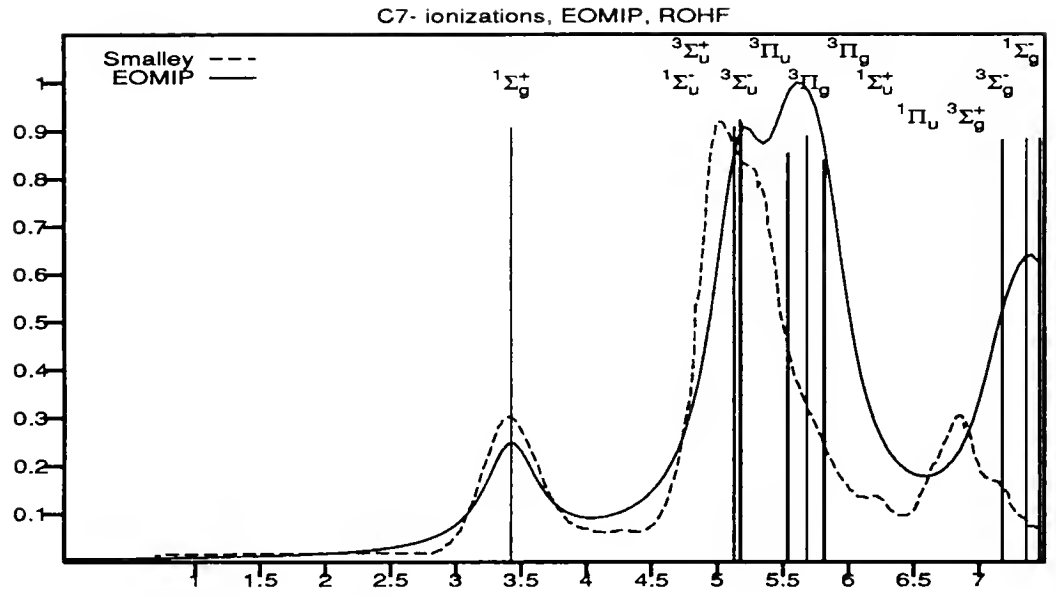

Figure 11.3: Ionization of C_7^-, ROHF basis

Table 11.8: C_7^- Ionization, ROHF orbitals

	Energy eV (Intensity)		
C_7 State	EOMIP		Expt.
$^1\Sigma_g^+$	3.425	(0.907)	3.538± 0.014[a]
			3.10[b]
			5.0(.9)[c]
$^1\Sigma_u^-$	5.130	(0.910)	
$^3\Sigma_u^+$	5.174	(0.925)	
$^3\Sigma_u^-$	5.187	(0.919)	
			5.25(.82 shoulder)[c]
$^3\Pi_u$	5.537	(0.854)	
$^3\Pi_g$	5.545	(0.855)	
$^1\Sigma_u^+$	5.685	(0.891)	
$^1\Pi_u$	5.813	(0.841)	
$^1\Pi_g$	5.824	(0.838)	
			6.8(.3)[c]
$^3\Sigma_g^+$	7.175	(0.883)	
$^3\Sigma_g^-$	7.359	(0.885)	
$^1\Sigma_g^-$	7.461	(0.885)	
$^1\Sigma_g^+$	7.727	(0.868)	

[a] As reported by Arnold et al. [36]
[b] As reported by Yang et al. [35]
[c] Maxima observed in plots by Yang et al. [35]

These calculations were performed using ROHF orbitals, in the DZP+*sp* basis because of the size of the calculation. Using D_{2h} symmetry, there were 129 α and 129 β functions in the SCF calculation. Dropping the 5 lowest-energy orbitals of each spin reduced that number to 124 each. Performing the calculation in the *p*VTZ+*sp* basis used for the smaller linear carbon clusters would have meant over 250 basis functions of each spin.

The first calculated ionization appears identical with the first experimental ionization. Although Smalley's group reports a vertical electron affinity of 3.10 eV, the available experimental plot has a maximum maximum closer to 3.40 eV, which gives almost perfect overlap between the experimental plot and the EOMIP results. This apparent improvement in the position of the first ionization energy compared to the C_5^- calculation is consistent with the results for smaller molecules, where reduction of the valence-type polarization functions leads to slightly smaller ionization energies, and slightly better agreement between theory and experiment, at least for the first ionization.

11.4.5 C_9^-

The disagreement of the UHF EOMIP calculation with experiment (figure 11.4) can be attributed to the unsuitability of the orbitals. Among the CCSD amplitudes, there is one large $T_1\alpha$ element, a π_{gx} valence excitation with amplitude .128. In the QRHF CCSD calculation, the situation is similar, and would presumably lead to similar EOMIP results

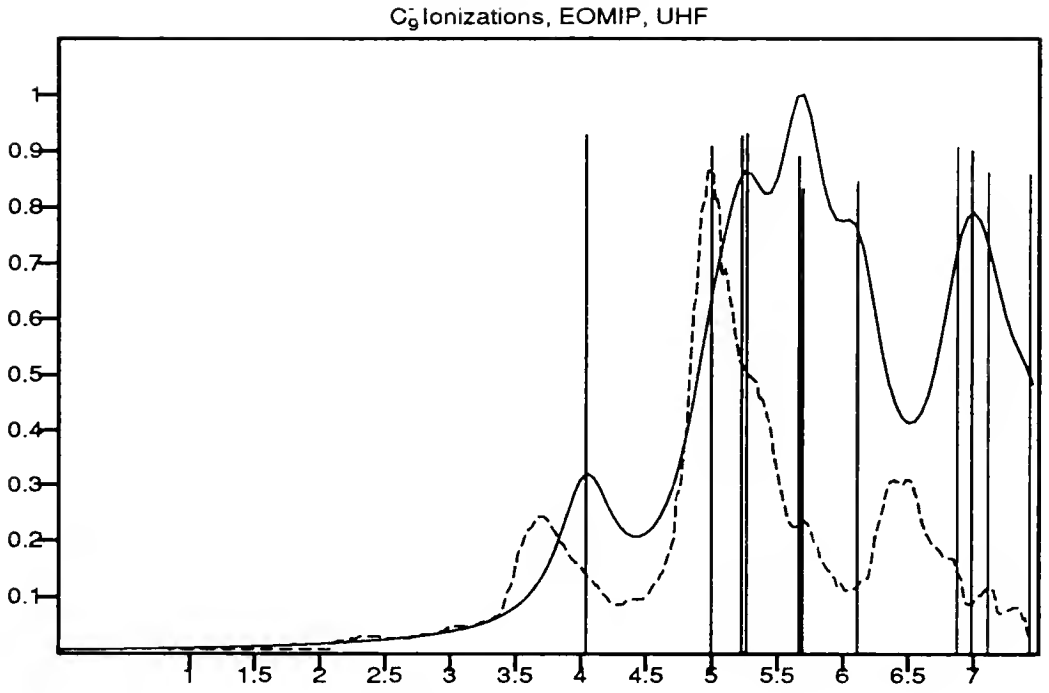

Figure 11.4: Ionization spectrum of C_9^-

Table 11.9: C_9^- Ionization, UHF orbitals

	Energy eV (Intensity)		
C_9 State	EOMIP		Expt.
$1\Sigma_g^+$	4.041	(0.928)	3.684 ± 0.01^a
			3.70^b
$1\Sigma_u^-$	4.997	(0.909)	
			5.0^c
$3\Sigma_u^-$	5.227	(0.927)	
$3\Sigma_u^+$	5.267	(0.931)	
$1\Sigma_u^+$	5.664	(0.891)	
$3\Pi_g$	5.693	(0.833)	
$3\Pi_u$	5.694	(0.833)	
$1\Pi_g$	6.112	(0.840)	
$1\Pi_u$	6.113	(0.846)	
			6.5^c
$3\Sigma_g^+$	6.875	(0.908)	
$3\Sigma_g^-$	6.985	(0.900)	
$1\Sigma_g^-$	7.109	(0.862)	
$1\Sigma_g^+$	7.429	(0.859)	

[a] As reported by Arnold et al. [36]

[b] As reported by Yang et al. [35]

[c] Maxima observed in plots by Yang et al. [35]

On the beta side, the UHF CCSD also has a large π_{gx} valence excitation, with amplitude -.115, while QRHF has one with amplitude -.058, which is not as severe. It would seem that the size of the T_1 amplitudes make the UHF orbitals the worst possible choice from the point of view of the size of the correlation correction – ΔE_{CCSD} is -1.131 for UHF, -1.068 for QRHF, and -1.040 for ROHF. Only the ROHF CCSD calculation doesn't show any T amplitudes over .1, which should indicate that EOMIP results would be improved if ROHF orbitals were used.

11.4.6 Even-Length Chains

A pervasive problem with calculations on C_4^-, C_6^-, and C_8^- is the partially-filled acetylenic valence π orbital, which inevitably leads to symmetry breaking because the calculations are carried out in the D_{2h} Abelian subgroup of the full $D_{\infty h}$ molecular symmetry. While an ROHF calculation on the ion will ensure that alpha and beta orbitals are identical, it cannot ensure that the π_x and π_y components of the partially filled valence π orbital will be identical. And while a QROHF calculation based on the ground state neutral will provide properly symmetric π_x and π_y orbitals, the mere fact that they are occupied differently in the reference will break the symmetry. The SRCC calculation cannot promote electron occupation from one irreducible representation to another, and so cannot "fix up" the broken symmetry. This means that certain states which should be degenerate in energy will not be. For example, Arnold *et al.* [36] cite experimental and theoretical evidence that C_4, C_6, and C_8 have low-lying $^1\Delta$ excited states. These arise in the photoelectron spectrum when an electron is

removed from a π orbital other than the one partially filled in the ground state ion or neutral. The possible results are a Σ^+, a Σ^-, and a Δ state. In the D_{2h} symmetry group, these choices reduce to two Σ^+ and two Σ^- states. If the molecular symmetry were preserved, one of the Σ^- states would clearly be degenerate with one of the Σ^+ states, with characteristic symmetry between the π_x and π_y orbitals. In CC EOMIP calculations on these even-length chains, the energies of such states will be split, and the wavefunctions will not show exact x-y symmetry. However, in cases of near degeneracy where the wavefunctions show something approaching the proper form, it may be presumed that the states are in fact an approximation to the proper Δ state.

11.4.7 C_2^-

EOMIP calculations in UHF and QRHF orbitals (table 11.10 and figure 11.4.7) tell approximately the same story. The relationship between the experimental and calculated spectra is slight. In addition to the afore-mentioned multi-reference problem (section 10.4), there is the problem of spin contamination in the open-shell singlet states of C_2. With the exception of the $^1\Sigma_g^+$ line, all the so-called singlet states are in fact severely spin contaminated, with an S^2 expectation value of 1.4. This means that the $^1\Pi_u$ line should be expected to move up in energy, narrowing the first peak, and moving its maximum slightly lower in energy, as well as decreasing the relative height of this peak.

The two-determinant MRCCSD calculation, like the EOMIP calculation, incorrectly places the C_2 $a^3\Pi_u$ state lower in energy than the ground $X^1\Sigma_g^+$ state. Triples

corrections are required to correctly order these states. The two-determinant calculation gives a singlet-triplet splitting of the Π states similar to that given by the EOMIP calculation, but gives a much larger splitting for the Σ_u^+ states (4.6 eV versus 1.17eV for the EOMIP). With the $^1\Sigma_u^+$ state near 9 eV, the two-determinant calculation gives a simulated spectrum much more similar to experiment than the EOMIP calculation does.

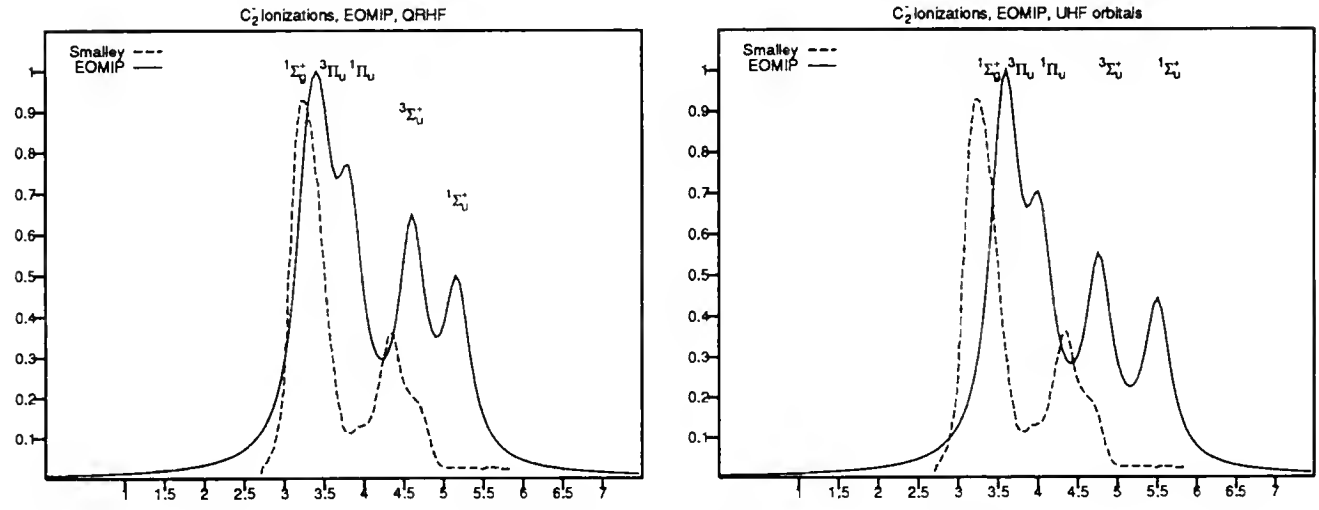

Figure 11.5: C_2^- Ionization spectrum, EOMIP calculation

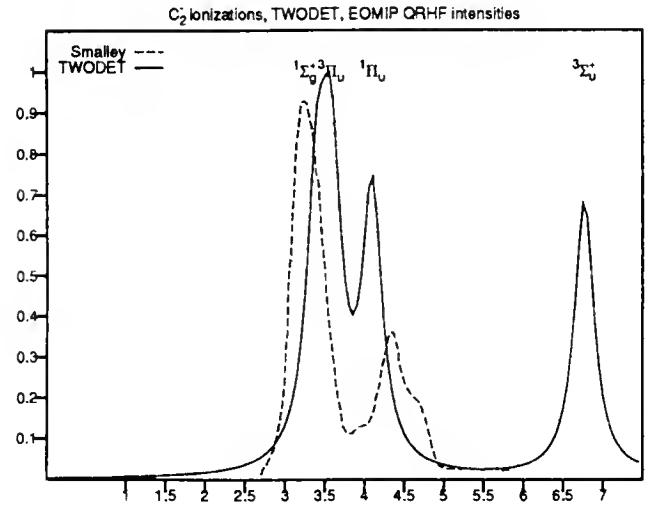

Figure 11.6: C_2^- ionization spectrum, two-determinant calculation

Table 11.10: C_2^- in pVTZ+sp basis, QRHF orbitals

			Energy eV (Intensity)		
C_2^-	C_2	Reference	EOMIP	Other	Experiment
$X^2\Sigma_g^+$					
	$X^1\Sigma_g^+$	$3\sigma_g^+$	4.05(.849)	3.359[a]	3.273[c]
					≈ 4.4[d]
	$a^3\Pi_u$	$1\overline{\pi}_u$	3.450(.891)	3.059[b]	3.351[c]
	$^3\Sigma_u^+$	$2\overline{\sigma}_u^+$	4.600(.893)	4.446[b]	
	$^1\Pi_u$	$1\pi_u$	4.954(.863)	4.090[b]	
	$^1\Sigma_u^+$	$2\sigma_u^+$	5.770(.640)	9.074[b]	
	$^3\Sigma_g^+$	$2\overline{\sigma}_g^+$, $2\pi_g^\dagger 2\sigma_u^+ 1\overline{\pi}_u$	11.952(.057)		
	$^1\Sigma_g^+$	$2\sigma_g^+$, $3\overline{\sigma}_g^{+\dagger} 2\overline{\sigma}_u^+ 2\sigma_u^+$	12.221(.100)		
	$^1\Sigma_u^+$	$2\sigma_u^+$, $2\overline{\pi}_g{}^\dagger 2\overline{\pi}_u 3\sigma_g^+$	12.395(.274)		
	$^3\Sigma_g^+$	$2\overline{\sigma}_g^+$, $2\pi_g^\dagger 2\sigma_u^+ 1\overline{\pi}_u$	14.015(.516)		
	$^1\Sigma_g^+$	$2\sigma_g^+$, $3\overline{\sigma}_g^{+\dagger} 2\overline{\sigma}_u^+ 2\sigma_u^+$	15.478(.175)		
	$^1\Sigma_g^+$	$2\sigma_g^+$, $3\overline{\sigma}_g^{+\dagger} 2\overline{\sigma}_g^+ 3\sigma_g^+$	19.69(.422)		

[a] ΔCCSD in pVTZ+sp basis

[b] TWODET MRCCSD calculation, QRHF orbitals

[c] Arnold et al. [36]

[c] Yang et al. [35]

11.4.8 C_4^-

In the spectrum of figure 11.7, one can confidently assign the $^1\Sigma_u^+$ line to the left shoulder of the first experimental peak, but beyond that it is difficult to associate calculated with experimental features. Arnold *et al.* assign a peak at 4.209 eV to a $^1\Delta$ state of C_4 In the QROHF orbitals, the character of the two wavefunctions differ enough that they do not approximate a Δ state. The $^1\Sigma_g^+$ state, for example, dominated by the $\cdots 1\pi_{gx}1\overline{\pi}_{gx}$ configuration, has the accompanying $\cdots 1\pi_{gy}1\overline{\pi}_{gy}$ configuration with the wrong sign to indicate a Δ state. And the $^1\Sigma_g^-$ state is perhaps closer to being a low-spin triplet than a singlet state

In the ROHF orbitals, however, the spin contamination and symmetry breaking problems are somewhat reduced in the two EOMIP wavefunctions, which do, when taken together resemble a $^1\Delta$ state, supporting the assignment made by Arnold *et al.* While the correlation correction in the ROHF orbitals is .03 Hartrees smaller than that in the QRHF orbital set (the total energies agree to a milliHartrees), some of the largest T_2 amplitudes in the ROHF set are up to 50% larger than the corresponding QRHF amplitudes, indicating a possible source of error in ROHF-based calculations. It is impossible, based on this evidence to draw a firm conclusion on the assignment of the peak.

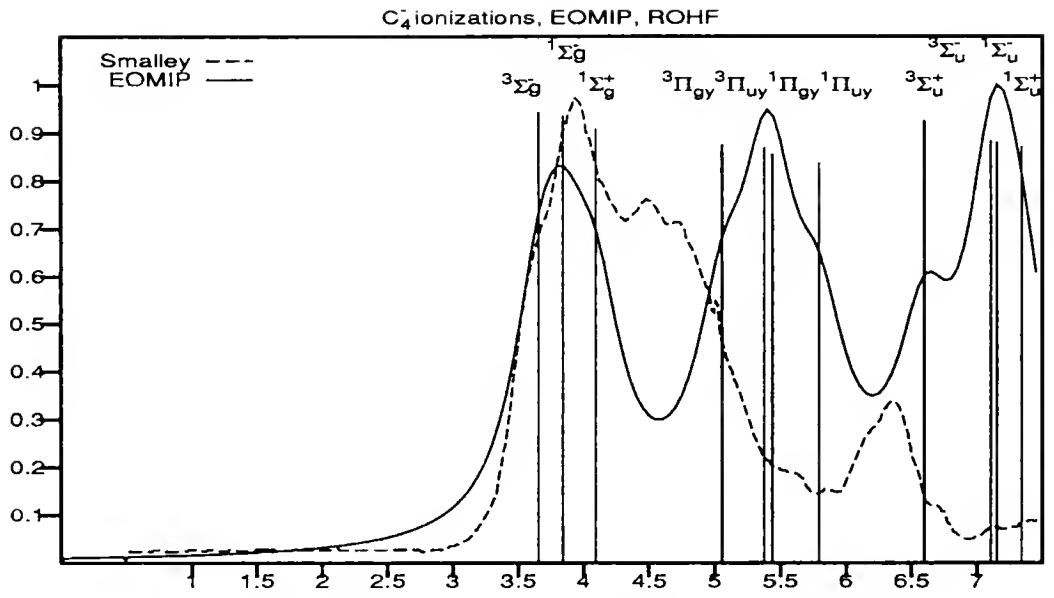

Figure 11.7: C_4^- ionization spectrum, ROHF orbitals

Table 11.11: Ionization of C_4^- in pVTZ+sp basis, ROHF orbitals

		Energy eV (Intensity)		
C_4 State	Reference	EOMIP		Experiment
$^3\Sigma_g^-$	$1\overline{\pi}_g$	3.655	(.944)	3.882± .01[a] 3.70[b]
$^1B_{1g}$	$1\pi_{gx}$	3.843	(.935)	
^1A_g	$1\pi_{gy}$	4.093	(.909)	
				4.209[a]
				4.5[c]
$^3\Pi_g$	$5\overline{\sigma}_g^+$	5.057	(.875)	
$^3\Pi_u$	$4\overline{\sigma}_u^+$	5.377	(.869)	
$^1\Pi_g$	$5\sigma_g^+$	5.439	(.855)	
$^1\Pi_u$	$4\sigma_u^+$	5.795	(.837)	
				6.4[c]
$^3\Sigma_u^+$	$1\overline{\pi}_{uy}$	6.598	(.925)	
$^3\Sigma_u^-$	$1\overline{\pi}_{ux}$	7.106	(.882)	
$^1\Sigma_u^-$	$1\pi_{ux}$	7.151	(.880)	
$^1\Sigma_u^+$	$1\pi_{uy}$	7.341	(.871)	

[a] As reported by Arnold et al. [36] [b] As reported by Yang et al. [35]

[c] Maxima observed in plots by Yang et al. [35]

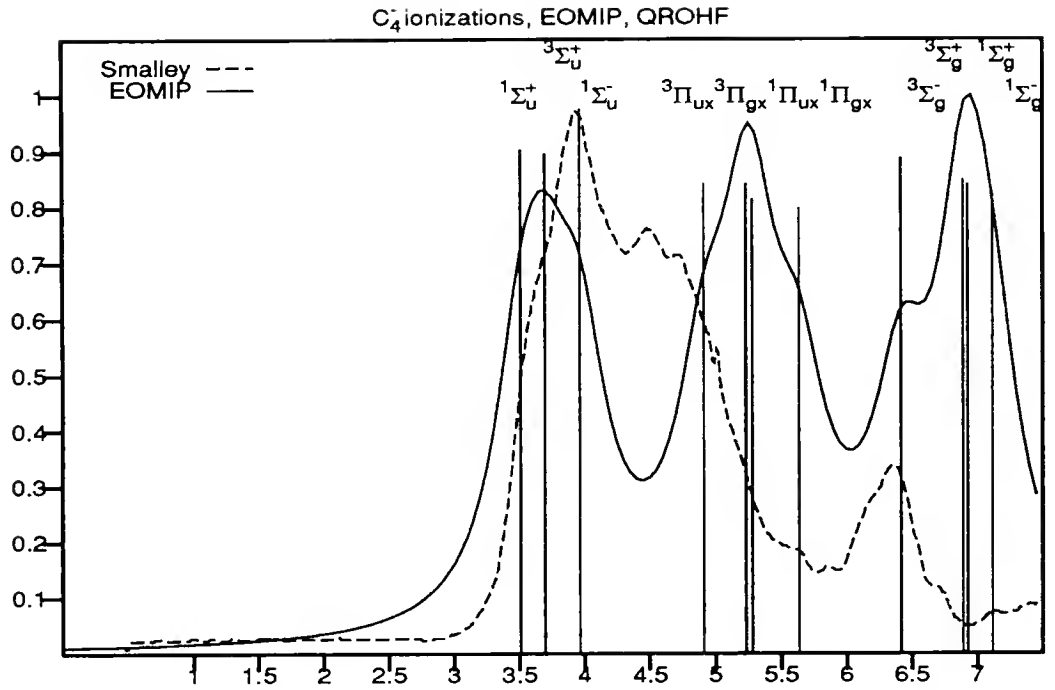

Figure 11.8: C_4^- ionization spectrum, QROHF orbitals

Table 11.12: Ionization of C_4^- in pVTZ+sp basis, QROHF orbitals

	Energy eV (Intensity)			
C_4 State	Reference	EOMIP		Experiment
$^3\Sigma_g^-$	$1\overline{\pi}_g$	3.512	(.904)	3.882± .01[a] 3.70[b]
$^1B_{1g}$	$1\pi_{gx}$	3.698	(.896)	4.209[a]
^1A_g	$1\pi_{gy}$	3.965	(.876)	
				4.5[c]
$^3\Pi_g$	$5\overline{\sigma}_g^+$	4.912	(.841)	
$^3\Pi_u$	$4\overline{\sigma}_u^+$	5.234	(.841)	
$^1\Pi_g$	$5\sigma_g^+$	5.281	(.814)	
$^1\Pi_u$	$4\sigma_u^+$	5.637	(.798)	
				6.4[c]
$^3\Sigma_u^+$	$1\overline{\pi}_{uy}$	6.415	(.888)	
$^3\Sigma_u^-$	$1\overline{\pi}_{ux}$	6.888	(.849)	
$^1\Sigma_u^-$	$1\pi_{ux}$	6.92	(.840)	
$^1\Sigma_u^+$	$1\pi_{uy}$	7.11	(.827)	

[a] As reported by Arnold et al. [36] [b] As reported by Yang et al. [35]

[c] Maxima observed in plots by Yang et al. [35]

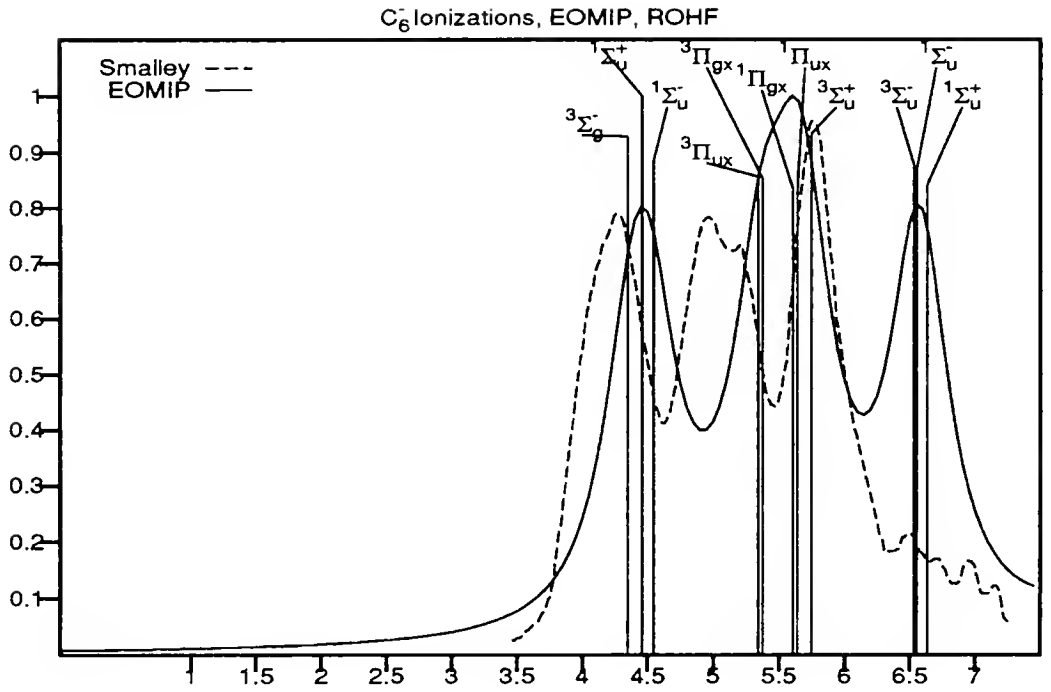

Figure 11.9: Ionization spectrum of C_6^-

Table 11.13: Ionization of C_6^-, ROHF orbitals

State	EOMIP		Expt.	Orbitals
$^3\Sigma_g^-$	4.347	(0.928)	4.185±0.006[a] 4.10[b]	$2\overline{\pi}_{ux}$
^1A_g	4.459	(1.000)	4.36[a] ($^1\Delta$)	$1\pi_{ux}$
$^1B_{1g}$	4.547	(0.884)		$1\pi_{uy}$
			5.0[c]	
			5.2[c]	
$^3\Pi_{ux}$	5.344	(0.856)		$7\overline{\sigma}_g$
$^3\Pi_{gx}$	5.377	(0.853)		$6\overline{\sigma}_u$
$^1\Pi_{ux}$	5.608	(0.834)		$6\sigma_g$
$^1\Pi_{gx}$	5.644	(0.833)		$7\sigma_u$
			5.7[c]	
$^3\Sigma_u^+$	5.750	(0.933)		$1\overline{\pi}_{gx}$
$^3\Sigma_u^-$	6.530	(0.878)		$1\overline{\pi}_{gy}$
$^1\Sigma_u^-$	6.554	(0.868)		$2\pi_{gx}$
$^1\Sigma_u^+$	6.633	(0.841)		$2\pi_{gy}$

[a] As reported by Arnold et al. [36] [b] As reported by Yang et al. [35]

[c] Maxima observed in plots by Yang et al. [35]

11.4.9 C_6^-

The EOMIP value for the first ionization of C_6^- is within .2 eV of the experimental value. Beyond that, the assignment of peaks becomes more difficult, although the theoretical and experimental spectra (figure 11.9 and table 11.13) are more similar here than they are for C_4^-. Assigning the cluster of EOMIP states between 5.344 and 5.644 eV to the two experimental peaks at about 5.0 and 5.2 eV implies EOMIP results in error by .3 to .44 eV in this region. While it would be convenient to assign the $^3\Sigma_u^+$ peak at 5.75 eV to the experimental 5.70 peak, an error this small seems unlikely in light of the errors at lower energy. Therefore, it would seem that the double-peaked experimental structure centered at about 5.1 eV is composed of transitions to the $^3\Pi_u$, $^3\Pi_g$, $^1\Pi_u$, $^1\Pi_g$, and $^3\Sigma_u^+$ states at energies ranging from 5.344 to 5.750 eV. In fact, the $^3\Sigma_u^+$ could be related to the small shoulder on the high-energy side of the 5.2 eV peak. This leaves the remaining peaks in the range, $^3\Sigma_u^-$, $^1\Sigma_g^+$, and $^1\Sigma_g^-$, to be assigned to the experimental 5.7eV peak, with an error somewhere in the range of .83 to .96 eV. The $^1\Sigma_g^-/^1\Sigma_g^+$ pair of peaks, separated by only .09 eV, show some Δ characteristics. Although the ratio of the two π_u^2 configurations is a little under 10:1 for the C_1 versus the C_2 amplitude, the signs are consistent with a $^1\Delta$ state, and the energies are close enough together to to be considered nearly degenerate. The Σ_u pair of states near 7 eV, on the other hand, despite their nearly-degenerate energies, do not display the characteristics of a $^1\Delta$ state, and show all evidences of being approximations to the true $^1\Sigma_u^-$ and $^1\Sigma_u^+$ states.

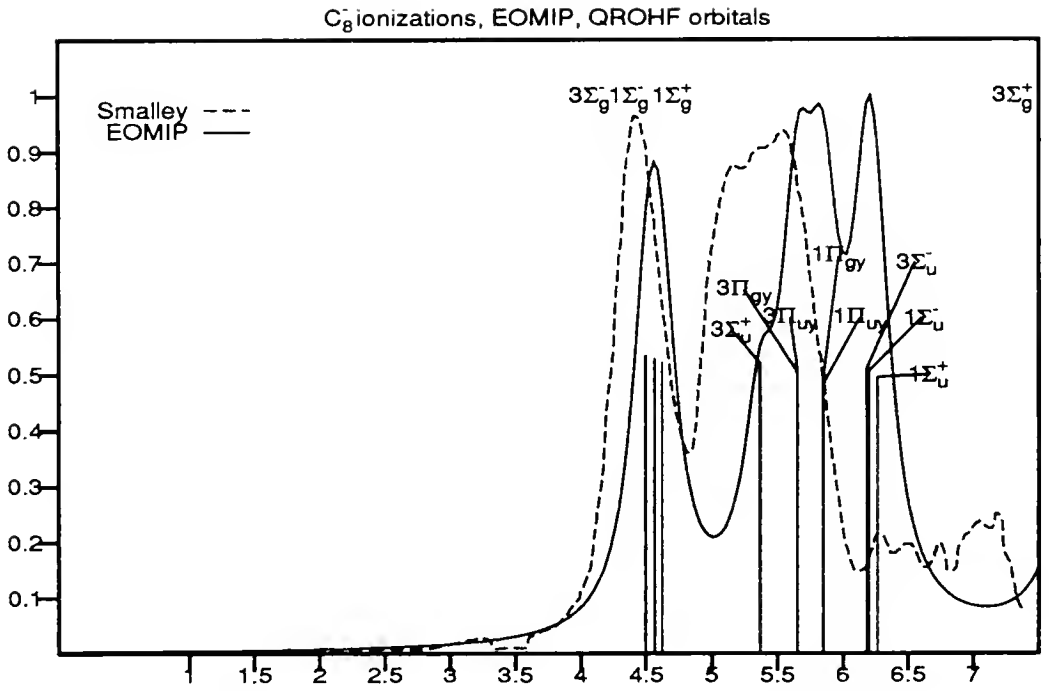

Figure 11.10: Ionization spectrum of C_8^-, QROHF orbitals

Table 11.14: C_8^- Ionization, QROHF orbitals

	Energy eV (Intensity)		
State	EOMIP		Expt.
$^3\Sigma_g^-$	4.498	(.889)	4.379±0.006[a]
			4.42[b]
^1A_g	4.566	(.882)	
$^1B_{1g}$	4.623	(.871)	
			4.449[a] ($^1\Delta$)
			5.2[c]
$^3\Sigma_u^+$	5.370	(.866)	
			5.4[c]
			5.5[c]
$^3\Pi_{gy}$	5.654	(.839)	
$^3\Pi_{uy}$	5.657	(.843)	
$^1\Pi_{gy}$	5.849	(.814)	
$^1\Pi_{uy}$	5.853	(.806)	
$^3\Sigma_u^-$	6.184	(.852)	
$^1\Sigma_u^-$	6.200	(.843)	
$^1\Sigma_u^+$	6.266	(.826)	
$^3\Sigma_g^+$	7.757	(.871)	

[a] As reported by Arnold et al. [36] [b] As reported by Yang et al. [35]

[c] Maxima observed in plots by Yang et al. [35]

11.4.10 C_8^-

The resemblance between the theoretical and experimental peaks for the ionization of C_8^- is even more striking than it is for the smaller even-length chains. The difference between the calculated first ionization and that of the next two calculated energies, at 4.566 and 4.623 eV, belong under the first experimental peak. For C_8^-, as for the C_4^- QROHF calculation, these two states do not exhibit $^1\Delta$ characteristics, and in act appear to be much more spin contaminated and symmetry broken than the $^1\Delta$ C_6 state wavefunctions were. It appears that the choice of QROHF orbitals causes additional difficulty in overcoming the spin and symmetry contamination problems of the reference.

11.4.11 Summary

The ROHF orbitals give good agreement with experiment for the first ionization of C_4^-, C_6^-, and C_8^- in the DZP+*sp* basis set. For higher-energy ionizations, there seems to be a problem with the distribution of the peaks. These even-length chains show considerable differences in bond lengths and the amount of bond-length alternation between the anion and the ground-state neutral. There is, as yet, no in-depth theoretical analysis of the bonding character or the electron density distribution of any of the excited states of the neutrals. Watts and Bartlett [65] observed that the anions exhibit considerable bond-length alternation, midway between the cumulenic

neutral ground state structure and the acetylenic dianion structure. This suggests that there are considerable differences in π orbital densities among these states, and likely among the various neutral excited states. Bernholdt noted that the size and direction of the FSCC third-order triples approximation differed between π and σ ionizations of C_5. It would require a more detailed examination of electron density and bonding in these states to answer these questions.

CHAPTER 12

SUMMARY

In this work, the author has

- Derived the CC EOMIP method for the study of electron-detached states. The implementation, in the CC EOMIP program, uses Nakatsuji's generalization of the Davidson diagonalization method in a thrifty and fast-converging approach to studying several states of a given molecule in a consistent framework.

- Developed procedures to follow desired roots from one iteration to the next and to search for the "shake-up" states which are important to the interpretation of photodetachment spectra, but difficult or impossible to obtain from other coupled-cluster based methods such as FSCC.

- Developed formulae for transition intensities based on CCLRT and the sudden approximation, and implemented two levels of approximation.

- Evaluated the predictive ability of EOMIP by applying it to several well-studied molecules, and compared its accuracy to that of ΔCC, EE-EOM, and two-determinant coupled-cluster approaches.

- Investigated photodetachment spectrum of the linear carbon cluster anions C_2^- through C_9^-, with special attention to its ability to interpret available experimental spectra. Various basis set and molecular orbital effects were observed.

- Demonstrated the formal correspondence between the EOMIP and FSIP methods, giving simple proofs of the invariance of the Fock-space method to the choice of active space, and of the size intensivity of the EOMIP method for principal ionizations.

As timings in table 12.1 indicate, the computational the required for converging these 12 roots is a very small compared to the time required for a CCSD calculation. Only 3.2% of the total central processing unit (CPU) time for the C_5^- job is spent on the EOMIP calculations. These timings are comparable to those for the FSCC calculation, which is to be expected since the formal equivalence of the two methods means that the terms to be encoded in either case are very similar.

From essentially single-reference starting points, the EOMIP method provides valence ionization energies useful for comparison to experiment, when used with high quality basis sets. Sufficient polarization functions are important to the representation of the wavefunction, but addition of diffuse, Rydberg-like functions to these basis sets make only very minor contributions. Using *p*VTZ+sp and DZP+sp basis sets in conjunction with the 2h1p CCSD-EOMIP method for small closed shell molecules gives quite reasonable results. There is a tendency for higher-energy roots to show increasingly positive errors. This tendency can be counteracted to some extent if core hole orbitals are used, bringing the core hole peak into better agreement with

Table 12.1: Computational times for EOMIP and FSCC calculations for electron detachment of C_5^- and N_2 using the PVTZ+*sp* basis set. An RHF and a UHF reference are used for N_2 and C_5^-, respectively. Timings are in seconds of Cray-YMP8 CPU time.

	Timings			
Computational step	N_2		C_5^-	
Integral evaluation	24		409	
SCF calculation	6		39	
Integral transformation	19		236	
Integral sorting	12		203	
CCSD calculation	27		845	
Subtotal	89		1732	
FSIP	4	(13 iters, 4 roots)	21	(17 iters, 12 roots)
EOMIP singlet	5	(12 iters, 4 roots)	33	(15 iters, 6 roots)
EOMIP triplet			24	(15 iters, 6 roots)

experiment as might be expected, but also improving agreement in the inner and outer valence regions. Using smaller basis with fewer polarizing functions can also counteract this tendency for the outer valence and core peaks, but accuracy in the inner-valence region suffers. The shake-up spectrum is poorly represented, with too much intensity concentrated in regions that are not important in the experimental spectrum.

While it might seem reasonable that some level of triples approximation would improve the position of the higher EOMIP peaks, perhaps lowering the energies too much, as is the case with the SRCC CCSD+T(CCSD) approximation (and less so with CCSD(T)), an examination of FSCC triples approximations does not bear this out. In Bernholdt's work, triples corrections increased the energies more often than decreased them. Either the triples approximations are poor approximations to the true triples (as is indicated by the size of fourth-order triples corrections in recent

work by Pal and Mukherjee[43]), or some higher order of excitation is as important as or more important than triples. In SRCC, for example, the quadruples which arise from T_2^2 are often more important to the wavefunction than the triples corrections, and such contributions are missing in the EOM or FSCC linear ansatz.

For cases (such as that of a multi-reference starting point) where double excitations not involving the annihilated electron have very different magnitudes in the N-1- than in the N-electron wavefunction, the method might be improved by the inclusion of some approximation to spectator triples in the EOMIP manifold space. This kind of triples correction might be most useful in cases such as the C_2 and C_2^- ionizations.

One source of difficulty with EOMIP calculations on open-shell systems is the spin contamination problem, especially for small molecules where the splitting between states with different S^2 eigenvalues is largest. There are two approaches which can be taken to this problem. One is simply to include one more level of excitation operator. For example, the UHF reference for C_2^- shows $\langle 0| S^2 |0\rangle = .770$, with an average multiplicity of 2.020. The CCSD wavefunction, because of the exponential form of the wave reaction operator, contains determinants of all excitation levels possible for the system, and effectively has had projected out of it the worst spin contaminants. The expectation value of S^2 is .751, with the approximate spin multiplicity in error by only .05%. Adding triple excitations to the EOMIP wavefunction would improve the spin-contamination situation by pushing the problem up one more level of excitation, where the dynamic correlation contributions should be smaller. This is a brute force approach, one which significantly increases the size of the EOMIP vector while adding

many new terms to the EOMIP equations, terms which require more operations to evaluate than coupled-cluster T_2 terms, although fewer than coupled-cluster T_3 terms.

The spin contamination problem can also be solved, somewhat more thriftily in terms of computational time and disk space, by the explicit spin adaptation of the EOMIP equations. This task must be undertaken separately for every spin case of interest, resulting in a proliferation of code. The easiest and most commonly required case is the open-shell singlet. Conceptually, one can think of creating two types of determinants at the EOMIP singles level – one based on removing an alpha electron from a reference with one unpaired alpha electron, the other based on removing a beta electron from a reference with one unpaired beta electron. Since the terms involving only those operators associated with one or the other of the references are identical to what is already coded, the only portion remaining is a block of terms involving an alpha-beta projection of $\bar{H}$. The amount of work involved in fully implementing these terms is similar to that involved in the implementation of the original terms, and is another possible course for future development.

Although the relevant condition for the EOMIP-SD to work well is that the amplitudes obtained from $T_1 * S_1$ aren't too different from the final $(T_1 * S1 + S2)$ amplitude for the same determinants, it seems that simply having smallish T1 and T2 amplitudes is a big help in general, something that can be most fully appreciated after a study of difficult molecules such as the small linear carbon cluster anions studied here. No doubt important reasons for this are

- The method is most applicable when the S_3 and higher amplitudes are pretty nearly small enough to neglect and
- large T_1 and T_2 amplitudes can create large contributions at the S_3 and higher level (as $T_1 * S_2$, $T_2 * S_1$, $T_2 * S_2$, etc.), in contradiction to the first point

There might be exceptional cases where a large $T_1 * S_2$ or $T_2 * S_1$ contribution to the S_3 part of the wavefunction is just exactly the one needed, or an erroneous S_3 contribution to the wavefunction is fortuitously in just the right direction energetically, but these cases are most likely exceptions to the rule.

The coupled-cluster EOMIP-SD has been shown useful for producing ionization spectra which compare well with experiment for inner and outer valence regions, including inner valence shake-up effects, as well as core hole primary ionizations, for both saturated and unsaturated closed shell molecules when high-quality basis sets are used. For the linear carbon cluster anions, all of which are open shell, most of

Table 12.2: EOMIP errors, pVTZ+ basis, small closed-shell molecules

	first ionization	outer valence	inner valence	core
closed shell	0.2	0.5	1.0 to 1.5	0.8
core hole	0.1	0.3	0.5 to 1.3	0.2

which are characterized by partially-filled π orbitals, the situation is different. The EOMIP approach has several advantages. First, it can be used to directly calculate many ionizations quickly and cheaply in terms of computer time, as compared to single-state methods which require an expensive correlated calculation for each state.

Second, EOMIP can be used to search the shake-up space. It is difficult or impossible to converge on desired shake-up peaks using conventional N-electron methods, and the use of the well-correlated CCSD reference state makes EOMIP more accurate than the 2h1p CI approach. The Davidson diagonalization method for the extraction of roots, along with the root finding and root following algorithms, makes the EOMIP approach less susceptible to the intruder state problems which can make it difficult to impossible to converge inner valence FSIP states. While highly correlated calculations such as CCSD(T) will provide better information about specific roots, EOMIP generally provides more information overall about more portions of the ionization spectrum. EOMIP can be reliably applied to systems with conventional bonding characteristics. More experience with unconventional bonding situations such as the even-length linear carbon cluster chains should shed some light on which types of roots are reliable in these situations, and what can be done to improve EOMIP performance. Co-development of triples approximations from FSCC and EOMIP standpoints should lead to better performance of both methods in most situations.

APPENDIX A

INVARIANCE OF FOCK-SPACE ENERGIES TO CHOICE OF ACTIVE SPACE

Invariance of the Ionization Energies

From the definitions given in section 4.1, the FSIP equations have been shown to satisfy

$$Q\left(\bar{H}_N\Omega - \Omega H_{eff}\right)P = Q\left(\bar{H}_N + \left(\bar{H}_N S\right)_c - \left(S H_{eff}\right)_c\right)P = 0 \tag{A.1}$$

$$\text{where } PH_{eff}P = P\left(\bar{H}_N + (\bar{H}_S)_c - (S\bar{H}_N)_c\right)P = P\left(\bar{H}_N + (\bar{H}_N S)_c\right)P \tag{A.2}$$

The operator equation $PH_{eff}PC = PC\mathcal{W}$, as well as the identity $QH_{eff}PC = 0$ can be written in matrix form:

$$\left(\bar{H}_N\Omega - \Omega H_{eff}\right)_{QP} = \left(\bar{H}_{QP} + \bar{H}_{QQ}S_{QP} - S_{QP}H_{eff}\right)C_{PP} = 0 \tag{A.3}$$

$$\begin{aligned} H_{eff}C_{PP} &= \left(\bar{H}_{PP} + \bar{H}_{PQ}S_{QP}\right)C_{PP} \\ &= C_{PP}\mathcal{W} \end{aligned} \tag{A.4}$$

Consider a partitioning of the active space into A and its complement in P, B $(= P - A)$. The complement to A in the full $(P + Q)$ space is Q' $(= Q + B)$. The

matrices appearing in the H_{eff} expression can be partitioned into A and B parts,

$$\bar{H}_{PP} = \begin{pmatrix} \bar{H}_{AA} & \bar{H}_{AB} \\ \bar{H}_{BA} & \bar{H}_{BB} \end{pmatrix} \qquad \bar{H}_{PQ} = \begin{pmatrix} \bar{H}_{AQ} \\ \bar{H}_{BQ} \end{pmatrix}$$
$$S_{QP} = \begin{pmatrix} S_{QA} & S_{QB} \end{pmatrix} \quad C_{PP} = \begin{pmatrix} C_{AA} & C_{AB} \\ C_{BA} & C_{BB} \end{pmatrix}$$
$$\mathcal{W} = \begin{pmatrix} \mathcal{W}_A & 0 \\ 0 & \mathcal{W}_B \end{pmatrix}, \qquad \textit{etc.}$$

which leads to

$$\begin{aligned} H_{eff} &= \left[\begin{pmatrix} \bar{H}_{AA} & \bar{H}_{AB} \\ \bar{H}_{BA} & \bar{H}_{BB} \end{pmatrix} + \begin{pmatrix} \bar{H}_{AQ}S_{QA} & \bar{H}_{AQ}S_{QB} \\ \bar{H}_{BQ}S_{QA} & \bar{H}_{BQ}S_{QB} \end{pmatrix} \right] \begin{pmatrix} C_{AA} & C_{AB} \\ C_{BA} & C_{BB} \end{pmatrix} \\ &= \begin{pmatrix} C_{AA}\mathcal{W}_A & C_{AB}\mathcal{W}_B \\ C_{BA}\mathcal{W}_A & C_{BB}\mathcal{W}_B \end{pmatrix}. \end{aligned} \tag{A.5}$$

The AA part of this equation can be written as

$$\Big(\big(H_{eff}\big)_{AA} + \big(H_{eff}\big)_{AB} C_{BA} C_{AA}^{-1} \Big) C_{AA} =$$
$$\Big(\bar{H}_{AA} + \bar{H}_{AB} C_{BA} C_{AA}^{-1} + \bar{H}_{AQ} S_{QA} + \bar{H}_{AQ} S_{QB} C_{BA} C_{AA}^{-1} \Big) C_{AA} = C_{AA} \mathcal{W}_A, \tag{A.6}$$

and the BA part as

$$\Big(\bar{H}_{BA} + \bar{H}_{BQ} S_{QA} + \bar{H}_{BB} C_{BA} C_{AA}^{-1} + \bar{H}_{BQ} S_{QB} C_{BA} C_{AA}^{-1} \Big) C_{AA} = C_{BA} \mathcal{W}_A. \tag{A.7}$$

The Bloch equation can also be expanded:

$$Q\Big(\bar{H}\Omega - \Omega H_{eff} \Big) P C_{PP} = 0$$
$$\left[\begin{pmatrix} (\bar{H}\Omega^A)_{QA} & (\bar{H}\Omega^A)_{QB} \end{pmatrix} + \begin{pmatrix} (\Omega^A H^A_{eff})_{QA} & (\Omega H^A_{eff})_{QB} \end{pmatrix} \right] \begin{pmatrix} C_{AA} & C_{AB} \\ C_{BA} & C_{BB} \end{pmatrix} = 0;$$

which gives, in the AA block of the product,

$$\Big(\bar{H}_{QA} + \bar{H}_{QB} C_{BA} C_{AA}^{-1} + \bar{H}_{QQ} S_{QA} + \bar{H}_{QQ} S_{QB} C_{BA} C_{AA}^{-1}$$
$$- S_{QA} H_{eff\,AA} - S_{QA} H_{eff\,AB} C_{BA} C_{AA}^{-1}$$
$$- S_{QB} H_{eff\,BA} - S_{QB} H_{eff\,BB} C_{BA} C_{AA}^{-1} \Big) C_{AA}$$

$$= \left(\bar{H}_{QA} + \bar{H}_{QQ}S^A_{QA} + \bar{H}_{QB}S^A_{BA} - S_{QA}C_{AA}\mathcal{W}_A C^{-1}_{AA} - S_{QB}C_{BA}\mathcal{W}_A C^{-1}_{AA}\right) C_{AA}$$

$$= 0 \tag{A.8}$$

Consider now the solution to the FS equations in the A model space

$$\left(\bar{H}_{Q'A} + \bar{H}_{Q'Q'}S^A_{Q'A} - S^A_{Q'A}H^A_{eff}\right)C^A_{AA} = 0 \tag{A.9}$$

$$H^A_{eff}C^A_{AA} = \left(\bar{H}_{AA} + \bar{H}_{AQ'}S^A_{QP}\right)C^A_{AA} = C^A_{AA}\mathcal{W}^A. \tag{A.10}$$

It will be shown that the solution to the FSIP equations in the smaller space is

$$C^A_{AA} \equiv C_{AA} \tag{A.11}$$

$$S^A_{BA} \equiv C_{BA}C^{-1}_{AA} \tag{A.12}$$

$$S^A_{QA} \equiv \left(S_{QA} + S_{QB}C_{BA}C^{-1}_{AA}\right) = S_{QA} + S_{QB}S^A_{BA} \tag{A.13}$$

$$\mathcal{W}^A \equiv \mathcal{W}_A. \tag{A.14}$$

In order to do this, two conditions must be satisfied:

$$1) \qquad H^A_{eff} = \bar{H}_{AA} + \bar{H}_{AB}S^A_{BA} + \bar{H}_{AQ}S^A_{AQ} = C_{AA}\mathcal{W}_A C^{-1}_{AA}; \tag{A.15}$$

and

$$2) \qquad \left(\bar{H}\Omega^A - \Omega^A H^A_{eff}\right)_{Q'A} = 0. \tag{A.16}$$

The satisfaction of the first condition relies on nothing more than the fact that $\bar{H}$ does not depend on the choice of active space. Expanding $A\left(\Omega^{A^{-1}}\bar{H}\Omega\right)A$ gives

$$\begin{aligned} H^A_{eff} &= \bar{H}_{AA} + \bar{H}_{AQ'}S^A_{Q'A} \\ &= \bar{H}_{AA} + \bar{H}_{AQ}S^A_{QA} + \bar{H}_{AB}S^A_{BA} \\ &= \left(H_{eff}\right)_{AA} + \left(H_{eff}\right)_{AB}S^A_{BA} \end{aligned} \tag{A.17}$$

Substitution of the definitions given in equations A.11 through A.14 into equation A.18 gives exactly the parenthetical expression in equation A.6.

For the proof that the second condition is satisfied, the QA portion of equation A.15 is compared to equation A.8, and the BA portion is shown to be zero.

$$\begin{aligned}
&\left(\bar{H}\Omega^A - \Omega^A H_{eff}\right)_{QA} C_{AA} \\
&= \left(\bar{H}_{QA} + \bar{H}_{QQ}S^A_{QA} + \bar{H}_{QB}S^A_{BA} - S^A_{QA}H^A_{eff}\right)C_{AA} \\
&= \left(\bar{H}_{QA} + \bar{H}_{QQ}S^A_{QA} + \bar{H}_{QB}S^A_{BA} - S_{QA}C_{AA}\mathcal{W}_A C^{-1}_{AA} - S_{QB}C_{BA}C^{-1}_{AA}\left(C_{AA}\mathcal{W}_A C^{-1}_{AA}\right)\right)C_{AA} \\
&= \left(\bar{H}_{QA} + \bar{H}_{QQ}S^A_{QA} + \bar{H}_{QB}S^A_{BA} - S_{QA}C_{AA}\mathcal{W}_A C^{-1}_{AA} - S_{QB}C_{BA}\mathcal{W}_A C^{-1}_{AA}\right)C_{AA} \qquad \text{(A.18)}
\end{aligned}$$

Since this is exactly the same expression as that given in equation A.8, the QA projection of the Bloch equation is satisfied. Finally using equation A.7 as well as the the definitions in equations A.11 through A.14,

$$\begin{aligned}
&\left(\bar{H}\Omega^A - \Omega^A H_{eff}\right)_{BA} C_{AA} \\
&= \left(\bar{H}_{BA} + \bar{H}_{BQ}S^A_{QA} + \bar{H}_{BB}S^A_{BA} - S^A_{BA}H^A_{eff}\right)C_{AA} \\
&= \left(C_{BA}\mathcal{W}_A C^{-1}_{AA} - C_{BA}C^{-1}_{AA}\left(C_{AA}\mathcal{W}_A C^{-1}_{AA}\right)\right)C_{AA} \\
&= 0, \qquad \text{(A.19)}
\end{aligned}$$

the BA projection is shown to be zero as well. Therefore, the definitions in equations A.11 through A.14 give the solution to the Fock-space equations in the smaller model space A and the energies are invariant to a reduction in the size of the model space. Any two model spaces for the IP problem, whether or not one is a subset of the other, are subsets of the "complete active space". The FSIP energies obtained in either case are identical to those obtained for the same model functions in the complete active

space, and therefore, if there are any model functions in common, to those obtained in each of the smaller model spaces.

A Modification of the Bloch Equation to Preserve Invariance in Any Sector

In the higher sectors, $\Omega^{(m,n)}$ $(= \left\{e^{S^{(m,n)}}\right\}_N)$ and $C^{(m,n)}$ give the solution to the $P^{(m,n)}$ model space problem, while $\Omega_{old}^{(m,n)}$ is the product of all $\Omega^{(l,k)}$ where $l+k < m+n$. In the discussion which follows, all the (m,n) superscripts will be dropped. The operators Ω, Ω_{old}, P, Q, and S will all be assumed to be those which correspond to the sector being discussed. $\bar{H}_N$ is the familiar ${\Omega^{(0,0)}}^{-1} H_N \Omega^{(0,0)} = e^{-T} H_N e^T$. From the definitions given above, it can be shown that

$$PH_{eff}P = P(R + (RS)_c - (SR)_c)P = P(R + (RS)_c)P, \tag{A.20}$$

where

$$R = \bar{H}_N \Omega_{old}.$$

The equation $PH_{eff}PC = PCW$, as well as the identity $QH_{eff}PC = 0$ can now be written in matrix form:

$$\begin{aligned} PH_{eff}PC &\Rightarrow \left(R_{PP} + R_{PQ}S_{QP} \right) C_{PP} \\ &= C_{PP}\mathcal{W} \end{aligned} \tag{A.21}$$

where

$$\begin{aligned} R_{PP} &= \bar{H}_{PP} + \bar{H}_{PQ}\left(\Omega_{old} - 1\right)_{QP} \\ R_{PQ} &= \bar{H}_{PQ} \end{aligned}$$

Since the S operators, by definition, can not cause scattering *into* the P space, the P projection on the left prevents any contribution from Ω^{-1}. The right projection by P and the normal ordering of Ω_{tot} prevents many products of S amplitudes from contributing. The surviving contributions from Ω_{tot} are $e^T\Big(\mathbf{1} + S + (\Omega_{old} - 1)\Big)$.

The model space spanned by P is defined by the choice of active orbitals. The usual development of the FS equations assumes that this same choice is used for all sectors. Suppose, however, that it were desirable to solve the lower-rank sectors in one active space, and the current one in a smaller model space than that defined by the original choice of active orbitals. The following discussion will show that it is possible in this smaller model space, by using all the S amplitudes from the lower-ranked sectors, to arrive at the same energies.

The new model space is a subset of the P model space, called A; its complement in P is B $(= P - A)$. The complement to A contains both Q and B, and will be referred to as Q'. The matrices appearing in the H_{eff} expression can be partitioned into A and B parts,

$$
\begin{aligned}
R_{PP} &= \begin{pmatrix} R_{AA} & R_{AB} \\ R_{BA} & R_{BB} \end{pmatrix} \qquad R_{PQ} = \begin{pmatrix} R_{AQ} \\ R_{BQ} \end{pmatrix} \\
S_{QP} &= \begin{pmatrix} S_{QA} & S_{QB} \end{pmatrix} \quad C_{PP} = \begin{pmatrix} C_{AA} & C_{AB} \\ C_{BA} & C_{BB} \end{pmatrix} \\
\mathcal{W} &= \begin{pmatrix} \mathcal{W}_A & 0 \\ 0 & \mathcal{W}_B \end{pmatrix}, \qquad\qquad etc.
\end{aligned}
$$

which leads to

$$
\begin{aligned}
H_{eff} &= \left[\begin{pmatrix} R_{AA} & R_{AB} \\ R_{BA} & R_{BB} \end{pmatrix} + \begin{pmatrix} R_{AQ}S_{QA} & R_{AQ}S_{QB} \\ R_{BQ}S_{QA} & R_{BQ}S_{QB} \end{pmatrix} \right] \begin{pmatrix} C_{AA} & C_{AB} \\ C_{BA} & C_{BB} \end{pmatrix} \\
&= \begin{pmatrix} C_{AA}\mathcal{W}_A & C_{AB}\mathcal{W}_B \\ C_{BA}\mathcal{W}_A & C_{BB}\mathcal{W}_B \end{pmatrix}. \qquad\qquad (A.22)
\end{aligned}
$$

The AA part of this equation can be written as

$$\Big((H_{eff})_{AA} + (H_{eff})_{AB}C_{BA}C_A A^{-1}\Big)C_{AA} = \tag{A.23}$$

$$\Big(R_{AA} + R_{AB}C_{BA}C_{AA}^{-1} + R_{AQ}S_{QA} + R_{AQ}S_{QB}C_{BA}C_{AA}^{-1}\Big)C_{AA} = C_{AA}\mathcal{W}_A. \tag{A.24}$$

If we define

$$S'_{BA} = C_{BA}C_{AA}^{-1} \tag{A.25}$$

$$\text{and } S'_{QA} = \Big(S_{QA} + S_{QB}C_{BA}C_{AA}^{-1}\Big), \tag{A.26}$$

it is possible to simplify the expression to

$$\Big(R_{AA} + R_{AB}S'_{BA} + R_{AQ}S'_{QA}\Big)C_{AA} = C_{AA}\mathcal{W}_A. \tag{A.27}$$

Similarly, the BA portion of this equation becomes

$$(H_{eff})_{BA} + (H_{eff})_{BB}C_{BA} =$$

$$\Big(R_{BA} + R_{BB}S'_{BA} + R_{BQ}S'_{QA}\Big)C_{AA} = C_{BA}\mathcal{W}_A. \tag{A.28}$$

If $\Omega' \equiv \{\exp(S')\}$ is defined, the AA expression has the form of an effective Hamiltonian, and can be written

$$A(R\Omega')_c C'A = C'A\mathcal{W}_A \tag{A.29}$$

If we define

$$H'_{eff} = \Big((\Omega')^{-1}R\Omega'\Big)_{AA} \tag{A.30}$$

$$= (H_{eff})_{AA} + (H_{eff})_{AB}C_{BA}C'_{AA} = C_{AA}\mathcal{W}_A C_{AA}^{-1} \tag{A.31}$$

$$= \bar{H}_{AA} + \bar{H}_{AQ}\Big(\Omega_{old} - 1\Big)_{QA} + \Big(\bar{H}_{AB} + \underline{\bar{H}_{AQ}(\Omega_{old} - 1)_{QB}}\Big)S'_{BA} + \bar{H}_{AQ}S'_{QA}$$

$$(H'_{eff})_{BA} = \left((\Omega')^{-1} R \Omega'\right)_{BA} \tag{A.32}$$

$$= (H_{eff})_{BA} + (H_{eff})_{BB} C_{BA} C_{AA}^{-1} = C_{BA} \mathcal{W}_A C_{AA}^{-1} \tag{A.33}$$

$$= \bar{H}_{BA} + \bar{H}_{BQ}\left(\Omega_{old} - 1\right)_{QA} + \left(\bar{H}_{BB} + \bar{H}_{BQ}(\Omega_{old} - 1)_{QB}\right) S'_{BA} + \bar{H}_{BQ} S'_{QA}$$

we can develop a method which is invariant to this reduction of the model space.

A new type of term has been introduced in the H'_{eff} expression (see the underlined term above). The $(H'_{eff})_{BA}$ term is created to appear in the modified FS equation, which is

$$Q'\left(\bar{H}_N \Omega - (\Omega_{old} - 1)(H'_{eff})_{BA} - \Omega H'_{eff}\right) A = 0, \tag{A.34}$$

and breaks down into

$$R_{QA} + R_{QB} S'_{BA} + R_{QQ} S'_{QA} - (\Omega_{old} - 1)_{QB} (H'_{eff})_{BA}$$

$$-(\Omega_{old} - 1)_{QA} H'_{eff} - S'_{QA} H'_{eff} = 0 \tag{A.35}$$

and

$$R_{BA} + R_{BB} S'_{BA} + R_{BQ} S'_{QA} - S'_{BA} H'_{eff} = 0. \tag{A.36}$$

More explicitly with all the "new" terms (excepting those in H'_{eff}) underlined this becomes

$$\bar{H}_{QA} + \bar{H}_{QQ}(\Omega_{old} - 1)_{QA} + (\bar{H}_{QB} + \underline{\bar{H}_{QQ}(\Omega_{old} - 1)_{QB}}) S'_{BA}$$

$$+\bar{H}_{QQ} S'_{QA} - \underline{(\Omega_{old} - 1)_{QB} (H'_{eff})_{BA}}$$

$$-(\Omega_{old} - 1)_{QA} H'_{eff} - S'_{QA} H'_{eff} = 0 \tag{A.37}$$

and

$$\bar{H}_{BA} + \bar{H}_{BQ}(\Omega_{old} - 1)_{QA} + (\bar{H}_{BB} + \underline{\bar{H}_{BQ}(\Omega_{old} - 1)_{QB}}) S'_{BA}$$

$$+\bar{H}_{BQ} S'_{QA} - S'_{QA} H'_{eff} = 0. \tag{A.38}$$

It is relatively easy to show that the S'_{BA} and S'_{QA} defined above satisfy these modified Bloch equations. Returning to the Bloch equation in the larger space,

$$Q(\bar{H}\Omega_{tot} - \Omega_{tot}H_{eff})P = 0$$

When partitioned, the Q-A block is

$$\begin{aligned}&\Big\{R_{QA} + R_{QQ}S_{QA} - (\Omega_{old} - 1)_{QB}(H_{eff})_{BA} \\ &-(\Omega_{old} - 1)_{QA}(H_{eff})_{AA} - S_{QA}(H_{eff})_{AA} - S_{QB}(H_{eff})_{BA}\Big\} = 0 \end{aligned} \quad \text{(A.39)}$$

and the Q-B block is

$$\begin{aligned}&\Big\{R_{QB} + R_{QQ}S_{QB} - (\Omega_{old} - 1)_{QB}(H_{eff})_{BB} \\ &-(\Omega_{old} - 1)_{QA}(H_{eff})_{AB} - S_{QA}(H_{eff})_{AB} - S_{QB}(H_{eff})_{BB}\Big\} = 0. \end{aligned} \quad \text{(A.40)}$$

Multiplying the Q-B block by $C_{BA}C_{AA}^{-1}$ and adding the two expressions yields

$$\begin{aligned}&\Big\{R_{QA} + R_{QB}C_{BA}C_{AA}^{-1} + R_{QQ}\left[S_{QA} + S_{QB}C_{BA}C_{AA}^{-1}\right] \\ &-(\Omega_{old} - 1)_{QB}\left[(H_{eff})_{BA} - (H_{eff})_{BB}C_{BA}C_{AA}^{-1}\right] \\ &-(\Omega_{old} - 1)_{QA}\left[(H_{eff})_{AA} - (H_{eff})_{AB}C_{BA}C_{AA}^{-1}\right] \\ &-S_{QA}\left[(H_{eff})_{AA} + (H_{eff})_{AB}C_{BA}C_{AA}^{-1}\right] \\ &-S_{QB}\left[(H_{eff})_{BA} + (H_{eff})_{BB}C_{BA}C_{AA}^{-1}\right]\Big\} = 0. \end{aligned} \quad \text{(A.41)}$$

This expression simplifies to

$$\begin{aligned}&\Big\{R_{QA} + R_{QB}S'_{BA} + R_{QQ}S'_{QA} \\ &-(\Omega_{old} - 1)_{QB}(H'_{eff})_{BA} \\ &-(\Omega_{old} - 1)_{QA}H'_{eff} \\ &-S_{QA}C_{AA}\mathcal{W}_A C_{AA}^{-1} - S_{QB}C_{BA}\mathcal{W}_A C_{AA}^{-1}\Big\} = 0. \end{aligned}$$

The last two terms reduce to

$$\begin{aligned} & -\left[S_{QA} + S_{QB}C_{BA}C_{AA}^{-1}\right] C_{AA}\mathcal{W}C_{AA}^{-1} \\ = \; & -S'_{QA}H'_{eff}, \end{aligned}$$

which allows the original Bloch equation to be expressed:

$$\begin{aligned} & \Big\{R_{QA} + R_{QB}S'_{BA} + R_{QQ}S'_{QA} - (\Omega_{old} - 1)_{QB}(H'_{eff})_{BA} \\ & -(\Omega_{old} - 1)_{QA}H'_{eff} - S'_{QA}H'_{eff}\Big\} = 0. \end{aligned} \tag{A.42}$$

This is identical to the modified Q-A projection of the Bloch equation expression in the reduced space.

The B-A part of the Bloch equation can be simplified to

$$\begin{aligned} & (H'_{eff})_{BA} - S'_{BA}H'_{eff} \\ = \; & C_{BA}\mathcal{W}_A C_{AA}^{-1} - (S_{BA}C_{AA}^{-1})C_{AA}\mathcal{W}_A C_{AA}^{-1} = 0 \end{aligned} \tag{A.43}$$

Therefore, the S'_{BA} and S'_{QA} satisfy the modified Bloch equations, and define a modified effective Hamiltonian, H'_{eff}. The eigenvalues are identical to a subset of those in the larger model space and H_{eff} eigenvectors are the projection into the smaller model space of those from the original, larger model space.

The Bloch Equation and Modified Bloch Equation

To make clear the differences between the equations used in an implementation of the original and modified Fock-space method that has been presented here, the equations for both will be presented in as much detail as possible.

Equations in the Original Model Space

The P-P projection of the effective Hamiltonian is:

$$(H_{eff})_{PP} = \bar{H}_{PP} + \bar{H}_{PQ}(\Omega_{old} - 1)_{QP} + \bar{H}_{PQ}S_{QP}, \tag{A.44}$$

and the equations which the S_{QP} amplitudes must satisfy are

$$\begin{aligned} &\bar{H}_{QP} + \bar{H}_{QQ}(\Omega_{old} - 1)_{QP} + \bar{H}_{QQ}S_{QP} \\ &-(\Omega_{old} - 1)_{QP}\left[\bar{H}_{PP} + \bar{H}_{PQ}(\Omega_{old} - 1)_{QP} + \bar{H}_{PQ}S_{QP}\right] \\ &-S_{QP}\left(H_{eff}\right)_{PP} \end{aligned} \tag{A.45}$$

Equations in the Reduced Model Space

The A-A projection of the modified effective Hamiltonian is

$$H'_{eff} = \bar{H}_{AA} + \bar{H}_{AQ}\left(\Omega_{old} - 1\right)_{QA} + \left(\bar{H}_{AB} + \underline{\bar{H}_{AQ}(\Omega_{old} - 1)_{QB}}\right)S'_{BA} + \bar{H}_{AQ}S'_{QA}. \tag{A.46}$$

The equations which the S'_{QA} and S'_{BA} amplitudes must satisfy are

$$\begin{aligned} &\bar{H}_{QA} + \bar{H}_{QQ}(\Omega_{old} - 1)_{QA} + \bar{H}_{QQ}S'_{QA} + \left[\bar{H}_{QB} + \underline{\bar{H}_{QQ}(\Omega_{old} - 1)_{QB}}\right]S'_{BA} \\ &\underline{-(\Omega_{old} - 1)_{QB}\left[\bar{H}_{BA} + \bar{H}_{BQ}(\Omega_{old} - 1)_{QA} + \bar{H}_{BQ}S'_{QA}\right.} \\ &\underline{\left.+\left\{\bar{H}_{BB} + \bar{H}_{BQ}(\Omega_{old} - 1)_{QB}\right\}S'_{BA}\right]} \\ &-(\Omega_{old} - 1)_{QA}\left[\bar{H}_{AA} + \bar{H}_{AQ}(\Omega_{old} - 1)_{QA} + \bar{H}_{AQ}S_{QA}\right. \end{aligned}$$

$$+\left\{\bar{H}_{AB}+\underline{\bar{H}_{AQ}(\Omega_{old}-1)_{QB}}\right\}S'_{BA}\Big]$$

$$-S'_{QA}H'_{eff} \tag{A.47}$$

and

$$\bar{H}_{BA}+\bar{H}_{BQ}(\Omega_{old}-1)_{QA}+\bar{H}_{BQ}S'_{QA}+\left[\bar{H}_{BB}+\underline{\bar{H}_{BQ}(\Omega_{old}-1)_{QB}}\right]S'_{BA}$$

$$-S'_{BA}H'_{eff} \tag{A.48}$$

where the terms that would not arise in the usual treatment have all been underlined for clarity.

APPENDIX B

THE IMPORTANCE OF TRIPLES – CC EOMIP-SDT PERTURBATION THEORY

As Mukherjee *et al.* have pointed out[10], the CC EOMIP equations for the principal ionizations are equivalent to the Fock Space IP equations. With a convenient, connected perturbation theory thus defined, it is a simple matter to use this perturbation theory to examine the importance of a triples correction to the CC EOMIP-SD theory presented and used in this thesis.

The CC EOMIP-SDT Equations

The full CC EOMIP-SDT equations can be written as

$$\begin{aligned}\omega^{\mathcal{K}} c_{\mathcal{I}}^{\mathcal{K}} &= -\sum_{\mathcal{M}} \langle \mathcal{M}|\, \bar{f}\, |\mathcal{I}\rangle\, c_{\mathcal{M}}^{\mathcal{K}} + \sum_{\mathcal{N}\mathcal{A}} \langle \mathcal{N}|\, \bar{f}\, |\mathcal{E}\rangle\, c_{\mathcal{I}\mathcal{N}}^{\mathcal{K}\mathcal{E}} - \frac{1}{2}\sum_{\mathcal{N}\mathcal{M}\mathcal{A}} \Big\langle \mathcal{N}\mathcal{M}\big|\big|\mathcal{I}\mathcal{E}\Big\rangle c_{\mathcal{N}\mathcal{M}}^{\mathcal{K}\mathcal{E}} \\ &\quad + \sum_{\mathcal{N}\mathcal{P}\mathcal{E}\mathcal{F}} \Big\langle \mathcal{N}\mathcal{P}\big|\big|\mathcal{E}\mathcal{F}\Big\rangle c_{\mathcal{I}\mathcal{N}\mathcal{P}}^{\mathcal{K}\mathcal{E}\mathcal{F}} \end{aligned} \tag{B.1}$$

$$\begin{aligned}\omega^{\mathcal{K}} c_{\mathcal{I}\mathcal{J}}^{\mathcal{K}\mathcal{A}} &= -\sum_{\mathcal{M}} \Big\langle \mathcal{M}\mathcal{A}\big|\big|\mathcal{I}\mathcal{J}\Big\rangle c_{\mathcal{M}}^{\mathcal{K}} + \sum_{\mathcal{B}} \langle \mathcal{A}|\, \bar{f}\, |B\rangle\, c_{\mathcal{I}\mathcal{J}}^{\mathcal{K}\mathcal{B}} - (1-P_{\mathcal{I}\mathcal{J}}) \sum_{\mathcal{N}} \langle \mathcal{N}|\, \bar{f}\, |\mathcal{I}\rangle\, c_{\mathcal{N}\mathcal{J}}^{\mathcal{K}\mathcal{A}} \\ &\quad + \frac{1}{2}\sum_{\mathcal{N}\mathcal{M}} \Big\langle \mathcal{N}\mathcal{M}\big|\big|\mathcal{I}\mathcal{J}\Big\rangle c_{\mathcal{N}\mathcal{M}}^{\mathcal{K}\mathcal{A}} + (1-P_{\mathcal{I}\mathcal{J}}) \sum_{\mathcal{N}} \Big\langle \mathcal{N}\mathcal{A}\big|\big|\mathcal{B}\mathcal{J}\Big\rangle c_{\mathcal{I}\mathcal{N}}^{\mathcal{K}\mathcal{B}} \\ &\quad - \frac{1}{2}\sum_{\mathcal{N}\mathcal{M}\mathcal{B}} \Bigg(\sum_{\mathcal{E}} \langle \mathcal{N}\mathcal{M}||\mathcal{B}\mathcal{E}\rangle\, t_{\mathcal{I}\mathcal{J}}^{\mathcal{E}\mathcal{A}} \Bigg) c_{\mathcal{N}\mathcal{M}}^{\mathcal{K}\mathcal{B}} + \sum_{\mathcal{P}\mathcal{F}} \langle \mathcal{P}|\, \bar{f}\, |\mathcal{F}\rangle\, c_{\mathcal{I}\mathcal{J}\mathcal{P}}^{\mathcal{K}\mathcal{A}\mathcal{F}} \\ &\quad - \frac{1}{2}(1-P_{\mathcal{I}\mathcal{J}}) \sum_{\mathcal{N}\mathcal{P}\mathcal{F}} \Big\langle \mathcal{N}\mathcal{P}\big|\big|\mathcal{J}\mathcal{F}\Big\rangle c_{\mathcal{I}\mathcal{N}\mathcal{P}}^{\mathcal{K}\mathcal{A}\mathcal{F}} + \frac{1}{2}\sum_{\mathcal{P}\mathcal{E}\mathcal{F}} \Big\langle \mathcal{A}\mathcal{P}\big|\big|\mathcal{E}\mathcal{F}\Big\rangle c_{\mathcal{I}\mathcal{J}\mathcal{P}}^{\mathcal{K}\mathcal{E}\mathcal{F}} \end{aligned} \tag{B.2}$$

$$
\begin{aligned}
\omega^{K} c^{K\,AB}_{I\,JK} \;=\; & -\sum_{M} \left\langle MAB\bar{|}|IJK\right\rangle c^{K}_{M} + \frac{1}{2}\sum_{MN\mathcal{E}}\left(\sum_{C}\left\langle MN\bar{|}|\mathcal{E}C\right\rangle t^{IJK}_{CAB}\right) c^{K\,\mathcal{E}}_{MN} \\
& + \mathcal{A}_{IJK}\sum_{\mathcal{E}}\left\langle AB\bar{|}|\mathcal{E}K\right\rangle c^{K\mathcal{E}}_{I\,J} - (1-P_{AB})\,\mathcal{A}_{IJK}\sum_{N}\left\langle IB\bar{|}|JK\right\rangle c^{K\,A}_{I\,N} \\
& - \mathcal{A}_{IJK}\sum_{M}\langle M|\,\bar{f}\,|I\rangle\, c^{K\,AB}_{M\,JK} + (1-P_{AB})\sum_{\mathcal{F}}\langle B|\,\bar{f}\,|\mathcal{F}\rangle\, c^{K\,A\mathcal{F}}_{I\,JK} \\
& + \frac{1}{2}\sum_{\mathcal{E}\mathcal{F}}\left\langle AB\bar{|}|\mathcal{E}\mathcal{F}\right\rangle c^{K\mathcal{E}\mathcal{F}}_{I\,JK} + \frac{1}{2}\mathcal{A}_{IJK}\sum_{MN}\left\langle MN\bar{|}|IJ\right\rangle c^{K\,AB}_{MNK} \\
& + (1-P_{AB})\mathcal{A}_{IJK}\sum_{PF}\left\langle PB\bar{|}|\mathcal{E}K\right\rangle c^{K\,A\mathcal{F}}_{I\,J\mathcal{P}} + \frac{1}{2}\mathcal{A}_{IJK}\sum_{PEF}\left\langle APB\bar{|}|\mathcal{E}\mathcal{F}K\right\rangle c^{K\mathcal{E}\mathcal{F}}_{I\,J\mathcal{P}} \\
& - \frac{1}{2}(1-P_{AB})\,\mathcal{A}_{IJK}\sum_{NPF}\left\langle NPB\bar{|}|JK\mathcal{F}\right\rangle c^{K\,A\mathcal{F}}_{I\,N\mathcal{P}}. \qquad \text{(B.3)}
\end{aligned}
$$

For the purpose of developing an EOMIP perturbation theory, it is convenient to write this in a compact matrix notation,

$$
\begin{aligned}
\omega^{K} c^{K}_{I} \;=\; & \sum_{M}\langle I|A|M\rangle c^{K}_{M} + \sum_{MN\mathcal{E}}\left\langle I|A|\begin{matrix}\mathcal{E}\\ MN\end{matrix}\right\rangle c^{K\,\mathcal{E}}_{MN} \\
& + \sum_{MNP\mathcal{E}\mathcal{F}}\left\langle I\middle|A\middle|\begin{matrix}\mathcal{E}\mathcal{F}\\ MNP\end{matrix}\right\rangle c^{K\,\mathcal{E}\mathcal{F}}_{MNP} \qquad \text{(B.4)}
\end{aligned}
$$

$$
\begin{aligned}
\omega^{K} c^{K\,A}_{I\,J} \;=\; & \sum_{M}\left\langle \begin{matrix}A\\ IJ\end{matrix}\middle|A\middle|M\right\rangle c^{K}_{M} + \sum_{MN\mathcal{E}}\left\langle \begin{matrix}A\\ IJ\end{matrix}\middle|A\middle|\begin{matrix}\mathcal{E}\\ MN\end{matrix}\right\rangle c^{K\,\mathcal{E}}_{MN} \\
& + \sum_{MNP\mathcal{E}\mathcal{F}}\left\langle \begin{matrix}A\\ IJ\end{matrix}\middle|A\middle|\begin{matrix}\mathcal{E}\mathcal{F}\\ MNP\end{matrix}\right\rangle c^{K\,\mathcal{E}\mathcal{F}}_{MNP} \qquad \text{(B.5)}
\end{aligned}
$$

$$
\begin{aligned}
\omega^{K} c^{K\,AB}_{I\,JK} \;=\; & \sum_{M}\left\langle \begin{matrix}AB\\ IJK\end{matrix}\middle|A\middle|M\right\rangle c^{K}_{M} + \sum_{MN\mathcal{E}}\left\langle \begin{matrix}AB\\ IJK\end{matrix}\middle|A\middle|\begin{matrix}\mathcal{E}\\ MN\end{matrix}\right\rangle c^{K\,\mathcal{E}}_{MN} \\
& + \sum_{MNP\mathcal{E}\mathcal{F}}\left\langle \begin{matrix}AB\\ IJK\end{matrix}\middle|A\middle|\begin{matrix}\mathcal{E}\mathcal{F}\\ MNP\end{matrix}\right\rangle c^{K\,\mathcal{E}\mathcal{F}}_{MNP}. \qquad \text{(B.6)}
\end{aligned}
$$

A review of the Rayleigh-Schrödinger Perturbation Theory

In a nutshell, Rayleigh-Schrödinger perturbation theory (RSPT) is:

$$
\begin{aligned}
(H-E)\,|I\rangle &= 0 \\
\left(H^0-E^0\right)\left|I^0\right\rangle &= 0 \\
H &= H^0+H^1 \\
|I\rangle &= \left|I^0\right\rangle+\left|I^1\right\rangle+\left|I^2\right\rangle+\left|I^3\right\rangle+\cdots \\
\left\langle I^0|I^0\right\rangle = 1,\ \left\langle I^0|I\right\rangle &= 1,\ \left\langle I^0|I^N\right\rangle = 0\ (N\neq 0) \\
E &= E^0+E^1+E^2+E^3+\cdots \\
\left((E^0-H^0)+(E^1-H^1)+E^2+E^3+\cdots\right)&\left(\left|I^0\right\rangle+\left|I^1\right\rangle+\left|I^2\right\rangle+\left|I^3\right\rangle+\cdots\right)=0.
\end{aligned}
$$

In order for the final equality above to hold true the equality,

$$
(E^0-H^0)\left|I^N\right\rangle+(E^1-H^1)\left|I^{N-1}\right\rangle+\sum_{k=0}^{N-2}E^{N-k}\left|I^k\right\rangle=0,
$$

must hold true for all N, $N=1,\infty$. This means that

$$
\begin{aligned}
\left\langle I^0\right|H^1\left|I^0\right\rangle-\left\langle I^0\right|E^1\left|I^0\right\rangle &= 0 \\
\left\langle I^0\right|E^1\left|I^{N-1}\right\rangle &= \left\langle I^0\right|H^1\left|I^{N-1}\right\rangle-\left\langle I^0\right|\sum_{k=0}^{N-2}E^{N-k}\left|I^k\right\rangle
\end{aligned}
$$

$$
\begin{aligned}
\left|I^N\right\rangle &= (E^0-H^0)^{-1}\left((H^1-E^1)\left|I^{N-1}\right\rangle-\sum_{k=0}^{N-2}E^{N-k}\left|I^k\right\rangle\right) \\
&= (E^0-H^0)^{-1}\left((H^1-E^1)\left|I^{N-1}\right\rangle-\left|I^0\right\rangle E^N-\sum_{k=1}^{N-2}E^{N-k}\left|I^k\right\rangle\right) \\
&= (E^0-H^0)^{-1}\left((H^1-E^1)\left|I^{N-1}\right\rangle-\left|I^0\right\rangle\left\langle I^0\right|(H^1-E^1)\left|I^{N-1}\right\rangle-\sum_{k=1}^{N-2}E^{N-k}\left|I^k\right\rangle\right) \\
&= (E^0-H^0)^{-1}\left(R^I(H^1-E^1)\left|I^{N-1}\right\rangle-\sum_{k=1}^{N-2}E^{N-k}\left|I^k\right\rangle\right)
\end{aligned}
$$

It is conceptually simplest to choose a Koopmans' or extended-Koopmans' zeroth-order wavefunction, and a zeroth-order array which is diagonal in these single-ionization wavefunctions. This means choosing A^0 to be either $\langle i|\, f\, |m\rangle\, \delta_{im}$ or $\langle i|\, \bar{f}\, |m\rangle\, \delta_{im}$. If the latter is chosen, the first order energy will disappear. The author has chosen the former. The quantities to be used in the perturbative development are:

$$\begin{aligned}
A^0 &\equiv \langle i|\, f\, |m\rangle\, \delta_{im} & \langle i|\, A^1\, |m\rangle &\equiv \langle i|\, \bar{f}\, |m\rangle - \langle i|\, f\, |i\rangle\, \delta_{im} \\
\left\langle \mathcal{K}^0 \right| &\equiv \mathcal{K}\, |0\rangle & P^{\mathcal{K}} &\equiv |\mathcal{K}^0\rangle\, \langle \mathcal{K}^0| \\
\left| \mathcal{K}^0 \right\rangle &\equiv \left(\left\langle \mathcal{K}^0 \right| \right)^\dagger = \langle 0|\, \mathcal{K}^\dagger & R^{\mathcal{K}} &\equiv 1 - P^{\mathcal{K}} \\
\omega^{\mathcal{K}0} &\equiv \left\langle \mathcal{K}^0 \right| f \left| \mathcal{K}^0 \right\rangle & Z^{\mathcal{K}} &\equiv (\omega^{\mathcal{K}0} - A^0) R^{\mathcal{K}}.
\end{aligned} \tag{B.7}$$

In the first order,

$$\begin{aligned}
\omega^{\mathcal{K}1} &= \left\langle \mathcal{K}^0 \right| A^1 R^{\mathcal{K}} \left| \mathcal{K}^0 \right\rangle = \langle \mathcal{K}|\, A^1\, |\mathcal{K}\rangle \\
c_i^{\mathcal{K}1} &= \langle i|\, A^1\, |\mathcal{K}\rangle\, / \Delta_i^{\mathcal{K}} \\
c_{i\ j}^{\mathcal{K}a1} &= \left\langle \begin{matrix} a \\ ij \end{matrix} \middle| A^1 \middle| \mathcal{K} \right\rangle / \Delta_{ij}^{ka} \\
c_{i\ jk}^{\mathcal{K}ab1} &= \left\langle \begin{matrix} ab \\ ijk \end{matrix} \middle| A^1 \middle| \mathcal{K} \right\rangle / \Delta_{ijk}^{\mathcal{K}ab},
\end{aligned}$$

where $\Delta_i^{\mathcal{K}} = \omega^{\mathcal{K}0} + f_{ii}$, $\Delta_{ij}^{ka} = \omega^{\mathcal{K}0} + f_{ii} + f_{jj} - f_{aa}$, etc.

In the second order,

$$\omega^{\mathcal{K}2} = \left\langle \mathcal{K}^0 \right| A^1 R^{\mathcal{K}} \left| \mathcal{K}^1 \right\rangle$$

$$= \sum_i \langle \mathcal{K}| A^1 |i\rangle c_i^{\mathcal{K}1} + \sum_{ija} \left\langle \mathcal{K}\middle| A^1 \middle|_{ij}^{a} \right\rangle c_{i\ j}^{\mathcal{K}a1} + \sum_{\substack{ab \\ ijk}} \left\langle \mathcal{K}\middle| A^1 \middle|_{ijk}^{ab} \right\rangle c_{i\ jk}^{\mathcal{K}ab1}. \quad \text{(B.8)}$$

The final term of equation B.8 represents the first triples correction to the EOMIP-SD energy. In a perturbation analysis of the CCSDT or CISDT equations, there would be no triples contribution to the energy until 4th order. Because $\bar{H}$ is not limited to 1- and 2-body terms, the EOMIP triples amplitude appears in order 1. And because only one $\langle ij||ab\rangle$ term is required to close the energy term (as opposed to one $\langle ij||ab\rangle$ and one $\langle ij||kb\rangle$ or $\langle cj||ab\rangle$ term for CC or CI), this triples term appears in the energy in order 2. In more detail, this term is:

$$\begin{aligned}
\omega_{\mathrm{T}}^{\mathcal{K}2}(ijkab) &= \left\langle \mathcal{K}|A^1|\begin{smallmatrix} ab \\ ijk \end{smallmatrix} \right\rangle c_{i\ jk}^{\mathcal{K}ab1} \\
&= \left\langle \mathcal{K}|A^1|\begin{smallmatrix} ab \\ ijk \end{smallmatrix} \right\rangle \left\langle \begin{smallmatrix} ab \\ ijk \end{smallmatrix}|A^1|\mathcal{K} \right\rangle / \Delta_{ijk}^{\mathcal{K}ab} \\
&= \left\langle jk\bar{|}ef \right\rangle \left\langle \begin{smallmatrix} ab \\ ijk \end{smallmatrix}|A^1|\mathcal{K} \right\rangle / \Delta_{ijk}^{\mathcal{K}ab} * \delta\mathcal{K}i \\
&= \left\langle jk\bar{|}ef \right\rangle \left(-\sum_m \langle jk||ab\rangle\langle \mathcal{K}m||\mathcal{K}j\rangle t_{ab}^{mk} + \sum_e \langle jk||ab\rangle\langle \mathcal{K}a||\mathcal{K}c\rangle t_{cb}^{jk} \right. \\
&\quad \left. - \sum_c \langle jk||ab\rangle\langle \mathcal{K}b||ck\rangle t_{ca}^{j\mathcal{K}} + \cdots \right) / \Delta_{ijk}^{\mathcal{K}ab} * \delta\mathcal{K}i \qquad \text{(B.9)}
\end{aligned}$$

The lowest contributions to the $\left\langle \begin{smallmatrix} ab \\ ijk \end{smallmatrix}|A^1|\mathcal{K} \right\rangle$ term are of order 2 in W, which makes this energy term, of order 2 in A, minimally of order 3 in W. This is still an order lower than the first triples contribution appearing in CCSD or CI, implying that triples are more important in the EOMIP problem than they are in the CC problem.

REFERENCES

[1] T. Koopmans, Physica, **1**, 104, 1933.

[2] S. A. Kucharski and R. J. Bartlett, Advances in Quantum Chemistry, **18**, 281, 1986.

[3] D. W. Turner, C. Baker, A. D. Baker, and C. R. Brundle, *Molecular Photoelectron Spectroscopy*. Wiley-Interscience, New York, 1970.

[4] R. L. Martin and D. A. Shirley, J. Chem. Phys., **64**, 3685, 1976.

[5] Ş. Süzer, S. T. Lee, and D. A. Shirley, Phys. Rev. A, **13**, 1842, 1976.

[6] R. L. Martin and E. R. Davidson, Chem. Phys. Lett., **51**, 1977.

[7] H. Nakatsuji, Chem. Phys. Lett., **59**, 362, 1978.

[8] H. Nakatsuji, Chem. Phys. Lett., **67**, 334, 1979.

[9] H. Nakatsuji, Chem. Phys. Lett., **76**, 283, 1983.

[10] D. Mukhopadhyay, S. Mukhopadhyay, R. Chaudhuri, and D. Mukherjee, Theoretica Chimica Acta, **80**, 441, 1983.

[11] I. Lindgren and D. Mukherjee, Physics Reports, **151**(2), 193, 1987.

[12] M. Barysz, H. J. Monkhorst, and L. Z. Stolarczyk, Theoretica Chimica Acta, **80**, 483, 1991.

[13] C. M. L. Rittby and R. J. Bartlett, Theoretica Chimica Acta, **80**, 469, 1991.

[14] U. Kaldor, Theoretica Chimica Acta, **80**, 427, 1991.

[15] R. P. Mattie. Applications of multi-reference coupled-cluster theory. In D. Mukherjee, editor, *Lecture Notes in Chemistry*, volume 50, pages 143–153. Springer-Verlag, Berlin, 1987.

[16] H. Koch and P. Jørgensen, J. Chem. Phys., **93**, 3333, 1990.

[17] P. Jørgensen and J. Simons, *Second Quantization-Based Methods in quantum chemistry*. Academic Press, New York, 1981.

[18] J. Paldus and J. Cizek, Advances in Quantum Chemistry, **9**, 105, 1975.

[19] Y. Öhrn and J. Linderberg, *Propagators in Quantum Chemistry.* Academic Press, New York, 1973.

[20] L. S. Cederbaum, Chemical Physics Letters, **25**, 562, 1974.

[21] J. Schirmer, L. S. Cederbaum, and O. Walter, Physical Review A, **28**, 1237, 1983.

[22] L. T. Redmon, G. Purvis, and Y. Öhrn, J. Chem. Phys., **63**, 5011, 1975.

[23] B. Weiner, H. J. A. Jensen, and Y. Öhrn, J. Chem. Phys., **80**, 2009, 1984.

[24] E. R. Davidson, J. Comp. Phys., **17**, 87, 1975.

[25] J. Baker and B. T. Pickup, Chem. Phys. Lett., **76**, 537, 1980.

[26] J. V. Ortiz, Chem. Phys. Lett., **199**, 530, 1992.

[27] M. Nooijen and J. G. Snijders, Int. J. Quant. Chem.Symp., **26**, 1992.

[28] C. W. Murray and E. R. Davidson, Chem. Phys. Lett., **190**, 231, 1992.

[29] H. Nakatsuji and K. Hirao, J. Chem. Phys., **68**(5), 2053, 1978.

[30] S. Pal, C. M. L. Rittby, and R. J. Bartlet, Chem. Phys. Lett., **160**, 212, 1989.

[31] J. Schirmer, L. S. Cederbaum, W. Domcke, and W. von Niessen, Chem. Phys., **26**, 149, 1977.

[32] Y. Öhrn and G. Born, Advances in Quantum Chemistry, **13**, 1, 1981.

[33] J. V. Ortiz, Chem. Phys. Lett., **216**, 319, 1993.

[34] C. M. L. Rittby and R. J. Bartlett, J. Chem. Phys., **92**, 3033, 1988.

[35] S. Yang, J. J. Taylor, M. J. Craycraft, J. Conceicao, C. L. Pettiette, O. Cheshnovsky, and R. E. Smalley, Chem. Phys. Lett., **144**(5), 431, 1988.

[36] D. W. Arnold, S. E. Bradforth, T. N. Kitsopoulos, and D. M. Neumark, J. Chem. Phys., **95**, 8753, 1991.

[37] S. A. Kucharski and R. J. Bartlett, J. Chem. Phys., **95**, 8227, 1991.

[38] A. Balkova and R. J. Bartlett, J. Chem. Phys., **101**, 8972, 1994.

[39] K. Hirao and H. Nakatsuji, J. Chem. Phys., **69**, 4548, 1978.

[40] D. E. Bernholdt. *Triple Excitation Effects in the Fock-Space Coupled Cluster Method.* PhD thesis, University of Florida, Gainesville, Florida, 1993.

[41] J. Olsen and P. Jørgensen, J. Chem. Phys., **83**(7), 3235, 1985.

[42] K. Hirao and H. Nakatsuji, J. Comp. Phys., **45**, 246, 1982.

[43] N. Vaval, K. B. Ghose, S. Pal, and D. Mukherjee, Chem. Phys. Lett., **209**, 292, 1993.

[44] S. Pal, M. Rittby, R. J. Bartlett, D. Sinha, and D. Mukherjee, Chem. Phys. Lett., **137**(3), 273, 1987.

[45] D. Sinha, S. K. Mukhopadhyay, R. Chaudhuri, and D. Mukherjee, Chem. Phys. Lett., **154**(6), 544, 1989.

[46] J. F. Stanton, R. J. Bartlett, and C. M. L. Rittby, J. Chem. Phys., **97**(8), 5560, 1992.

[47] J. D. Watts, C. M. L. Rittby, and R. J. Bartlett, J. Amer. Chem. Soc., **111**, 4155, 1989.

[48] J. F. Stanton, J. Gauss, J. D. Watts, W. J. Lauderdale, and R. J. Bartlett, *ACES II: A Quantum Chemical Program Package.* The Quantum Theory Project, University of Florida, Gainesville.

[49] R. P. Mattie, *CC EOMIP, A Coupled-Cluster Equation-of-Motion Program.* The Quantum Theory Project, University of Florida, Gainesville, 1995.

[50] T. H. Dunning, Jr, J. Chem. Phys., **55**, 716, 1971.

[51] R. A. Kendall, T. H. Dunning, Jr, and R. J. Harrison, J. Chem. Phys., **96**, 6796, 1992.

[52] M. S. Banna and D. A. Shirley, J. El. Spec., **8**, 255–270, 1976.

[53] K. Siegbahn, C. Nordling, G. Johansson, J. Hedman, P. F. Heden, K. Hamrin, U. Gelius, T. Bergmark, L. O. Werme, R. Manne, and Y. Baer, *ESCA Applied to Free Molecules.* Amsterdam, 1969.

[54] H. Nakatsuji, J. Chem. Phys., **80**, 3703, 1984.

[55] Herzberg, *Molecular Spectra and Molecular Structure. III. Electronic Spectra and Electronic Structure of Polyatomic Molecules.* Van Nostrand, Princeton, 1965.

[56] Cederbaum et al., J. Chem. Phys., **69**, 1591, 1978.

[57] U. Gelius, J. El. Spec., **5**, 985, 1974.

[58] A. J. Dixon, S. T. Hood, E. Weigold, and G. R. J. Williams, J. El. Spec.Rel. Phen., **14**, 267, 1978.

[59] M. P. Keane, A. N. de Brito, N. Correia, S. Svenssson, L. Karlsson, B. Wannberg, U. Gelius, S. Lunell, W. R. Salaneck, M. Lögdlund, D. B. Swanson, and A. G. MacDiarmid, Phys. Rev. B, **45**, 6390, 1992.

[60] A. Lisini, G. Fronzoni, and P. DeCleva, Int. J. Quant. Chem., **52**, 527, 1994.

[61] A. O. Bawagan, R. Müller-Fiedler, C. E. Brion, E. R. Davidson, and C. Boyle, Chem. Phy., **120**, 1988.

[62] M. S. Banna and D. A. Shirley, J. Chem. Phys., **63**, 1975.

[63] D. A. Allison and R. G. Cavell, J. Chem. Phys., **68**, 1978.

[64] A. Bawagan, C. E. Brion, E. R. Davidson, and D. Feller, Chem. Phy., **113**, 19, 1987.

[65] J. D. Watts and R. J. Bartlett, J. Chem. Phys., **97**, 3445, 1992.

[66] J. D. Watts and R. J. Bartlett, J. Chem. Phys., **96**, 6073, 1992.

[67] P. F. Bernath, K. W. Hinkle, and J. J. Keady, Science, **244**, 562, 1989.

[68] K. W. Hinkle, J. J. keady, and P. F. Bernath, Science, **241**, 1319, 1988.

[69] P. Gerhardt, S. Loffler, and K. H. Homann, Chem. Phys. Lett., **137**, 306, 1987.

[70] W. Weltner, Jr and R. J. van Zee, Chem. Rev., **89**(8), 1715, 1989.

[71] P. L. Jones, R. D. Mead, B. E. Kohler, S. D. Rosner, and W. C. Lineberger, J. Chem. Phys., **73**, 4419, 1980.

[72] T. N. Kitsopoulos, C. J. Chick, Y. Zhao, and D. M. Neumark, J. Chem. Phys., **95**(7), 5479, 1991.

[73] J. Drowart, R. P. Burns, G. DeMaria, and M. G. Inghram, J. Chem. Phys., **31**, 1131, 1959.

[74] V. H. Dibbler and S. K. Liston, J. Chem. Phys., **47**(11), 4548, 1967.

[75] C. Petrongolo, P. J. Bruna, S. D. Peyerimhoff, and R. J. Buenker, J. Chem. Phys., **74**(8), 4595, 1981.

[76] R. A. Whiteside, R. Krishnan, D. J. DeFrees, and J. A. Pople, Chem. Phys. Lett., **78**, 538, 1981.

[77] D. H. Magers, R. J. Harrison, and R. J. Bartlett, J. Chem. Phys., **84**, 3284, 1986.

[78] K. Raghavachari and J. S. Binkley, J. Chem. Phys., **85**, 2191, 1987.

[79] D. E. Bernholdt, D. H. Magers, and R. J. Bartlett, J. Chem. Phys., **89**, 3612, 1988.

[80] R. J. van Zee, R. F. Ferrante, K. J. Zeringer, and W. Weltner, Jr, J. Chem. Phys., **88**, 3465, 1988.

[81] J. D. Watts, J. Gauss, J. F. Stanton, and R. J. Bartlett, J. Chem. Phys., **97**, 8372, 1992.

[82] J. D. Watts and R. J. Bartlett, J. Chem. Phys., **101**, 409, 1994.

[83] L. Adamowicz, Chem. Phys. Lett., **178**, 259, 1991.

[84] L. Adamowicz, J. Chem. Phys., **95**, 8669, 1991.

[85] C. C. Arnold, Y. Zhao, T. N. Kitsopoulos, and D. M. Neumark, J. Chem. Phys., **97**, 6121, 1992.

BIOGRAPHICAL SKETCH

Renée Peloquin was born in Washington, D.C., on July 1, 1964, and except for 18 months in Solana Beach, California, attended Catholic and public schools in Prince George's County, Maryland. In September of 1982, she entered the halls of higher education at the Johns Hopkins University in Baltimore, Maryland, and embarked upon graduate studies in 1985 at the Quantum Theory Project of the University of Florida, Gainesville. Nearly a decade later, she emerged with a new name, a Ph.D. in Physical Chemistry, a home in Pennsylvania, and a cat. It has been a long decade. She is looking forward to applying her skills to some real chemistry, and to spending a good deal more time with her husband of seven years than she has been able to do lately.

acceptable standards of scholarly presentation and is fully adequate, in scope and quality, as a dissertation for the degree of Doctor of Philosophy.

Rodney J. Bartlett, Chairman
Graduate Research Professor of Chemistry

I certify that I have read this study and that in my opinion it conforms to acceptable standards of scholarly presentation and is fully adequate, in scope and quality, as a dissertation for the degree of Doctor of Philosophy.

N. Yngve Öhrn
Professor of Chemistry

I certify that I have read this study and that in my opinion it conforms to acceptable standards of scholarly presentation and is fully adequate, in scope and quality, as a dissertation for the degree of Doctor of Philosophy.

Samuel Trickey
Professor of Physics

I certify that I have read this study and that in my opinion it conforms to acceptable standards of scholarly presentation and is fully adequate, in scope and quality, as a dissertation for the degree of Doctor of Philosophy.

William Weltner
Professor of Chemistry

I certify that I have read this study and that in my opinion it conforms to acceptable standards of scholarly presentation and is fully adequate, in scope and quality, as a dissertation for the degree of Doctor of Philosophy.

Kermit Sigmon
Associate Professor of Mathematics

This dissertation was submitted to the Graduate Faculty of the Department of Chemistry in the College of Liberal Arts and Sciences and to the Graduate School and was accepted as partial fulfillment of the requirements for the degree of Doctor of Philosophy.

August 1995

Dean, Graduate School